TABLE OF CONTENTS

LIST OF TABLES

LIST OF FIGURES

LIST OF SYMBOLS

Symbol	Definition
F_I	Instantaneous bouyancy term $\frac{3gQ_I}{4c_pT\pi\rho}$ (m^4/s^2)
FM	Percentage by weight of pollutant material in the fuel
H_L, H_S	Respective heat contents of liquid and solid fuels (cal/gm)
M	Molecular weight (gm/mole)
P	Ambient pressure (mb)
$P\ z_{TK}$	Integral of the Gaussian probability function between minus infinity and the top of the Kth layer z_{TK} $P\left\{\frac{z_{TK} - z_{mI}}{\sigma}\right\}$
Q	Total weight of exhaust products in the stabilized exhaust cloud (gm) $(Q_R)(t_R\{z_{mI}\})(FM)$
Q_F	Rate of heat released by burning fuel (cal/s) $H_L \cdot W_L + H_S \cdot W_S$
Q_I	Effective heat released (cal)
Q_K	Source strength in units of mass per unit depth of the Kth layer (gm/m)
T	Ambient air temperature (K)
W_L, W_S	Respective fuel expenditure rates, liquid and solid fuel (g/s)
z	Height above ground of any selected layer (m)
c_p	Specific heat of air at constant pressure 0.24 cal/K gm
g	Gravitational acceleration (9.8 m/s^2)

Symbol	Definition
r_R	Initial cloud radius at the surface (m)
$S=\frac{g}{T}\frac{\partial \theta}{\partial z}$	Stability parameter ($1/s^2$)
t^*	Time of layer breakdown (s)
t_H	Time after ignition required for the cloud to reach the stabilization height (s)
t_R	Time after ignition (s)
t_{sI}	Time required for the cloud to achieve stabilization in an adiabatic atmosphere (s)
$t_R\{z_{mI}\}$	Time in seconds required for the vehicle to reach the height z_{mI} of maximum ris of the ground cloud (obtained from equation 1)
$\bar{u}$	Mean wind speed (m/s)
z	Height of stabilized cloud (m)
z'	Midpoint of the Kth layer (m) $(z_{BK} + z_{TK})/2$
z_{BK}	Height of the base of the Kth layer (m)
z_{TK}	Height of the top of the Kth layer (m)
z_{TL}	Height of the top of the Lth layer (m)
z_R	Altitude above the pad (m)
γ_C	Entrainment constant (continuous) (dimensionless)
γ_I	Entrainment constant (instantaneous) (dimensionless)
σ	Standard deviation of the concentration distribution of the stabilized ground cloud (m)
σ_{xK}	Standard deviation of the alongwind concentration distribution in the Kth layer at distance x (m)
σ_{xLK}	Standard deviation of the alongwind concentration distribution in the Lth layer for the source originating in the Kth layer (m)
$\sigma_{xo}\{K\}$	Standard deviation of the alongwind concentration distribution in the Kth layer at cloud stabilization (m)
$\sigma_{yo}\{K\}$	Standard deviation of the crosswind concentration distribution in the Kth layer at cloud stabilization (m)

Symbol	Definition
$\sigma_{zo}(K)$	Standard deviation of the vertical concentration distribution in the Kth layer at cloud stabilization (m)
σ_{yK}	Standard deviation of the crosswind concentration distribution in the Kth layer at distance x (m)
ρ	Density of ambient air (g/m^3)
$\frac{\partial \Phi}{\partial z}$	Vertical gradient of ambient potential temperature (K/m)
χ_p	Peak or centerline concentration (ppm)
keV	Kilo electron volt
s	Seconds

NASA Technical Paper 1073

Research in the Use of Electrets in Measuring Effluents From Rocket Exhaust of the Space Shuttle (6.4 Percent Scaled Model) and Viking I Launch

Michael Susko

NOVEMBER 1977

NASA

NASA Technical Paper 1073

Research in the Use of Electrets in Measuring Effluents From Rocket Exhaust of the Space Shuttle (6.4 Percent Scaled Model) and Viking I Launch

Michael Susko
George C. Marshall Space Flight Center
Marshall Space Flight Center, Alabama

NASA
National Aeronautics
and Space Administration

Scientific and Technical
Information Office

1977

ACKNOWLEDGMENTS

The author is grateful to Drs. W. W. Vaughan, G. H. Fichtl, and Robert E. Turner of the Space Sciences Laboratory, Marshall Space Flight Center, for their encouragement and enthusiastic support of this work.

The excellent cooperation of Drs. Walter Frost, Basil Antar, Kenneth R. Kimble, and Kapuluru C. Reddy of the University of Tennessee Space Institute is sincerely appreciated.

The associates at Marshall Space Flight Center, Mr. David Nicolas of the Electronics Development Division and Mr. Don Donald and Mr. Charley Watson of the Test Division, were very cooperative in laboratory and field tests.

The assistance of Dr. Ron Dawbarn and Dr. Max Kinslow (of Arnold Engineering Development Center, Tullahoma, Tennessee) in the chamber tests is appreciated.

The use of the electrets in the studies of rocket exhaust effluents was made possible through collaboration with the inventor, Dr. P. K. C. Pillai of the Physics Department, Indian Institute of Technology, New Delhi, India, who was a National Research Council postdoctoral research associate at NASA/ Marshall Space Flight Center.

CHAPTER I

INTRODUCTION

The primary objective of this report is to demonstrate the feasibility of using electrets, a new measuring device developed by the Space Sciences Laboratory of Marshall Space Flight Center (MSFC) to measure the chemical composition of rocket exhaust from space vehicles. The secondary objective is to evaluate the NASA/MSFC Multilayer Diffusion Model versus standard hydrogen chloride (HCl) detectors. It is noted there are over 50 measuring techniques available to detect atmospheric contamination. The instrumentation used operationally by the Booster Exhaust Study Test Team (BEST) which was composed of personnel from Langley Research Center (LaRC), Kennedy Space Center (KSC), and MSFC during the sampling of the ground cloud from the Titan IIIC launch of Viking I mission to Mars from Cape Kennedy, Florida, on August 20, 1975 and the instruments used for the measurement of gases in MSFC's static test firings of the 6.4 percent scaled model of the Space Shuttle are presented.

Several of these instruments have been used in previous attempts to obtain measurements of HCl concentrations downwind of actual launches of solid rockets, both at KSC and Vandenberg Air Force Base, California. However, due to the problems in trying to predict the path of the ground cloud and thereby prelocate the instruments, minimal data had been obtained. In such field tests, it soon becomes apparent that one must either deploy an extensive grid of measuring devices or have the instruments highly mobile and capable of following the cloud. It has been shown there is a general complication with all these types of instruments, i.e., a lack of multipollutant capabilities or a need for the development of a method of high sensitivity, simplicity, and speed of measurement, and for multipollutant capabilities. The electrets can overcome this complication. The experiments with the electrets have shown that they have unique properties that are useful in practical exhaust studies. They may be deployed over a large area and used to augment the more sophisticated detectors.

The research is reported in the following manner. Chapter II discusses the background, the preparation, and the use of electrets to measure effluents from Solid Rocket

Boosters (SRB's). Chapter III discusses the standard instruments used to detect HCl during the static tests, chamber tests, and Viking I mission. Chapter IV presents the meteorological input which is vital to the NASA/MSFC Multilayer Diffusion Model to predict the HCl concentration. Chapter V discusses the NASA/MSFC Multilayer Diffusion Model. Chapters II, III, IV, and V present the necessary background information to evaluate realistically the electrets. Chapter VI evaluates electrets by reporting the results of the static tests, chamber tests, and Viking I's mission. Comparisons are made with the diffusion model and standard instruments. Finally, Chapter VII presents the conclusions of the investigation.

CHAPTER II

EXPERIMENTAL ELECTRETS

Electrets have been known since the latter part of the 19th century. A substantial amount of work has been done on electrets, and a few practical applications, particularly in the area of communications, have been made. In general, however, only qualitative descriptions of the various processes are known.

The particles in tests that have been conducted have either a positive or negative charge and are attracted to the electret's surface. These collected particles or ions on the electrets are then analyzed by taking the mass spectra of the sample.

Electrets have been made in a variety of ways, but the method used most often has been to make "thermoelectrets." A thermoelectret is made by placing a dielectric material between two electrodes, heating the dielectric material to near its softening point, and applying a high direct current field to the material between electrodes. The field is maintained while the dielectric is cooled to room temperature, and the electric field is removed. If the treated dielectric exhibits electric polarization, it is called an electret [1].

It has been found that thermoelectrets of polymers with stable surface charges on either side are suitable devices for attracting charged particles and ions to their surface. Therefore, it was decided to use these electrets for effectively measuring charged gases, vapors, or particles in the atmosphere. The thermoelectret characteristics of polytetrafluorethylene (Teflon) from experimental studies were analyzed by collecting vapors of xylene and acetone under different experimental conditions. Thermoelectrets were prepared by keeping a Teflon foil of 0.0125 cm thickness between two aluminum electrodes. Further details are in Reference 2. Mass spectra of the unexposed electret and the exposed electret were taken by using the Varian M-66 cycloidal mass spectrometer. The experiment results indicated that even small quantities of the gases give a characteristic mass spectra and the peak height of the mass spectra can be considered as a measure of the quantity of the material collected over the surface of the electret.

Electrets are being used to measure the effluents from the propellants in SRB's. The most widely used propellant in SRB's is ammonium perchlorate as the oxidizer with powdered aluminum filler that acts in part as a fuel and partially as a stabilizer to control the burning rate. The exhaust products from this type of fuel contain HCl, aluminum oxide (Al_2O_3), and water (H_2O). To assess the impact of these products in the atmosphere, it is necessary to know not only their quantity but also their distribution in the ground cloud that develops at the launch site after a rocket firing.

Electrets of polymers were used successfully for the first time in collecting rocket exhaust effluent measurements. The exposed electrets were analyzed by scanning electron microscope (SEM) and X-ray microprobe analyses. It was possible by these studies to identify the various effluents coming from the rockets at the time of firing. Direct comparisons of values with electrets were made with the results obtained from the chemiluminescent, bubbler, coulometer, and millipore filters for samples kept under identical conditions. This aided in calibrating the intensity of the X-ray spectra with respect to the concentration of the products collected on the electret surfaces. The results of these comparisons show a high degree of correlation. The entire spectra of the pollutants coming from the rocket may be obtained from the electrets. Other methods showed only the concentration of HCl. However, more extensive investigations must be performed to obtain quantitative results with electrets. This report discusses the use of electrets to measure the effluents.

A typical computer output of the scanning electron microscope (SEM) and X-ray microprobe analysis [2] of the rocket exhaust effluents is shown in Figure 1 and listed in Table 1. Figure 1 illustrates the X-ray energy spectra obtained from the electret during the Viking I launch (Test V11). Table 1 lists the peak count of X-ray energy for each element. The surface topology of the electret for this test is shown in Figure 2. Because this method has the added advantage of obtaining the entire spectrum of pollutants from a rocket exhaust, it is a powerful tool in studying contaminants.

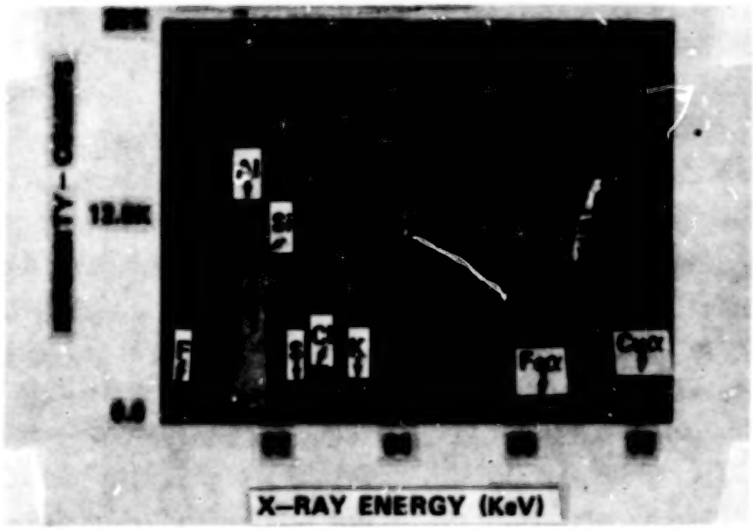

Figure 1. X-ray energy spectra from Test V11, Viking I mission.

Table 1. Data Output from Analyzer, Test V11, Viking I Mission

X-ray Energy (KeV)	Counts (2000 s)	Symbol
0.707	13 632	F
1.497	121 644	Al
1.749	90 720	Si
2.105	4 647	Au
2.306	18 156	S
2.626	24 992	Cl
3.317	16 415	K
3.660	3 146	Ca
5.409	3 094	Cr α
5.880	79	Cr β
6.388	10 469	Fe α
7.035	1 233	Fe β
8.010	24 390	Cu α

Figure 2. Surface topology from Test V11, Viking I mission.

CHAPTER III

INSTRUMENTS

The following instruments were used to detect and measure the concentration of HCl in these tests:

1. Chemiluminescent HCl detector (Geomet)
2. Bubblers
3. Millipore filter
4. Coulometer.

A brief discussion of each of the instruments and its evaluation follows.

A. Chemiluminescent HCl Detector (Geomet)

This detector was developed under contract for NASA and is now available commercially. The HCl detector is designed to continuously monitor HCl air concentrations from 0.1 to 50 ppm. In this concentration range, the response time to 90 percent signal and 10 percent recovery is a few seconds. Since these terms will be used again, an explanation is presented as follows [3]:

> Response time has been defined as that time required for the output of the detector to reach 90 percent of its final (equilibrated) output upon exposure to a fixed pollutant concentration. Time zero for a response time measurement is that time at which the pollutant concentration is introduced into the inlet of the detector. Recovery time is defined as that time required for the output of the detector sampling a fixed concentration to decay to 10 percent of the original value after removing source of the pollutant gas stream from the inlet of the detector. Time zero for a recovery time measurement is that time at which the source of pollutant is removed from the inlet of the detector.

HCl is detected by chemiluminescence accompanying the reaction of luminol. The inlet column for the sampling stream is coated with NaBr and $NaBr0_3$. HCl reacts with this coating to produce hypochlorite, hypobromite, and possibly bromine, all of which react with luminol to produce chemiluminescence which is proportional to the concentration of HCl in the incoming stream. With most other instruments sufficient HCl, especially at low concentrations, is removed by the adsorption or reaction at the inlet to cause a lag in response of the instrument. However, in this chemiluminescent instrument,

this adsorption or reaction produces species that are essential to the detection process. The response of this instrument is rapid in comparison to other HCl detecting instruments. Laboratory and field evaluations of the chemiluminescent HCl detector have shown the unit to be a reliable HCl detector [3]. Laboratory results have shown detector limits of 0.05 ppm and an absolute accuracy of at least ±5 percent. Field results have shown similar detection limits and stable operation at ambient temperatures of 40°C. Future laboratory evaluations will be in the area of interference studies and detection of HCl (gas) and HCl (aerosol) mixtures. Based on the results in Reference 3, the following conclusions apply:

1. The detection limit for the HCl detector is less than 0.05 ppm.
2. In the range of 0.05 to 50 ppm, the accuracy of the HCl detector is 5 percent.
3. Response time for the HCl detector ranges from less than 1 s at 50 ppm to approximately 20 s at 0.05 ppm.

B. Bubblers

Basically, the bubbler is a dosage type instrument. It sucks air at a rate of 3000 cm^3/min into 20 cm^3 of distilled water. It uses coulometric detection for the detection of chloride.

There is a detection limit of 3 nanograms (ng)/20 μliters of water. Also, the detection limit is a function of how pure one can get the water. Basically, the detection limit is 80 to 100 ppm-s, which is marginal. As an example, if the concentration is 0.8 ppm for 10 s, no measurement is obtained. However, if a 0.8 ppm measurement for 100 s is made, a measurement may be obtained. The accuracy is 10 percent of the reading above 200 ppm-s; below this the accuracy increases [4].

C. Millipore Filter

A millipore filter consists of a plastic membrane backed with a cellulose pad. The membrane and pad are housed in a disposable plastic container. The accuracy of the

determination of an HCl concentration using this device is defined by the various measurements that must be made, i.e., time of exposure, flow rate through filter, quantity of water used in the analysis, and the hydrogen ion concentration. Assuming reasonable uncertainties for each of these measurements yields a net uncertainty of ±15 percent in the HCl concentration.

The pore size of the millipore filter membrane is 0.4 μm. The flow rate to sample the exhaust gas is 5 liters/min. The membrane is 3.28 cm (1.5 in.) in diameter. The membrane collects the aluminum oxide particles. The HCl is absorbed by the membrane and the cellulose backing pad. The dosage absorbed by a specific filter is determined by removing the membrane and pad and macerating them in 20 cm^3 of distilled water. The resulting pH change in the water is then measured. Thus, the hydrogen ion concentration can be determined, and the quantity of HCl follows from this determination [4].

D. Coulometer

The coulometer used in these tests was supplied and operated by personnel from the U.S. Air Force School of Aerospace Medicine, Brooks Air Force Base, Texas. It is a standard laboratory microcoulometric titrating system which has been modified to accept a continuous sample of gas bubbled through the electrolyte. The cell is composed of two pairs of electrodes immersed in a 70 percent (vol./vol.) aqueous glacial acetic acid solution made approximately 1×10^{-7} molar in silver ions. One pair of electrodes is used to sense the concentration of silver ions and the other pair is used to generate silver ions. When a sample of HCl is introduced into the cell, it reacts with the silver ions to produce AgCl as a precipitate. As the concentration of the silver ions in the electrolyte varies, a change in the output voltage across the sensing electrodes is developed. This voltage is fed to an amplifier and after being amplified and properly phased is applied to the generating electrodes to replenish the silver ions.

The potential drop across a precision resistor in series with the generating electrodes is monitored by a recorder. Thus, the total charge needed to regenerate the silver ions appears as a peak on the recorder. The area under this peak is related by Faraday's Law to the Cl^- ion concentration. The threshold detection limit for batch injection of HCl is approximately 3 nanograms (ng). The total quantity is calculated from

$$W = \frac{36.45}{96\,501} \frac{\text{gm/mole}}{\text{coulomb}} \times 10^6 \left(\frac{A}{R}\right)$$

where

W = weight of HCl nanograms (ng)

A = coulogram peak area millivolts-seconds (mV-s)

R = precision resistor ohms (Ω)

When the instrument is sampling a steady-state mixture of HCl and air, the resulting constant current supplied to the generating electrodes can be directly related to the HCl concentration. The range of HCl concentrations which can be measured by the instrument can be adjusted by changing the rate at which the sampled gases are drawn through the electrolyte. However, there are limits, imposed by the excessive turbulence of the electrolyte caused by high flow rates and poor mixing at low sampling rates, which set the optimum instrument range from 0.1 to 20 ppm of HCl. A typical sampling rate is 0.1 liter/min.

The coulometer has been employed as a standard to check HCl mixtures used as calibration gases for other instruments. In this role the coulometer samples the mixture for a specific time; from the determination of the weight of the total chloride ion sensed, the flow rate of the gas through the electrolyte, and the time interval, the concentration of the HCl is calculated. Using a chain rule analysis with estimates on the precision of each measured quantity indicates an expected uncertainty of ±6 percent when the coulometer is sampling at its upper limit of 17 ppm [4].

CHAPTER IV

METEOROLOGICAL DATA

Meteorological data are used as weather input into the NASA/MSFC Multilayer Diffusion Model to compute the HCl isopleth concentration versus downwind distance and HCl centerline concentration as given in Chapter VI of this report.

The atmospheric soundings for the Space Shuttle Vehicle's (SSV's) static test firings were made by the Atmospheric Research Test Facility of MSFC with the following equipment:

a. Radiosonde – A balloon-borne instrument for the simultaneous measurement and transmission of meteorological data. The instrument consists of transducers for the measurement of pressure, temperature, and humidity.

b. Rawin – A method of upper-air observation consisting of an evaluation of the wind speed and direction, temperature, and relative humidity aloft by means of a balloon-borne radiosonde tracked by a radar or by a ground meteorological detector. Height data pertaining to levels aloft are computed from the radiosonde data, while wind data are derived by trigonometric computation.

c. AF Type Radiosonde – At the KSC meteorological station, the rawin flights were made with an AF type radiosonde using the GMD-4 rather than the National Weather Service (NWS)/National Oceanic and Atmospheric Administration (NOAA) radiosonde system to obtain weather data during Viking I's launch. The temperature and humidity sensor data are transmitted ten times per minute in the AF sonde by a clock-actuated switch rather than the aneroid barometer switch used in the NOAA radiosonde. Both systems measure azimuth and elevation with the GMD. A transponder in the AF sonde is used to obtain the slant range to the radiosonde, enabling the calculation of altitude. The pressure is then calculated according to the hydrostatic equation. The equations used in the computer program to calculate various thermodynamic quantities from the basic altitude, temperature, and relative humidity data are given in Appendix A.

A. Static Tests' Weather Data for Diffusion Model

Tables 2 through 19 present a collection of atmospheric soundings of the environment at MSFC's Test Facility 116, Huntsville, Alabama, during the SSV 6.4 percent model static test firings.

B. Viking I's Weather Data for Diffusion Model

Table 20 is the atmospheric soundings for the Viking I launch. The Viking I mission to Mars was a Titan IIIE launch from Pad 41 at KSC at 1722 EDT on August 20, 1975.

The test day occurrences of the 18 static test firings were as follows: two in August, two in November, one in December, nine in January, three in February, and one in March. The nine tests in January were particularly favorable for model testing of HCl downwind concentrations because of the extreme wind shears, temperature inversions, and cold temperatures.

Table 2. GMD Sounding for Test Firing No. 1, August 16, 1974, 1440 CST, MSFC Test Facility 116[a]

Height (m)	Wind Speed (m/s)	Wind Direction (degree)	Temperature (°C)	Pressure (mb)
0.0	2.6	240.0	29.3	999.0
107.0	3.6	229.8	26.9	987.0
197.0	4.6	219.6	26.9	977.0
306.0	4.0	207.7	25.9	965.0
434.0	4.4	210.5	24.5	951.0
573.0	4.2	214.6	22.4	936.0
695.0	4.1	209.6	21.3	923.0
837.0	4.2	208.7	20.0	908.0
971.0	3.9	208.9	19.4	894.0
1087.0	4.1	209.6	18.5	882.0

a. Standard deviation of the surface wind angle – 4.0°; surface air density – 1156.0 gm/m^3.

Table 3. GMD Sounding for Static Test Firing No. 2, August 30, 1974, 1302 CST, MSFC Test Facility 116[a]

Height (m)	Wind Speed (m/s)	Wind Direction (degree)	Temperature (°C)	Pressure (mb)
0.0	3.6	250.0	25.3	997.9
123.0	4.6	246.5	24.4	984.0
221.0	5.7	243.0	23.4	973.0
357.0	5.9	238.4	22.1	958.0
485.0	6.6	236.0	21.0	944.0
679.0	8.3	234.0	19.2	923.0
897.0	8.9	230.6	18.2	900.0
1090.0	9.4	222.4	17.8	880.0

a. Standard deviation of the surface wind angle – 4.0°; surface air density – 1218.9 gm/m^3.

Table 4. GMD Sounding for Static Test Firing No. 3, November 19, 1974, 2131 CST, MSFC Test Facility 116[a]

Height (m)	Wind Speed (m/s)	Wind Direction (degree)	Temperature (°C)	Pressure (mb)
0.0	0.5	100.0	13.6	989.0
170.0	3.9	153.6	14.3	979.0
284.0	7.3	207.2	14.9	965.0
408.0	7.6	219.2	15.1	951.0
542.0	8.3	278.3	13.5	936.0
687.0	9.6	236.2	12.1	920.0
834.0	10.1	243.2	10.6	904.0
973.0	10.6	244.7	9.6	889.0
1105.0	11.6	250.3	8.3	875.0

a. Standard deviation of the surface wind angle – 4.0°; surface air density – 1215.95 gm/m^3.

Table 5. GMD Sounding for Static Test Firing No. 4, November 22, 1974, 1830 CST, MSFC Test Facility 116[a]

Height (m)	Wind Speed (m/s)	Wind Direction (degree)	Temperature (°C)	Pressure (mb)
0.0	0.5	90.0	7.1	1000.0
101.0	4.0	127.6	16.0	988.0
248.0	7.6	165.2	15.1	971.0
407.0	4.6	157.0	14.4	953.0
523.0	2.0	162.9	13.6	940.0
649.0	1.8	196.2	12.6	926.0
745.0	1.4	243.4	12.2	910.0
925.0	2.6	276.2	12.6	896.0
1057.0	3.4	270.9	12.8	882.0

a. Standard deviation of the surface wind angle – 4.0°; surface air density – 1244.4 gm/m^3.

Table 6. GMD Sounding for Static Test Firing No. 5, December 12, 1974, 1350 CST, MSFC Test Facility 116[a]

Height (m)	Wind Speed (m/s)	Wind Direction (degree)	Temperature (°C)	Pressure (mb)
0.0	4.1	190.0	17.1	997.9
136.0	5.2	187.1	14.4	982.0
265.0	6.3	184.2	13.2	967.0
397.0	6.9	191.2	12.0	952.0
511.0	7.5	198.6	11.1	939.0
627.0	8.5	199.4	9.6	926.0
736.0	9.4	204.0	8.8	914.0
845.0	10.2	208.2	7.9	902.0
955.0	10.7	211.0	7.7	890.0
1077.0	10.0	213.3	7.9	877.0

a. Standard deviation of the surface wind angle – 4.0°; surface air density – 1197.7 gm/m^3.

Table 7. GMD Sounding for Static Test Firing No. 6, January 7, 1975, 1759 CST, MSFC Test Facility 116[a]

Height (m)	Wind Speed (m/s)	Wind Direction (degree)	Temperature (°C)	Pressure (mb)
0.0	2.6	130.0	12.7	997.0
132.0	6.9	144.4	12.4	979.0
291.0	11.3	158.9	12.0	963.0
404.0	12.2	165.8	11.2	950.0
528.0	12.5	172.0	10.8	936.0
645.0	13.5	177.1	10.1	923.0
772.0	13.3	182.8	9.7	909.0
919.0	12.8	189.8	9.1	893.0
1069.0	12.4	197.5	8.4	877.0

a. Standard deviation of the surface wind angle – 4.0°; surface air density – 1218.9 gm/m^3.

Table 8. GMD Sounding for Static Test Firing No. 7, January 9, 1975, 1758 CST, MSFC Test Facility 116[a]

Height (m)	Wind Speed (m/s)	Wind Direction (degree)	Temperature (°C)	Pressure (mb)
0.0	5.2	110.0	14.3	991.5
141.0	9.3	129.0	13.9	975.0
290.0	13.5	148.1	13.5	958.0
450.0	13.8	162.8	13.2	940.0
604.0	13.2	181.4	14.1	923.0
733.0	12.8	198.3	15.1	909.0
846.0	13.3	208.4	14.7	897.0
979.0	14.3	212.4	14.1	883.0
1114.0	15.3	215.2	13.2	869.0

a. Standard deviation of the surface wind angle – 4.0°; surface air density – 1199.12 gm/m^3.

Table 9. GMD Sounding for Static Test Firing No. 8, January 11, 1975, 1435 CST, MSFC Test Facility 116[a]

Height (m)	Wind Speed (m/s)	Wind Direction (degree)	Temperature (°C)	Pressure (mb)
0.0	2.6	230.0	12.5	996.4
198.0	3.0	255.0	10.3	973.0
396.0	3.4	280.1	8.4	950.0
571.0	3.4	271.7	6.4	930.0
749.0	4.2	264.5	4.3	910.0
939.0	4.9	257.3	2.8	889.0
1113.0	5.4	246.6	0.9	870.0

a. Standard deviation of the surface wind angle – 4.0°; surface air density – 1212.64 gm/m^3.

Table 10. GMD Sounding for Static Test Firing No. 9, January 15, 1975, 1550 CST, MSFC Test Facility 116[a]

Height (m)	Wind Speed (m/s)	Wind Direction (degree)	Temperature (°C)	Pressure (mb)
0.0	1.0	270.0	10.3	1001.6
130.0	2.0	252.9	8.9	986.0
273.0	3.1	238.8	7.8	969.0
410.0	4.7	241.7	6.2	953.0
540.0	6.5	242.6	5.3	938.0
698.0	7.7	246.5	4.5	920.0
841.0	7.9	261.0	4.3	904.0
968.0	8.1	276.1	4.1	890.0
1106.0	8.7	287.3	2.8	875.0

a. Standard deviation of the surface wind angle – 4.0°; surface air density – 1230.60 gm/m^3.

Table 11. GMD Sounding for Static Test Firing No. 10, January 16, 1975, 1640 CST, MSFC Test Facility 116[a]

Height (m)	Wind Speed (m/s)	Wind Direction (degree)	Temperature (°C)	Pressure (mb)
0.0	1.6	330.0	7.2	1006.4
135.0	4.7	350.1	6.8	990.0
260.0	7.8	10.3	5.8	975.0
361.0	7.5	12.8	4.6	963.0
472.0	7.3	11.7	3.4	950.0
566.0	7.2	16.4	2.2	939.0
678.0	7.8	16.7	1.3	926.0
810.0	7.7	16.0	0.4	911.0
943.0	6.6	11.8	−0.8	896.0
1069.0	5.0	359.5	−1.3	892.0

a. Standard deviation of the surface wind angle – 4.0°; surface air density – 1249.88 gm/m^3.

Table 12. GMD Sounding for Static Test Firing No. 11, January 18, 1975, 1450 CST, MSFC Test Facility 116[a]

Height (m)	Wind Speed (m/s)	Wind Direction (degree)	Temperature (°C)	Pressure (mb)
0.0	0.5	350.0	11.7	996.3
138.0	4.4	294.2	11.9	980.0
275.0	8.4	238.5	11.3	964.0
415.0	10.7	246.7	10.6	948.0
557.0	13.2	248.8	9.7	932.0
701.0	16.4	247.7	8.9	916.0
847.0	17.5	252.8	7.7	900.0
986.0	17.7	256.4	7.5	885.0
1126.0	18.2	260.1	6.6	870.0

a. Standard deviation of the surface wind angle – 4.0°; surface air density – 1245.46 gm/m^3.

Table 13. GMD Sounding for Static Test Firing No. 12, January 21, 1975, 1145 CST, MSFC Test Facility 116[a]

Height (m)	Wind Speed (m/s)	Wind Direction (degree)	Temperature (°C)	Pressure (mb)
0.0	3.1	120.0	7.5	1004.0
132.0	4.7	130.4	7.3	988.0
266.0	6.3	140.9	6.0	972.0
402.0	7.6	150.3	4.8	956.0
539.0	7.6	155.7	2.7	940.0
678.0	6.9	165.3	1.4	924.0
801.0	6.5	177.2	1.6	910.0
944.0	6.7	192.2	3.2	894.0
1081.0	7.3	308.8	3.6	879.0

a. Standard deviation of the surface wind angle – 4.0°; surface air density – 1249.87 gm/m^3.

Table 14. GMD Sounding for Static Test Firing No. 13, January 23, 1975, 1958 CST, MSFC Test Facility 116[a]

Height (m)	Wind Speed (m/s)	Wind Direction (degree)	Temperature (°C)	Pressure (mb)
0.0	0.5	40.0	6.0	1003.8
139.0	1.4	80.7	9.5	987.0
266.0	2.3	121.4	8.7	972.0
403.0	2.5	125.0	7.6	956.0
524.0	3.0	144.3	7.3	942.0
639.0	3.7	163.6	6.4	929.0
736.0	5.1	180.0	8.0	915.0
900.0	6.7	198.0	9.1	900.0
1039.0	8.1	213.7	9.3	885.0

a. Standard deviation of the surface wind angle – 4.0°; surface air density – 1215.70 gm/m^3.

Table 15. GMD Sounding for Static Test Firing No. 14, January 27, 1975, 1822 CST, MSFC Test Facility 116[a]

Height (m)	Wind Speed (m/s)	Wind Direction (degree)	Temperature (°C)	Pressure (mb)
0.0	2.6	160.0	18.2	996.6
144.0	7.1	174.3	19.5	980.0
259.0	11.6	188.7	19.2	967.0
393.0	14.5	190.8	18.6	952.0
529.0	15.2	196.9	16.4	937.0
656.0	16.8	202.0	15.0	923.0
795.0	17.8	209.2	14.6	908.0
936.0	18.1	219.2	14.2	893.0
1070.0	19.3	229.7	14.8	879.0

a. Standard deviation of the surface wind angle – 4.0°; surface air density – 1195.11 gm/m^3.

Table 16. GMD Sounding for Static Test Firing No. 15, February 8, 1975, 1254 CST, MSFC Test Facility 116[a]

Height (m)	Wind Speed (m/s)	Wind Direction (degree)	Temperature (°C)	Pressure (mb)
0.0	2.1	220.0	7.8	1000.2
158.0	2.1	215.1	3.7	981.0
325.0	2.2	210.3	1.8	961.0
485.0	4.0	217.5	0.3	942.0
657.0	5.4	231.0	–1.4	922.0
823.0	6.3	236.0	–1.5	903.0
938.0	7.8	241.2	–0.4	890.0
1056.0	8.3	243.6	–0.7	877.0

a. Standard deviation of the surface wind angle – 4.0°; surface air density – 1243.70 gm/m^3.

Table 17. GMD Sounding for Static Test Firing No. 16, February 12, 1975, 1700 CST, MSFC Test Facility 116[a]

Height (m)	Wind Speed (m/s)	Wind Direction (degree)	Temperature (°C)	Pressure (mb)
0.0	2.6	340.0	5.8	999.0
106.0	4.9	357.0	4.0	986.0
214.0	7.2	14.1	2.5	973.0
323.0	7.4	17.4	1.5	960.0
433.0	7.3	13.3	0.6	947.0
543.0	8.2	19.0	−0.3	934.0
673.0	8.8	22.5	−1.3	919.0
795.0	9.6	30.4	−2.2	905.0
929.0	10.3	39.3	1.2	890.0
1048.0	11.0	44.7	5.2	877.0

a. Standard deviation of the surface wind angle – 4.0°; surface air density – 1251.30 gm/m^3.

Table 18. GMD Sounding for Static Test Firing No. 17, February 22, 1975, 1528 CST, MSFC Test Facility 116[a]

Height (m)	Wind Speed (m/s)	Wind Direction (degree)	Temperature (°C)	Pressure (mb)
0.0	7.2	130.0	13.8	993.8
151.0	10.0	134.4	11.7	976.0
298.0	12.9	138.8	10.2	959.0
447.0	18.1	154.0	9.9	942.0
590.0	20.8	169.3	11.4	926.0
700.0	23.1	178.9	14.1	914.0
831.0	26.3	184.8	14.7	900.0
973.0	25.9	191.1	13.7	885.0
1097.0	25.5	195.9	12.3	872.0

a. Standard deviation of the surface wind angle – 4.0°; surface air density – 1210.02 gm/m^3.

Table 19. GMD Sounding for Static Test Firing No. 18, March 25, 1975, 1700 CST, MSFC Test Facility 116[a]

Height (m)	Wind Speed (m/s)	Wind Direction (degree)	Temperature (°C)	Pressure (mb)
0.0	6.7	300.0	12.9	998.0
177.0	7.5	302.7	11.6	977.0
350.0	8.8	305.5	9.7	957.0
524.0	9.4	298.3	7.9	937.0
702.0	10.2	294.1	5.9	917.0
882.0	11.7	286.6	3.8	897.0
1037.0	13.6	283.7	2.0	880 0

a. Standard deviation of the surface wind angle – 4.0°; surface air density – 1215.8 gm/m^3.

Table 20. Titan T-0 Sounding, August 20, 1975, 1722 EDT (2122Z)[a]

Height (m)	Wind Speed (m/s)	Wind Direction (degree)	Temperature (°C)	Pressure (mb)
5.0	3.0	110.0	28.7	1018.3
166.0	4.0	95.0	26.8	1000.0
220.0	4.0	91.0	26.2	994.0
305.0	4.0	89.0	25.5	984.5
610.0	2.0	83.0	24.5	951.1
619.0	2.0	82.0	24.5	950.0
638.0	2.0	82.0	24.5	948.0
814.0	1.0	87.0	21.8	918.5
1078.0	0.1	77.0	20.7	902.0
1090.0	0.1	80.0	20.6	900.0
1219.0	0.1	109.0	20.0	886.9
1524.0	1.0	169.0	17.7	856.1
1583.0	1.0	166.0	17.4	850.0
1829.0	1.0	162.0	16.8	826.1
1987.0	3.0	167.0	15.4	811.0
2100.0	4.0	170.0	15.5	800.0
2134.0	4.0	170.0	15.6	797.1
2211.0	5.0	171.0	15.6	790.0
2438.0	4.0	159.0	11.7	769.0

a. Surface air density – 1162.670 g/m^3; height of surface mixing layer 1090 m.

CHAPTER V

NASA/MSFC MULTILAYER DIFFUSION MODELS PROGRAM

The NASA/MSFC Multilayer Diffusion Models Program is designed to calculate the following quantities downwind from normal and abnormal launches of rocket vehicles:

a. Concentration and dosage patterns

b Time interval (minutes) – concentration

c. Average cloud concentration

d. Time of cloud passage

e. Ground-level deposition patterns due to gravitational settling or precipitation scavenging.

Programs options include the calculation of concentration, dosage, and time-mean concentration patterns with partial reflection of material at the surface, with time-dependent exponential decay, and/or with depletion due to precipitation scavenging. Also, the program is capable of calculating ground-level deposition due to gravitational settling with partial reflection at the surface. Provision is also made (in Model 4) to account for changes in meteorological structure along the cloud trajectory. Model 4 also may be used to determine concentration and dosage fields in the surface mixing layer downwind from a source in which the source strength varies with height in the layer [5].

Program output options include:

a. Printing of all data inputs

b. Printing of the results of all model calculations

c. Plotting of maximum centerline concentration, dosage, time-mean concentration, and deposition versus distance along the cloud trajectory

d. Plotting of concentration, dosage, time-mean concentration, and deposition isopleths.

A simplified block diagram illustrating major features of the program is shown in Figure 3.

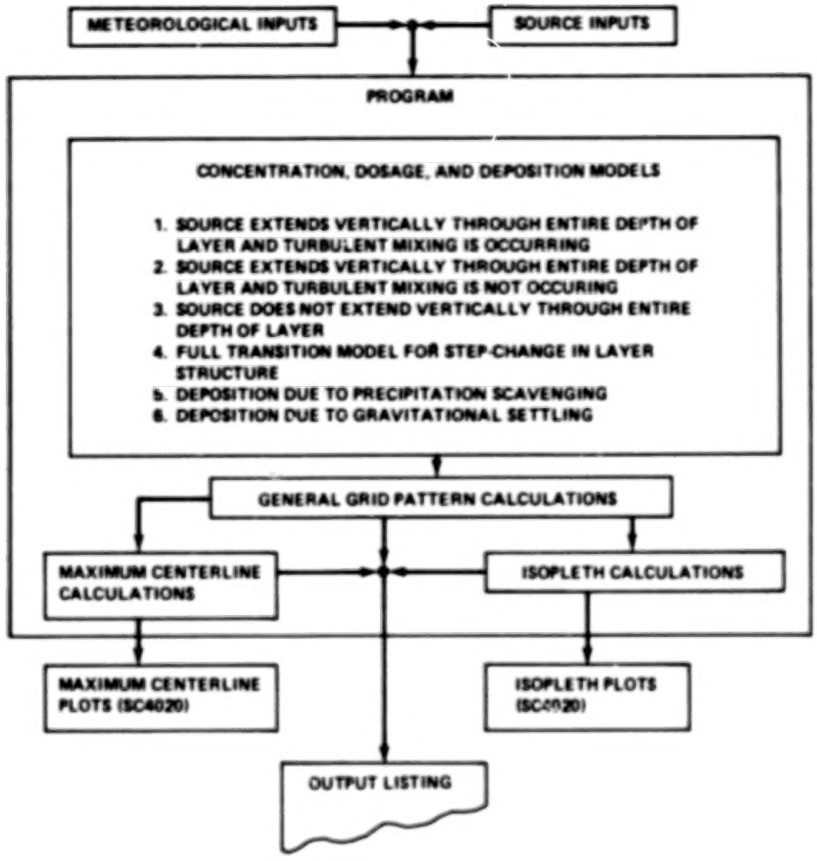

Figure 3. Simplified block diagram of the computer program for the NASA/MSFC Multilayer Diffusion Models.

With the increasing knowledge of the environmental impact of air pollution, special attention is now being placed on the emission into the atmosphere of aerospace vehicle exhaust effluents and by-products. Limited concern was placed on this problem in the past, especially because vehicles using solid rocket motors were small in size and few were tested and launched. National, state, and local air pollution laws are also becoming more stringent to prevent environmental damage which places additional restrictions on any organization or private citizen in regard to pollution of many types.

To determine the ground level concentrations, the procedure is to apply the proper atmospheric diffusion models to calculate downwind concentrations and dosages from various engine and SRB exhaust by-products. A major effort is being made to gather detailed data on the chemical reactions that take place between the exhaust effluents and the atmosphere. While little is currently known about this problem, research is underway throughout the aerospace research community to determine initial and long term source characteristics.

This chapter includes statements on the basic diffusion estimation formulas. This is a summary of the salient facets of the effluent material transport problem which is found in referenced literature. Other than normal exhaust releases and abnormal releases, brief statements will follow on leaks and inadvertent spills. Cloud rise formulas for use in source identification are included and meteorological inputs are covered.

A. Definitions

Concentration is the mass of a pollutant per unit volume at a point in space and is referenced to the ambient atmosphere (units: parts per million, milligrams per cubic meter, etc.).

Dosage is the time-integrated concentration at a point in space and has the units of concentration multiplied by the unit of time.

The generalized concentration and dosage models describe the behavior of the cloud of toxic material after the cloud establishes equilibrium in the mixing layer. This equilibrium point is known as the cloud source and serves as the origin for the Cartesian coordinate system such that the x-axis is in the mean azimuth wind direction, y is the crosswind or lateral direction, and z is the vertical height above the ground. (The location of the source cloud is addressed later.) It is also assumed that this is an expanding volumetric cloud about a moving reference point in a homogeneous fluid. For diagnostic and interpretation flexibility, these models are formatted in a modular form [5,6].

The generalized concentration model for a nearly instantaneous source is expressed as the product of seven modular terms:

$$\text{Concentration} = \{\text{Peak Concentration Term}\} \times \{\text{Alongwind Term}\} \times \{\text{Lateral Term}\} \times \{\text{Vertical Term}\} \times \{\text{Depletion Term}\} \times \{\text{Scavenging Term}\} \times \{\text{Surface Absorption Term}\}$$

whereas, the generalized dosage model for a nearly instantaneous source is defined by the product of six modular terms:

Dosage = {Peak Dosage Terms} × {Lateral Term}
× {Vertical Term} × {Depletion Term}
× {Scavenging Term} × {Surface Absorption Term}

Thus, the mathematical description for the concentration and dosage models permitsflexibility in application to various sources and for changing atmospheric parameters while always maintaining a rigorous mass balance.

Two obvious differences exist. First, the peak concentration term refers to the concentration at the point x, y = O, z = H and is defined by the expression

$$\text{Point Peak Concentration} = \frac{Q}{(2\pi)^{3/2}\,\sigma_x\sigma_y\sigma_z} \tag{5.1}$$

where Q is the source strength and σ_i is the standard deviation of the concentration distribution in the ith direction; whereas, the peak dosage term is given by

$$\text{Point Peak Dosage} = \frac{Q}{2\pi\bar{u}\sigma_y\sigma_z} \tag{5.2}$$

where $\bar{u}$ is the mean wind speed. The second difference between these models is that the concentration contains a modular alongwind term to account for downstream temporal effects not considered in the dosage model. The alongwind term affords an exponential decay in concentration as a function of cloud transit time, concentration distribution, and the mean wind speed.

The lateral term, common to both models, is another exponential decay term and is a function of the Gaussian spreading rate and the distance laterally from the mean wind azimuth. The vertical term, again common to both models, is a rather complex decay function since it contains a multiple reflection term for the point source which stops the vertical cloud development at the top of mixing layer and eventually changes the form of the vertical concentration distribution from Gaussian to rectangular. The last remaining three terms represent the options. The deposition term accounts for gravitational settling. The scavenging term accounts for precipitation of effluents by rain falling

through the exhaust cloud. The surface absorbtion term accounts for the fraction of material absorbed at a surface.

The ground cloud is formed during the first several minutes and contains all of the exhaust by-products formed by the rocket engines from the time of engine ignition until the vehicle passes through the stabilization height, "height of maximum buoyancy rise of the hot exhaust products," of the ground cloud. If the stabilization height is such that some of the ground cloud is contained in a thermally stable layer, only a fraction of the total amount of exhaust products in the ground cloud is available for mixing to the ground surfaces.

The exhaust trail plume is the plume of stabilized exhaust products formed by rocket engine emissions occurring above the stabilization height of the ground cloud.

B. Description of Models

The normal launch environment will usually involve an atmospheric structure comprised of several horizontal meteorological layers with distinctive wind velocity, temperature, and humidity regimes between the surface and 5 km altitude. Large horizontal spatial variation in these meteorological parameters may also occur in the surface layer as a consequence of changes in terrain or land-water interfaces, which is accounted for by the absorbtion coefficient. The general diffusion model for concentration [equation (5.1)] and the dosage [equation (5.2)] assumes an expanding volume about a moving point of reference in a homogeneous environment.

To overcome the obvious shortcomings of the general diffusion model but to stay within the accepted bounds of classical fluid mechanics [6], a multiple layer concept is introduced to cope with the vertical and horizontal atmospheric gradients. Here, the general diffusion model is applied to individual horizontal layers in which the meteorological structure is reasonably homogeneous and independent of the neighboring layers. These layers have boundaries which are placed at points of major discontinuities in the vertical profiles of wind velocity, temperature, and humidity. Since the NASA/MSFC Multilayer Diffusion Model [5] is an empirical model and has imposed the general restriction of layer independence (no flux of particles or gases entering or leaving an individual layer), special provision must be made for spatial changes in the horizontal meteorology and for

gravitational settling or precipitation scavenging. In addition, the type of source within a layer must be considered, that is, whether there is a ground cloud source or a plume cloud source.

The NASA/MSFC Multilayer Diffusion Model has six submodels to deal with the stages of the development of the exhaust cloud and the complex potentially varying meteorological conditions. These submodels can be used alone to describe all the environmental layers or in combinations where variations in layer meteorology require different modeling. For the introductory overview, however, these combinations will not be considered. The primary output of all submodels is a mapping of the regimes of the concentration and dosage isopleths.

Model 1 is the basic model for the dispersive description of exhaust material from rocket plume. In this model it is assumed that the source extends vertically through the entire layer with a uniform distribution of the concentration of exhaust material, whereas, the horizontal distribution of the material being dispersed along the layer (x and y directions) has a Gaussian distribution. In addition, it is assumed that there is turbulent mixing.

An analogous model would be the wave generated by dropping a rock in a river, where the wave disperses across the surface of the moving river. The significance of the supposition of turbulent mixing is that this mixing action disperses the effluent material across the layer similar to the way the wave is dispersed across the surface of the water. This model is an effective description of the plume cloud where the action of the vehicle passing through a layer leaves a cylindrical cloud of exhaust effluents.

Model 2 is the same as Model 1 except it is assumed that there is no turbulent mixing. This implies that the exhaust material meanders along the layer without dispersing, very much like a small oil puddle moves on the surface of a river. While Model 2 is not generally used, movies of rocket firings clearly show that under some special meteorological conditions (temperature inversion) this model is required. While the multilayer diffusion model is general in applicability, it is specific in meteorological parameters and launch description.

From the standpoint of environmental impact, the description of the fields of the ground deposition of materials from the ground cloud is of primary significance – this description is afforded by Model 3. Generally, this model is employed in the surface

layer, but can be employed in any layer where the source does not extend through the entire layer. In this model, a Gaussian distribution is assumed along all three axes with turbulent mixing occurring.

Model 3 is similar to Model 1 except that, rather than the plane two-dimensional dispersion of Model 1, there is a three-dimensional dispersion of the exhaust cloud as the cloud is transported downstream. When the cloud reaches the top of the mixing layer, the distribution of material is reflected back into the expanding vertical distribution. Thus, after a certain time period Model 3 is identical with Model 1. A clear understanding can be obtained if the formulation for this model is examined.

The first three models can be summarized as describing initial transport of the effluents after the cloud reaches equilibrium. While the equations given for Model 3 are in the general form for any Kth layer, it should be noted that K = 1 (the surface layer) is used in most applications of this model. If after launch the rocket explodes in a layer, this can be studied with this model by setting K equal to that layer number.

The remaining models are specialized models which afford a second order description of the transport of the vehicle exhaust materials. These three models incorporate considerations for changes in meteorological conditions and particle effects.

Model 4 updates the diffusion model with changes in meteorological conditions and structure which can occur as the toxic cloud propagates downstream. This model assumes that the vertical concentration of material has become uniform throughout each layer when a step-change in the meteorological conditions is introduced. This step-change results in the destruction of the original layer boundaries and the formation of new layer boundaries. The concentration fields which exist at this time are treated as new sources. In those new layers which now comprise more than one old layer, the old concentration is mapped as two independent concentration sources and then superimposed for the resulting concentration and dosage mappings.

Model 5 accounts for precipitation scavenging. An example of where Model 5 must be used is in solid rocket launches during the occurrence of rain, because the HCl will be scavenged by the rain.

Model 6 describes the ground deposition due to gravitational settling of particles of droplets. Wind shears are incorporated in this model to account for the effect of the

settling velocity of the particulate matter. There are two forms for the source in this model, namely:

1. The source that extends vertically through the entire layer with a uniform distribution (this is the same source model as used with Models 1 and 2)

2. A volume source in the Kth layer (this is the same source model as used with Model 3).

Model 6 is very important in the analysis of the settling of Al_2O_3 particles released in solid rocket firings.

In summary, the Multilayer Diffusion Model is composed of six submodels. Models 1 and 3 are designed to distinguish between the two sources of toxic cloud formation – the ground cloud during the initial launch phase (Model 3) and the plume cloud after the initial launch phase (Model 1). Model 2 was injected to account for a lack of turbulent mixing which can occur in the upper atmosphere. Model 4 is employed when a change in meteorological condition occurs during the downstream transport of the cloud. In the event of rain, the precipitation scavenging, both of gases and particles, can be accounted for in Model 5. The fallout of particulate matter on the ground is the domain of Model 6. These six submodels form the basic algorithms which are available to treat the diffusion problem. To model a specific launch of a vehicle, it is necessary to blend these algorithms together and adjust the model parameters to the specific meteorological conditions of the launch, to the specific terrain (use of absorbtion coefficient) around the launch site, and to the specific vehicle being launched; this is the degree of complexity in the diffusion model.

C. Cloud Rise Calculations

The burning of rocket engines during normal launches results in the formation of a cloud of hot exhaust products which subsequently rises and entrains ambient air until an equilibrium with ambient conditions is achieved. Experience in predicting the buoyant rise [7] from normal launches of solid-fueled vehicles indicates the rise is best predicted using a cloud rise model for instantaneous sources. For solid-fueled vehicles, residence times near the pad are relatively short.

Each of the models for cloud height is subdivided into two categories to account for the atmospheric temperature lapse rate. The model assumes that the atmosphere is

either quasi-adiabatic or stable. Here the quasi-adiabatic is where the adiabatic atmosphere is the limit, which means that the potential temperature difference ($\Delta\theta$) is zero or less, where the potential temperature difference is given by

$$\Delta\theta = \theta_{\text{max cloud height}} - \theta_{\text{surface}} \quad . \tag{5.3}$$

If this potential temperature difference is positive, then the atmosphere is stable. Since in most cases of interest there will be an inversion layer present, the stable cloud rise formula is the normally utilized relation [8].

The maximum rise z_{ml} for an instantaneous source is given by the expression in a stable atmosphere as

$$z_{ml} = \left[\frac{8F_l}{\gamma_l^3 S} + \left(\frac{r_R}{\gamma_l}\right)^4\right]^{1/4} - \frac{r_R}{\gamma_l} \tag{5.4}$$

whereas the maximum cloud rise z_{ml} downwind from an instantaneous source in a quasi-adiabatic atmosphere is given by

$$z_{ml} = \left[\frac{2F_l t_{sl}^2}{\gamma_l^3} + \left(\frac{r_R}{\gamma_l}\right)^4\right]^{1/4} - \frac{r_R}{\gamma_l} \quad . \tag{5.5}$$

In deriving equation (5.4), it is assumed that the initial upward momentum imparted to the exhaust gases by reflection from the ground surface and launch pad hardware is insignificant in comparison with the effect of thermal buoyancy. Based on limited experience in predicting cloud rise from launches at Vandenberg Air Force Base, California, this assumption appears to be justified. The time required for the cloud to reach the stabilization height is given by the expression

$$t_H = \frac{\pi}{S^{1/2}} \quad . \tag{5.6}$$

In calculating z_{ml} from equations (5.4) and (5.5), the instantaneous heat released Q_l is obtained from the relationship

$$Q_l = Q_F t_R \{z_{ml}\} \quad . \tag{5.7}$$

Inspection of the previously given equations reveals an interdependence between the calculated maximum cloud rise z_{mI}, the height over which the potential temperature gradient $\partial\Phi/\partial z$ is measured, and the value of $t_R\{z_{mI}\}$ used in obtaining Q_I. Thus, the final value of maximum cloud rise must be found through iteration of either equation (5.4) or (5.5). The height over which $\partial\Phi/\partial z$ is measured and the time $t_R\{z_m\}$ are thus made consistent with the value of z_{mI} calculated from the model.

D. Cloud Dimensions and Vertical Distribution of Exhaust Products

Source inputs required for the diffusion model calculations include the stabilization height of the exhaust cloud and cloud dimensions, as well as the vertical distribution of exhaust products in the stabilized cloud. The calculation of the stabilization height z_m was described on page 29. The calculation of the dimensions of the stabilized cloud and the vertical distribution of exhaust products is described in the following paragraphs.

The general formula used to calculate the radius of the stabilized cloud at height z is given by the expression

$$r\{z\} = \begin{cases} \gamma z & ; z \leq z_m \\ \gamma(2z_m - z) \geq 200 \text{ m}; & z \geq z_m \end{cases} \qquad (5.8)$$

where

$$\gamma = (\gamma_I) = 0.64 \quad .$$

Note that for $z > z_m$, the minimum radius of the stabilized cloud is set equal to 200 m.

The cloud is assumed to be symmetrical about a vertical axis through the cloud centroid. The alongwind and crosswind source dimensions of the cloud in each of the layers are calculated under the following assumptions:

1. The distribution of exhaust products within the cloud is Gaussian in the horizontal plane.

2. The concentration of exhaust products at a lateral distance of one radius from the cloud vertical axis is 10 percent of the concentration at the cloud axis.

The entrainment coefficient is defined to be the ratio of cloud radius to the cloud centroid height. This empirical coefficient is very difficult to evaluate because of the complex cloud geometry and because it varies so much with height. Current entrainment coefficients ($\gamma = 0.64$) were obtained from cloud photographs [8,9].

The alongwind and crosswind source dimensions required for input to the NASA/ MSFC Multilayer Diffusion Models are defined for each layer by

$$\sigma_{xo}\{K\} = \sigma_{yo}\{K\} = \begin{cases} \gamma z'/2.15 & ; z \leqslant z_m \\ \gamma(2z_m - z')/2.15 \geqslant 93 \text{ m}; & z \geqslant z_m \end{cases} \tag{5.9}$$

where

z' = midpoint of the Kth layer

$= (z_{BK} + z_{TK})/2$.

The quantities z_{TK} and z_{BK} are, respectively, the height of the top and base of the Kth layer.

The corresponding vertical source dimension for each layer was calculated from the expression

$$\sigma_{zo}\{K\} = (z_{TK} - z_{BK})/\sqrt{12} \tag{5.10}$$

Equation (5.10) applies to a rectangular material distribution which has been assumed to apply along the vertical in the Kth layer.

E. Calculation of the Vertical Source Strength Distribution

The fraction of material by weight in each of the K layers $F\{K\}$ for the launches was calculated from the expression

$$F\{K\} = \begin{cases} QP\{z_{TK}\} & ; K = 1 \\ Q(P\{z_{TK}\} - P\{z_{BK}\}); & K > 1 \end{cases} \tag{5.11}$$

$P\{z_{BK}\}$ is the integral of the Gaussian probability function between minus infinity and the base of the Kth layer z_{BK}, and is equal to $P\{z_{BK} - z_{ml}/\sigma\}$. Sigma ($\sigma$) is equal to $\gamma\{z = z_{ml}\}/2.15$.

The NASA/MSFC Multilayer Diffusion Models described here require that source strength in each of the K layers be specified per unit height. Since the desired concentration units for HCl and CO are parts per million, the complete expression for the source strength model input for the Kth layer is

$$Q_K = \left(\frac{F\{K\}}{(z_{TK} - z_{BK})}\right)\left(\frac{10^3\ mg}{g}\right)\left(\frac{22.4}{m}\right)\left(\frac{1013.2}{P}\right)\left(\frac{T(z_R)}{273.16}\right) \qquad (5.12)$$

For Al_2O_3, the desired concentration units are milligrams per cubic meter and the complete expression for source strength in the Kth layer is

$$Q_K = \frac{F\{K\}}{(z_{TK} - z_{BK})}\left(\frac{10^3\ mg}{g}\right) \quad . \qquad (5.13)$$

Equations (5.11) and (5.12) were used to obtain the model input values of Q_K for the various static test results.

F. Composition of Rocket Exhaust Effluents

The composition of the rocket exhaust effluents varies between vehicles in accord with vehicle sizes and motor types. The two major rocket classes are the ones that use liquid and solid rocket propellants.

When calculating downwind concentrations from fractional weights of materials in the exhaust, definite uncertainties evolve. The actual amounts of elements or compounds available after the exhaust material combines with the ambient atmosphere is difficult to obtain. Factors that may cause the fractional amounts of effluents to change in the ground cloud are: (1) the exhaust flame evaporates thousands of gallons of deluge water within the flame trench and other water being sprayed on the launcher towers, (2) significant amounts of materials are ablated such as concrete, steel, and paint, and (3) other matter such as dust, ocean salt, grease, etc., are vaporized and are contained within the ground cloud. Subsequently, a great deal of research must be accomplished before accurate source inventory data can be made available. This is especially needed for exhaust ground cloud chemistry as such clouds will be composed of both solid and liquid exhaust

by-products. Exhaust chemistry, especially after reaction with the air and extraneous material, is essential for identifying initial ground cloud source composition to make atmospheric diffusion computations.

G. Meteorological Inputs

Reliable atmospheric, thermodynamic, and kinematic profiles are required to compute diffusion estimates. Consideration must be given to such factors as: (1) local climatology, (2) large scale atmospheric conditions,(3) local atmospheric conditions, (4) topographical features, (5) land-water interfaces, and (6) exhaust source chemistry which may form new compounds with the ambient air, etc. One of the most important factors is having a sound definition of the Earth's planetary boundary layer phenomena. This is the main atmospheric layer of concern when determining downwind dispersion of exhaust effluents.

The meteorological inputs for diffusion modeling are as follows: (1) wind direction, (2) wind speed, (3) standard deviations of vertical and horizontal wind, (4) humidity, (5) atmospheric pressure, (6) temperature profile data, (7) height of stable layers, and (8) air density [10,11]. Precipitation, cloud heights and types, pressure gradient conditions, and other features of the synoptic state must also be considered. The height of the stable layer is needed because it dictates the height the hot buoyant exhaust clouds will stabilize, especially when dealing with the larger vehicle exhausts.

CHAPTER VI

EVALUATION OF ELECTRETS

To evaluate the electrets, the total chlorine counts obtained from the SEM from the surface of the electret after exposure to pollution is a measure of the quantity of material collected. The counts were converted to ppm and compared with HCl measuring equipment and computed values from the NASA/MSFC Multilayer Diffusion Model.

A total of 18 static test firings were conducted at MSFC Atmospheric Test Facility 116. For each of the test firings, meteorological data were obtained (Tables 2 through 19, pages 12 through 21) and the NASA/MSFC Multilayer Diffusion Model was used to predict the downwind concentration of HCl. A test matrix for the static tests is presented in Table 21. The coulometer, millipore filter, and bubblers used in these tests were supplied and operated by personnel from Arnold Engineering Development Center, Tullahoma, Tennessee. The calibration of the electrets was made from Test 18 when all the instrumentation appeared to assess the ground cloud for an exposure time of 10 s. Photographic data and personal observation indicated that the ground cloud passed uniformly over the instruments during this interval. Hence, the calibration of the electrets was made from this test and is used in reporting the comparison of the electrets with the diffusion model and various HCl measuring devices.

An evaluation of the electrets was done during the chamber tests at Arnold Engineering Development Center to verify the previously mentioned results. The electrets compared with the millipore filter.

During the Viking I launch to Mars from KSC on August 20, 1975, an array of electrets was placed alongside standard HCl instrumentation, bubblers, and coulometers, 0.25 km from the launch pad. During this initial flight, all power was turned off from T minus ten to T plus ten minutes at the launch complex. No direct comparison could be made with the HCl measuring equipment, but comparisons were made with the computed NASA/MSFC Multilayer Diffusion Model. These comparisons were made at various distances from the launch pad, 0.25 to 2.59 km on land and 6.80 km on the ocean.

Table 21. Test Matrix of MSFC Static Tests

Test No.	Date	Time (CST)	Place	Configuration	Measuring Devices					NASA/ MSFC Diffusion Model	Radiosonde
					Electrets	Bubbler	Geomet	Coulometer	Millipore Filter		
1	August 16, 1974	1442	MSFC	Solid Motor		X			X	X	X
2	August 30, 1974	1302	MSFC	Solid Motor						X	X
3	November 19, 1974	2131	MSFC	Solid and LOX Engines	X					X	X
4	November 22, 1974	1830	MSFC	Solid and LOX Engines	X	X			X	X	X
5	December 22, 1974	1340	MSFC	Solid and LOX Engines	X					X	X
6	January 7, 1975	1759	MSFC	Solid and LOX Engines						X	X
7	January 9, 1975	1758	MSFC	Solid and LOX Engines		X			X	X	X
8	January 11, 1975	1435	MSFC	Solid and LOX Engines						X	X
9	January 15, 1975	1550	MSFC	Solid and LOX Engines						X	X
10	January 16, 1975	1640	MSFC	Solid and LOX Engines		X			X	X	X
11	January 18, 1975	1450	MSFC	Solid and LOX Engines						X	X
12	January 21, 1975	1145	MSFC	Solid and LOX Engines						X	X
13	January 23, 1975	1958	MSFC	Solid and LOX Engines	X					X	X
14	January 27, 1975	1822	MSFC	Solid and LOX Engines						X	X
15	February 8, 1975	1254	MSFC	Solid and LOX Engines		X	X	X	X	X	X
16	February 12, 1975	1700	MSFC	Solid and LOX Engines						X	X
17	February 22, 1975	1528	MSFC	Solid and LOX Engines						X	X
18	March 25, 1975	1700	MSFC	Solid and LOX Engines	X	X	X	X	X	X	X

A. Static Test Firings

A summary of the data obtained from 18 static tests is presented in this chapter. From the computed NASA/MSFC Multilayer Diffusion Model, two figures are shown. The first figure is the computed HCl isopleths versus the crosswind and downwind distance. The second figure is the computed HCl maximum centerline concentration versus downwind distance. Figure 4 is the HCl isopleths versus the crosswind and downwind distance for Static Test No. 1.

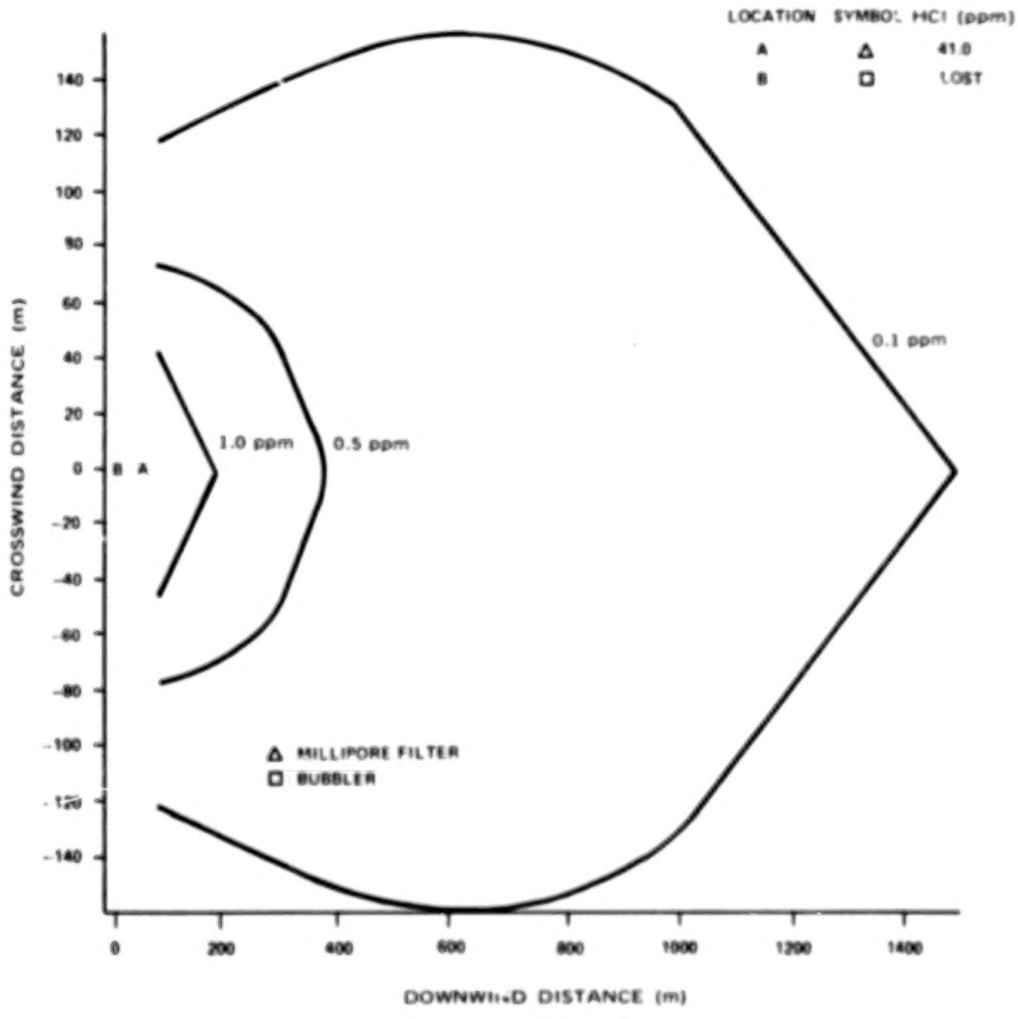

Figure 4. Comparison of HCl concentration isopleths computed by NASA/MSFC Multilayer Model with measured values: Test No. 1 using Model 4 (height 2.0 m, azimuth bearing 43.0°).

The MSFC Test Facility 116 is shown in Figure 5. The Tomahawk missile is situated in the test stand ready for Static Test No. 1. Figure 6 illustrates a closeup of the rocket exhaust effluents being fired by the Tomahawk missile during Static Test No. 1.

Static Test No. 1

This was the first 6.4 percent SSV static test at MSFC Test Facility 116. The bubblers which were positioned in the superstructure were swept away by the force of the exhaust. The millipore filter which was 75 m from the flame trench measured a dosage of 410 ppm-s. The cloud passed by this detector in approximately 10 s, giving a concentration of 41.0 ppm [4]. Subsequent tests indicated there is a dramatic drop in concentration at the ground level when the cloud rises and becomes airborne. Photographs indicated the ground cloud was airborne before 100 m. At 100 m downwind distance, the MSFC Multilayer Diffusion Model indicated 1.2 ppm. Figure 7 shows the maximum HCl centerline concentration versus downwind distance. The photo sequence for the static test is shown in Figure 8. The movie sequence was taken with a 35 mm Automax camera with a focal length of 50 mm and a frame speed of 2/s from the Saturn Static Test Stand (Building 4670), approximately 1400 m due west from Test Stand 116. At 80 and 90 s, the dark cloud area was due to a grass fire.

Static Test No. 2

The exhaust cloud from Static Test No. 2 was photographed for eight minutes after cloud stabilization, illustrating its travel downwind.

The photosequence is shown in Figure 9 taken from the Saturn Static Test Stand. Figures 10 and 11 illustrate the HCl isopleths and HCl centerline downwind concentration, respectively.

Static Test No. 3

The electrets were experimentally used for the first time in Test 3. From the experience gained from the two previous tests, it was determined that to obtain measurement it was necessary to get close and in line with the flame trench, which directs the exhaust away from the pad but not close enough to lose the electrets from the force of the rocket exhaust. The electret was placed 75 m in line with the flame trench. Also, during the previous tests it was observed from the block house (Building 4596) that the

Figure 5. MSFC Test Facility 116 (6.4 percent scaled model of Space Shuttle).

Figure 6. Tomahawk missile being test fired at MSFC Test Facility 116.

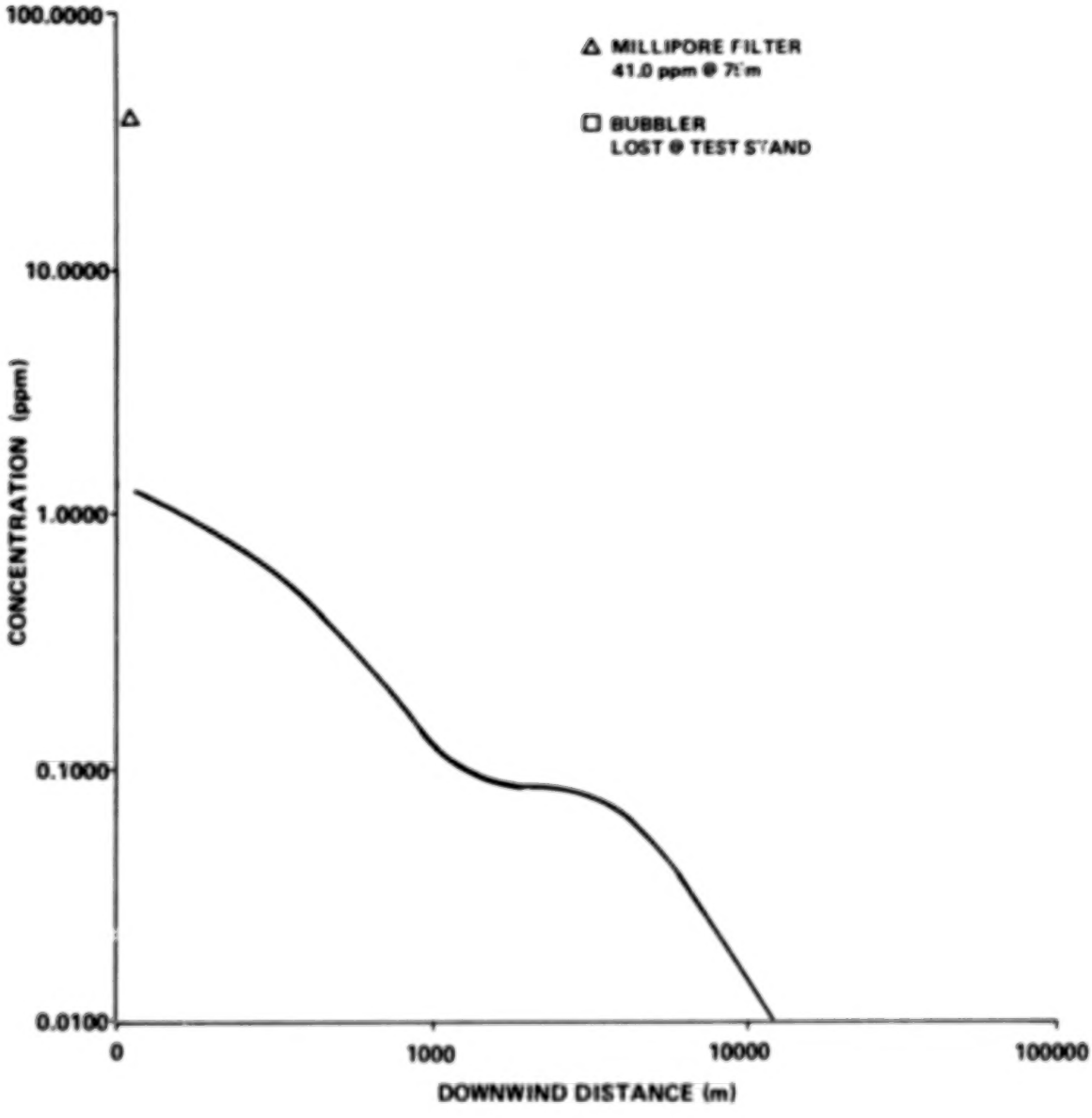

Figure 7. Computed maximum centerline HCl concentrations and measured values: Static Test No. 1 (height 2.0 m, azimuth bearing 43.0°).

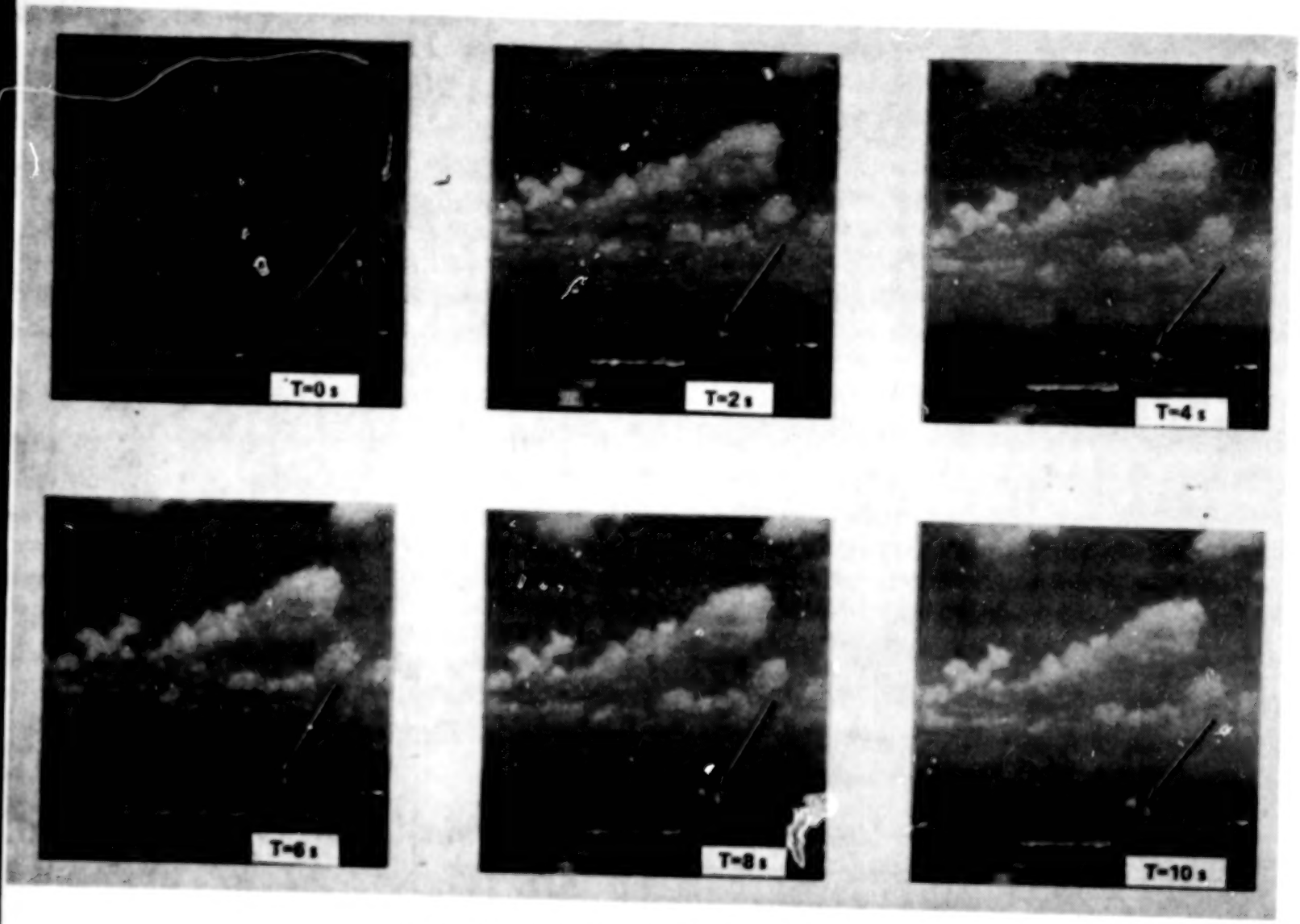

Figure 8. Photo sequence for MSFC Test No. 1.

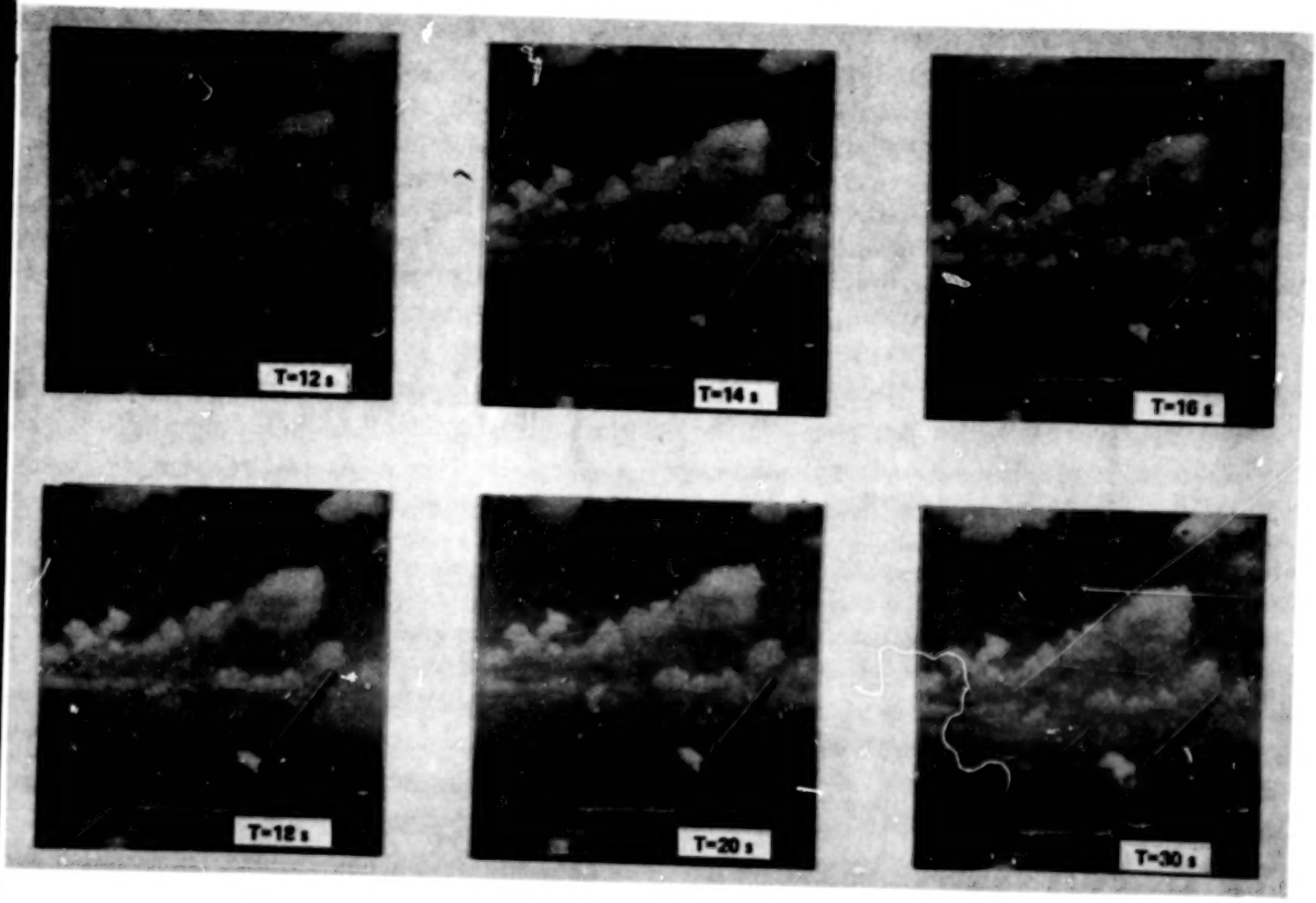

Figure 8. (Continued).

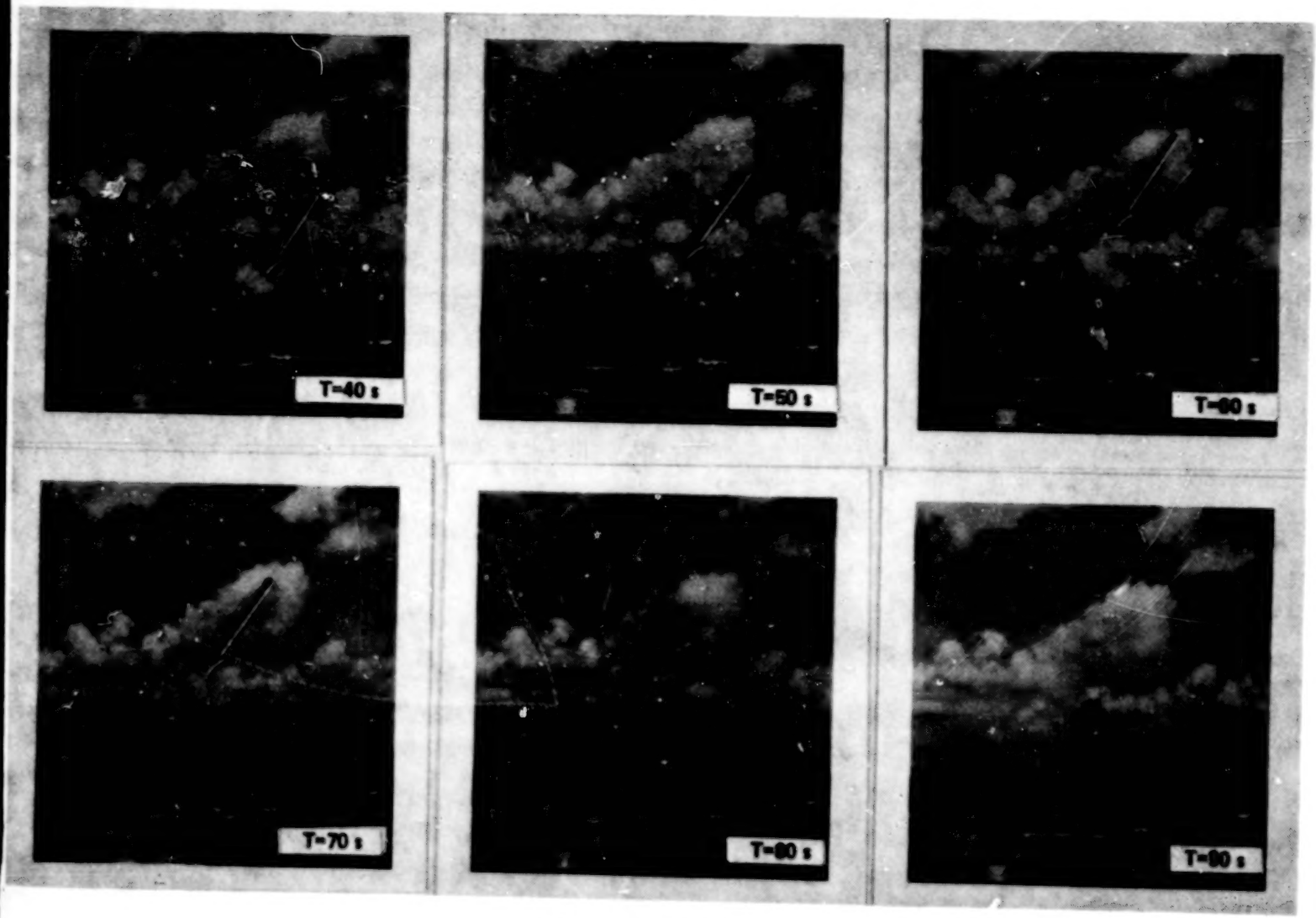

Figure 8. (Continued).

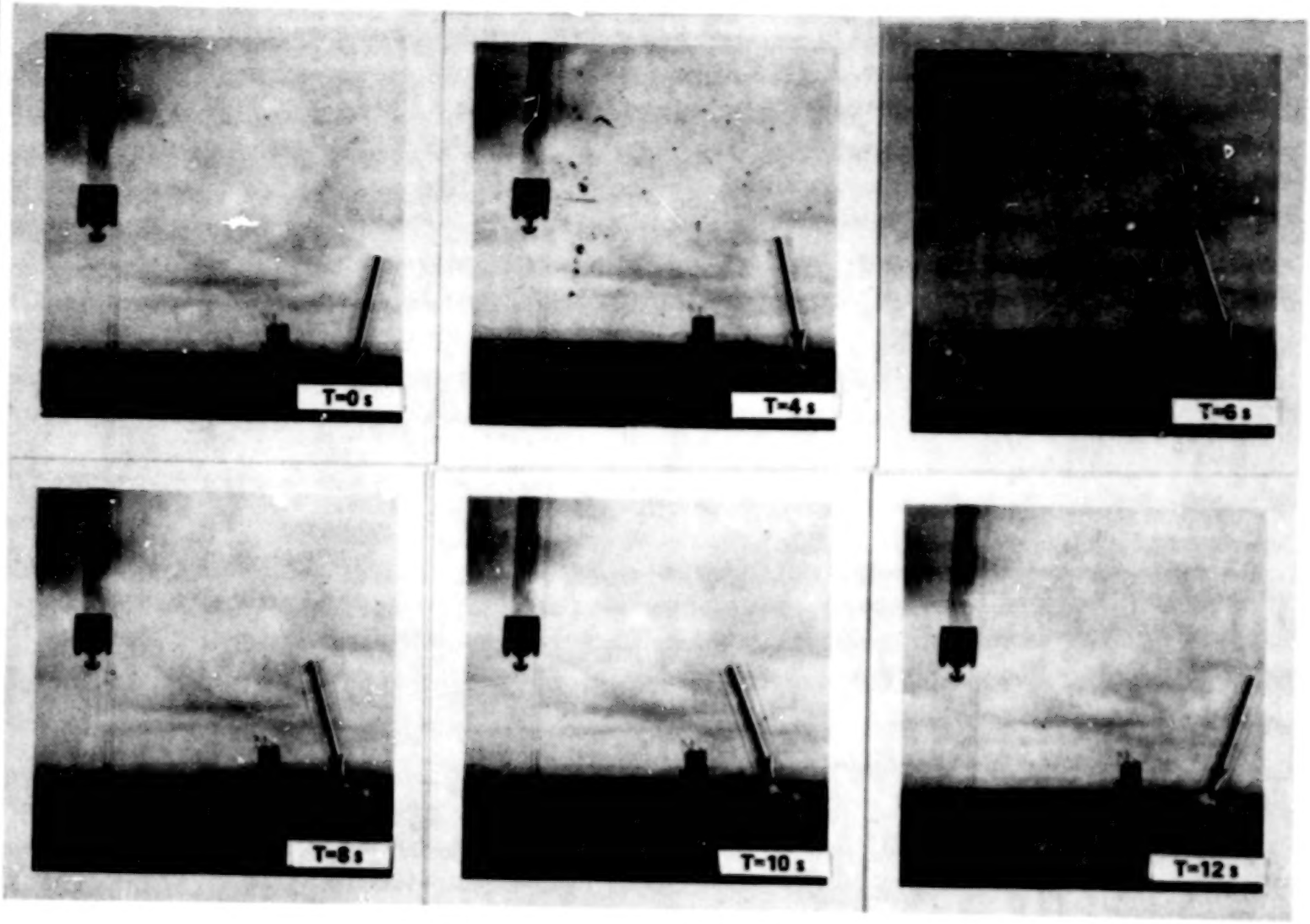

Figure 9. Photo sequence for MSFC Test No. 2.

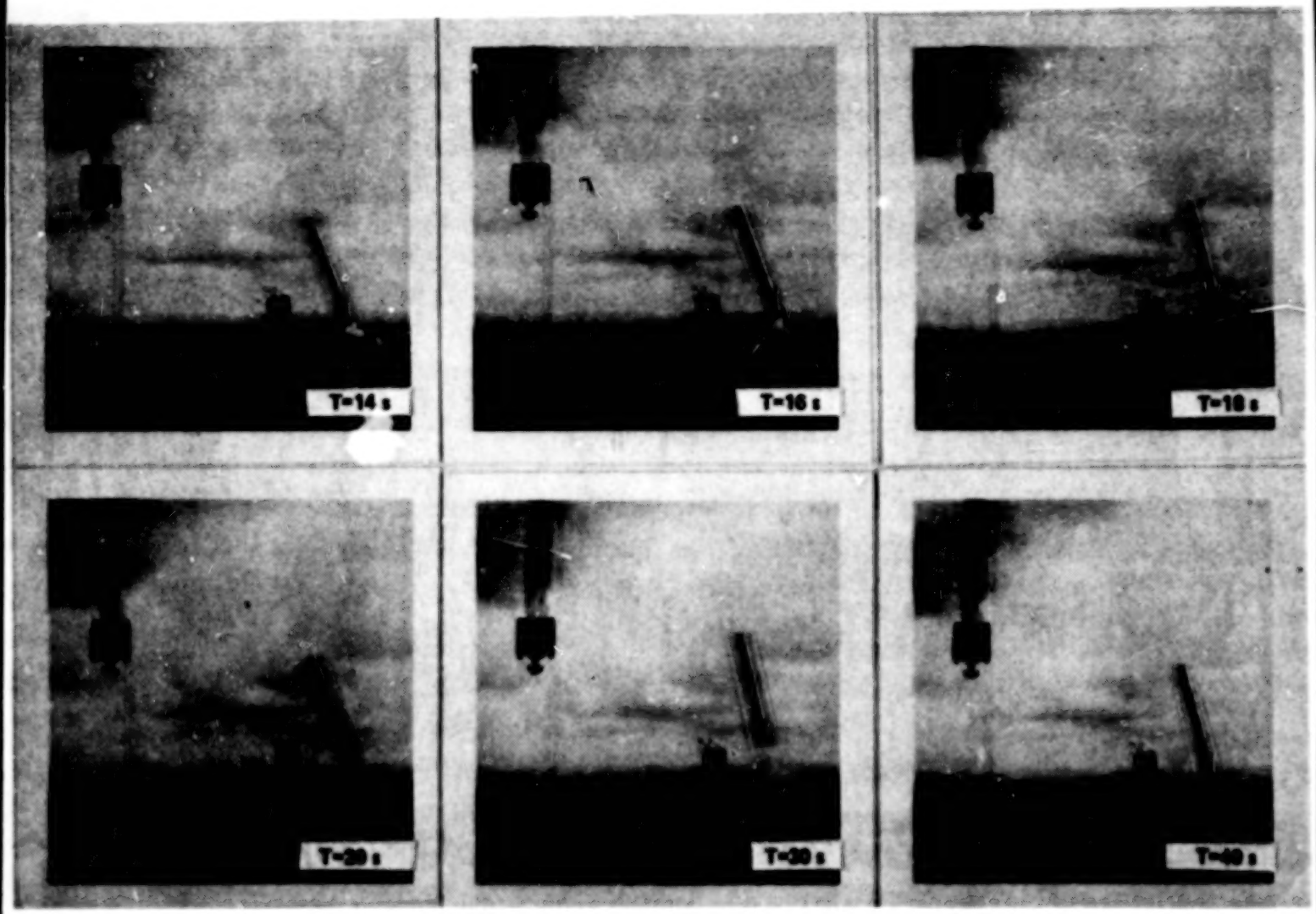

Figure 9. (Continued).

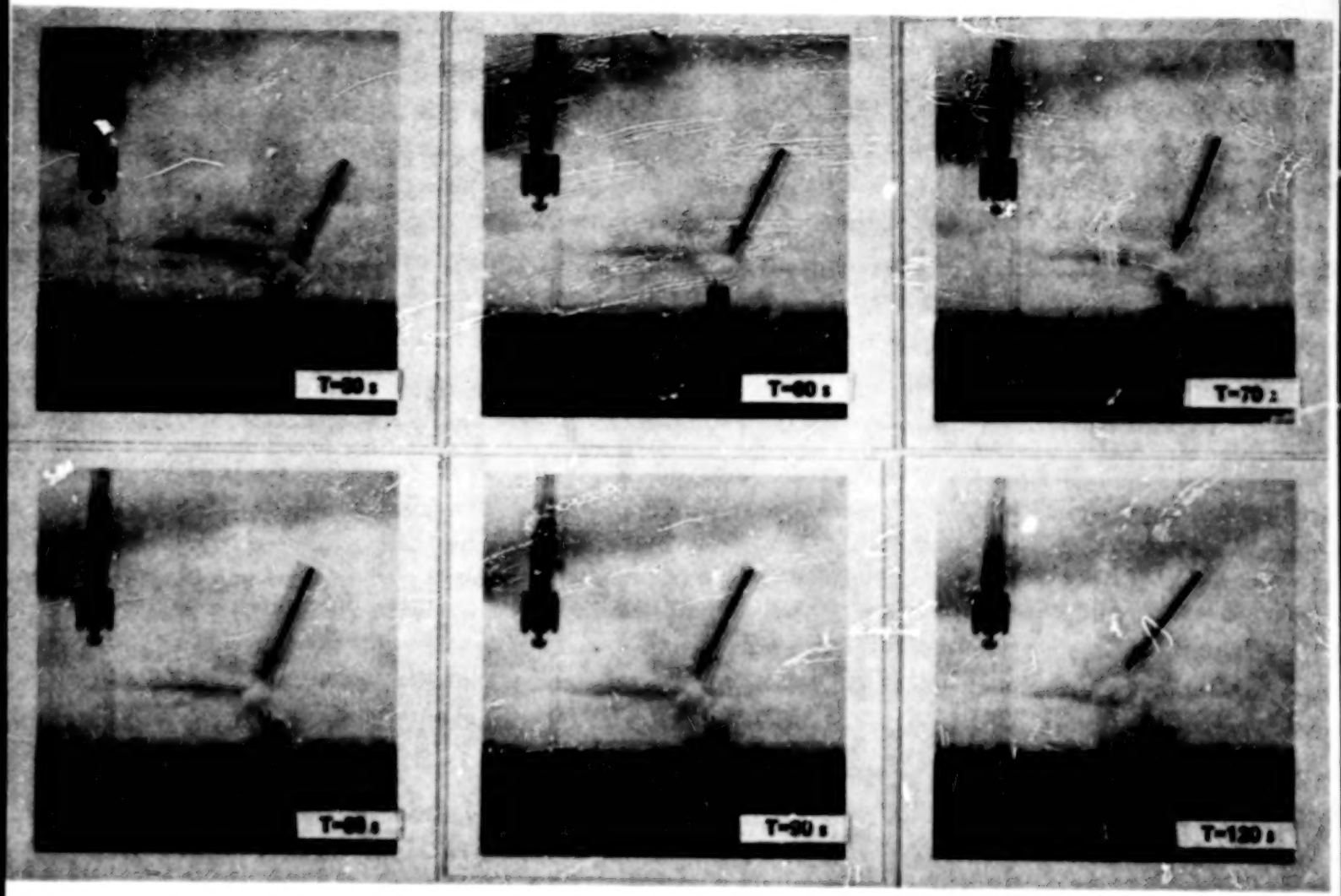

Figure 9. (Continued).

Figure 9. (Continued).

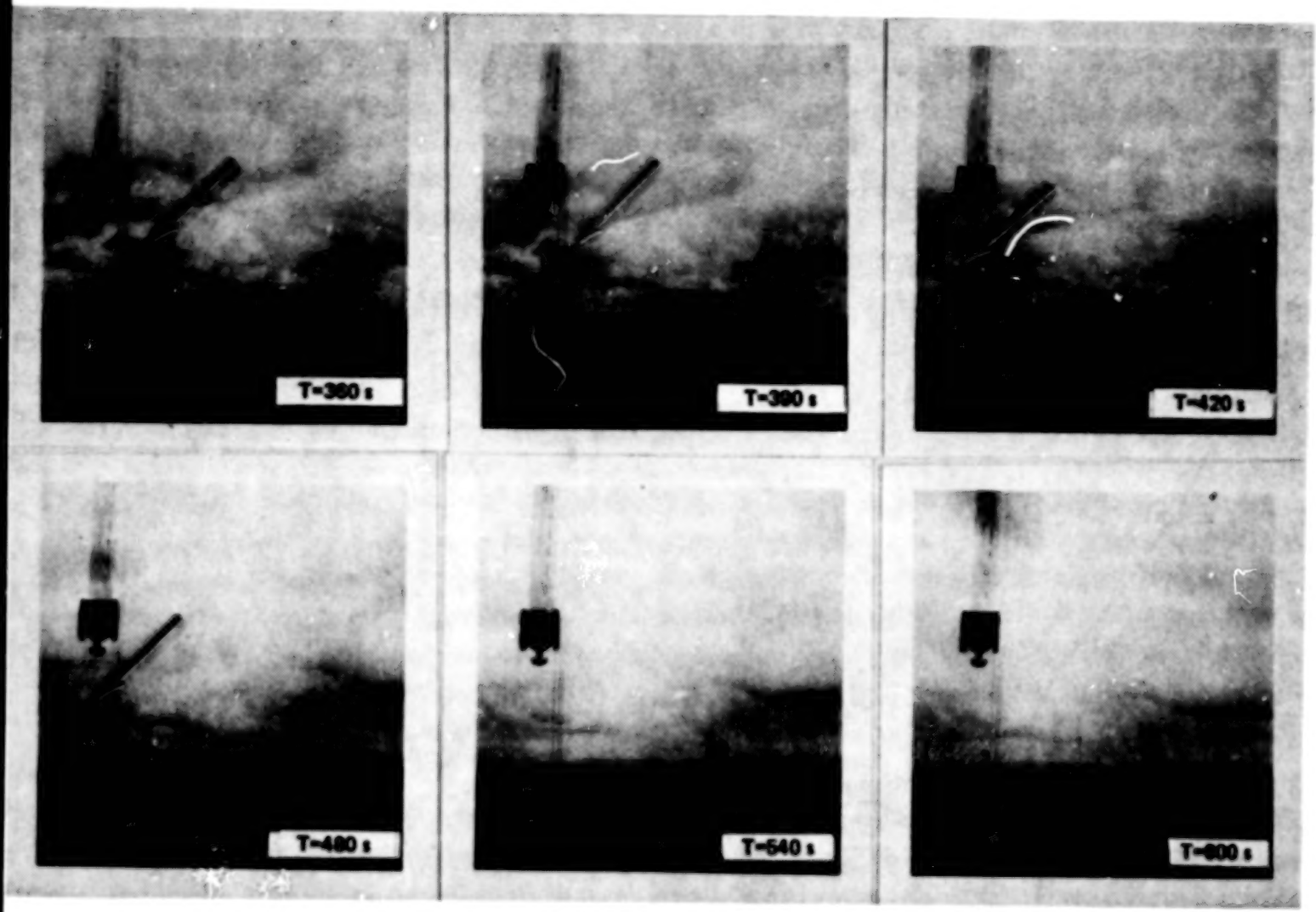

Figure 9. (Continued).

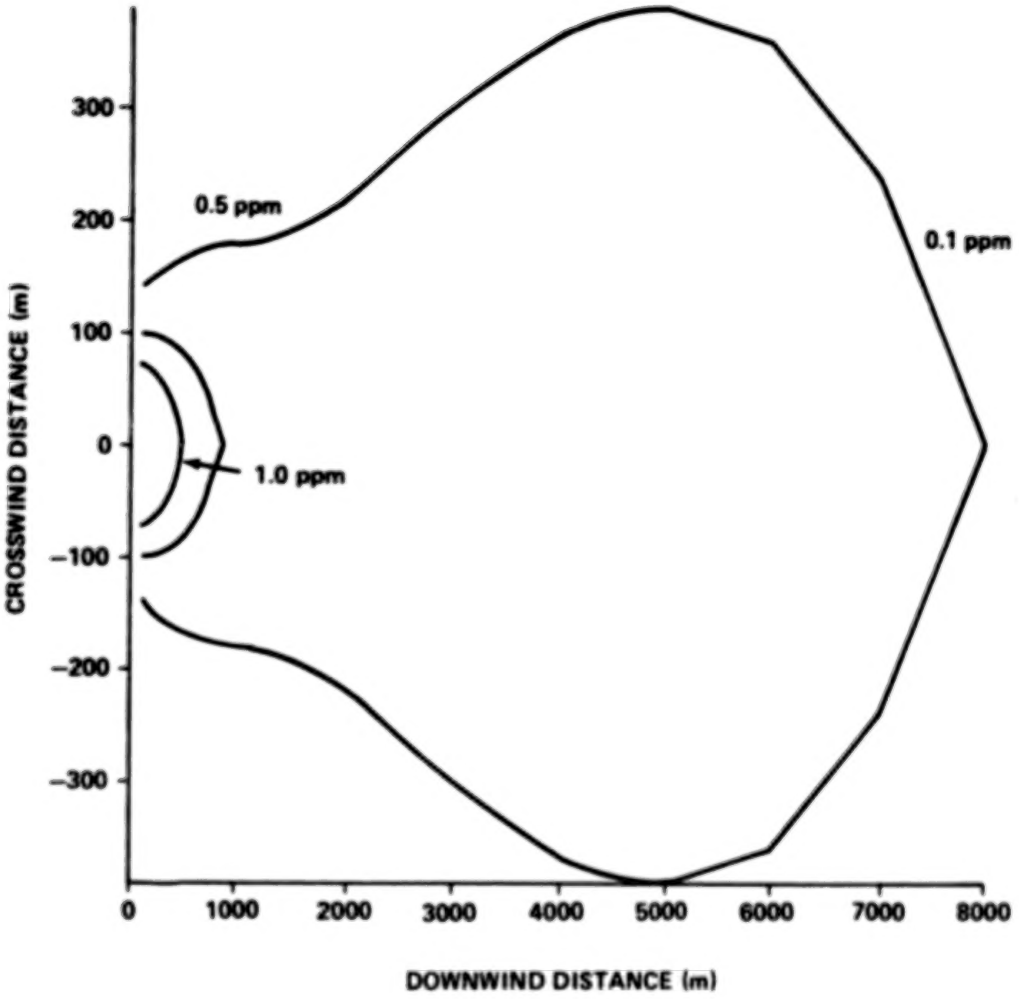

Figure 10. Computed HCl concentration isopleths from NASA/MSFC Multilayer Diffusion Model: Static Test No. 2 using Model 4 (height 2.0 m, azimuth bearing 64.2°).

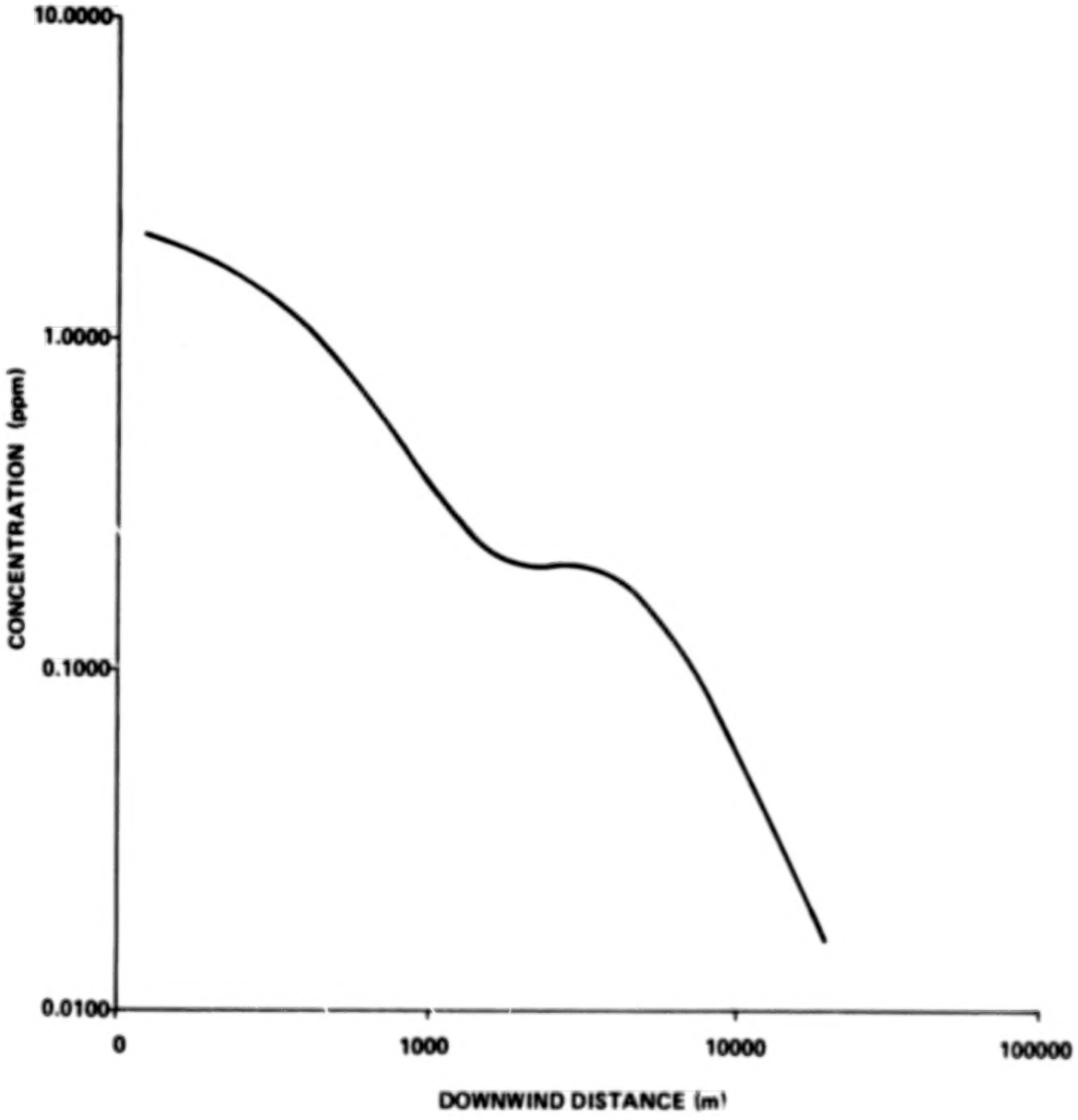

Figure 11. Computed maximum centerline HCl concentration from Model 4 for Static Test No. 2 (height 2.0 m, azimuth bearing 64.2°).

cloud definitely passed over the electrets and that measurements should be obtained. It also was observed that the ground cloud hugged the ground for approximately 10 s and then became airborne. Later tests (15 and 18) indicated that the chemiluminescent HCl detector (Geomet) shows on the oscillograph the exhaust cloud passage for approximately 10 s where measurements of 5.0 ppm and >40.0 ppm were obtained. Most importantly, after the exhaust cloud became airborne, the concentration dropped dramatically to zero. Although there were no standard measurements taken during Static Test No. 3, a comparison with the NASA/MSFC Multilayer Diffusion Model indicated approximately 22.6 ppm at 100 m. The electrets were positioned at approximately 75 m, and a measurement of 49.1 ppm was obtained. (See Test 18 for calibration data.) Figure 12 illustrates the HCl maximum centerline concentration, while Figure 13 shows the HCl isopleths versus downwind distance.

Static Test No. 4

During this test, standard HCl instrumentation and the electrets were used. The millipore filter and bubblers were positioned 150 m from the flame trench. Only one measurement was obtained by a millipore filter, 29 ppm-s, averaged over 10 s to a concentration value of 2.9 ppm. Two bubblers measured zero. This firing occurred after dark and the visual observation indicated that the winds were very light, and the exhaust cloud lifted over the samples. Low ground level concentrations are obtained after the cloud becomes airborne. The electrets were positioned closer to the flame trench with the intention of obtaining a measurement. At 75 m, a measurement of 39.4 ppm was obtained in the ground cloud. Figure 14 illustrates the comparison of the measured values from the electrets, millipore filter, and bubbler with model. As shown in Figure 15, a measurement of approximately 79.0 ppm at 100 m was obtained from the NASA/MSFC Multilayer Diffusion Model. As indicated by Dumbauld et al. [5], measurements very close to the pad are uncertain for modeling purposes.

Static Test No. 5

A measurement of 5.7 ppm was obtained from the electrets positioned at 75 m from the flame trench. Figure 16 illustrates the HCl isopleths versus crosswind

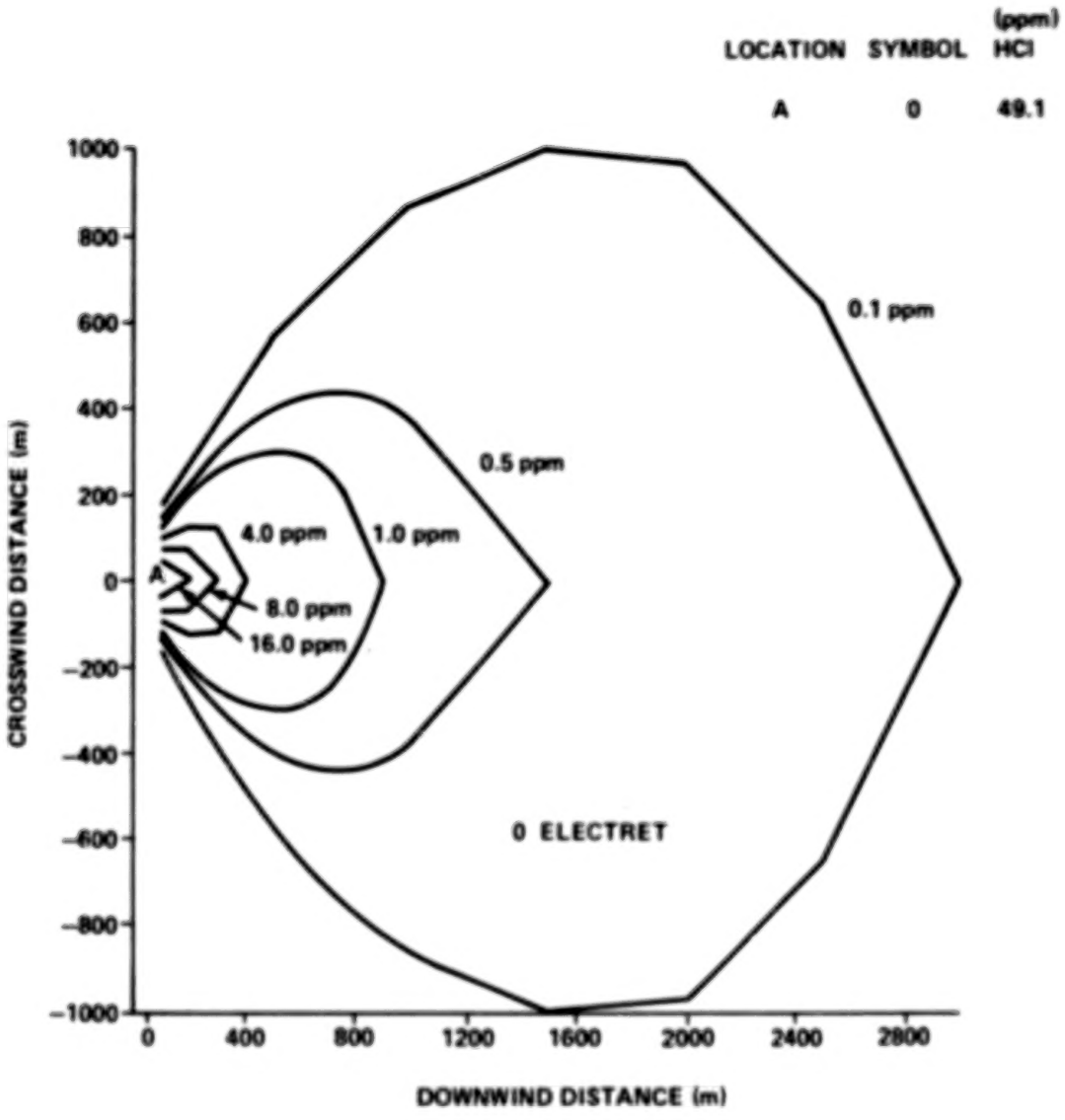

Figure 12. Comparison of HCl concentration isopleths computed by NASA/MSFC Multilayer Diffusion Model with measured values: Static Test No. 3 using Model 4 (height 2.0 m, azimuth bearing 333.6°).

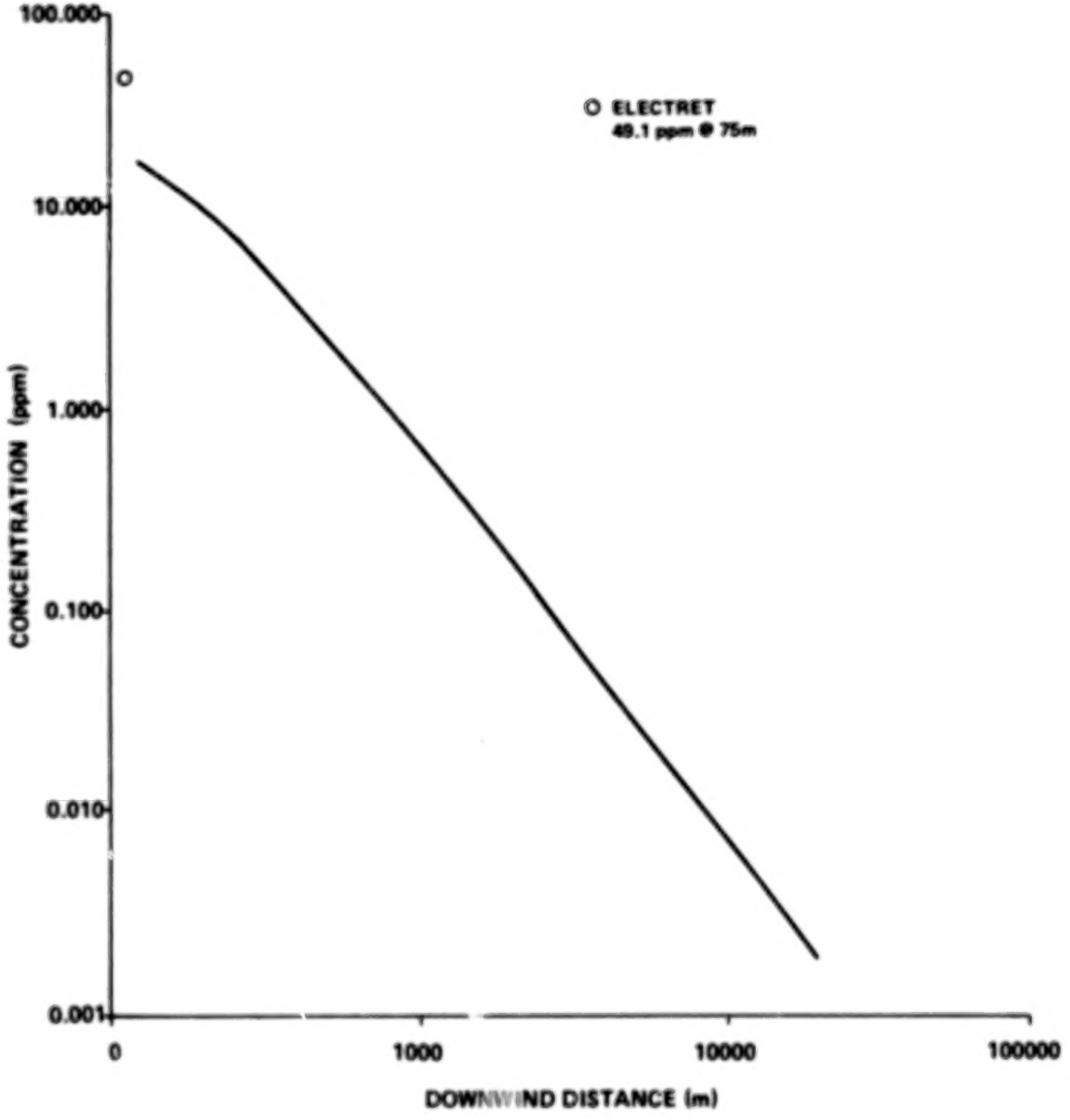

Figure 13. Computed maximum centerline HCl concentration from Model 4 and measured values: Static Test No. 3 (height 2.0 m, azimuth bearing 333.6°).

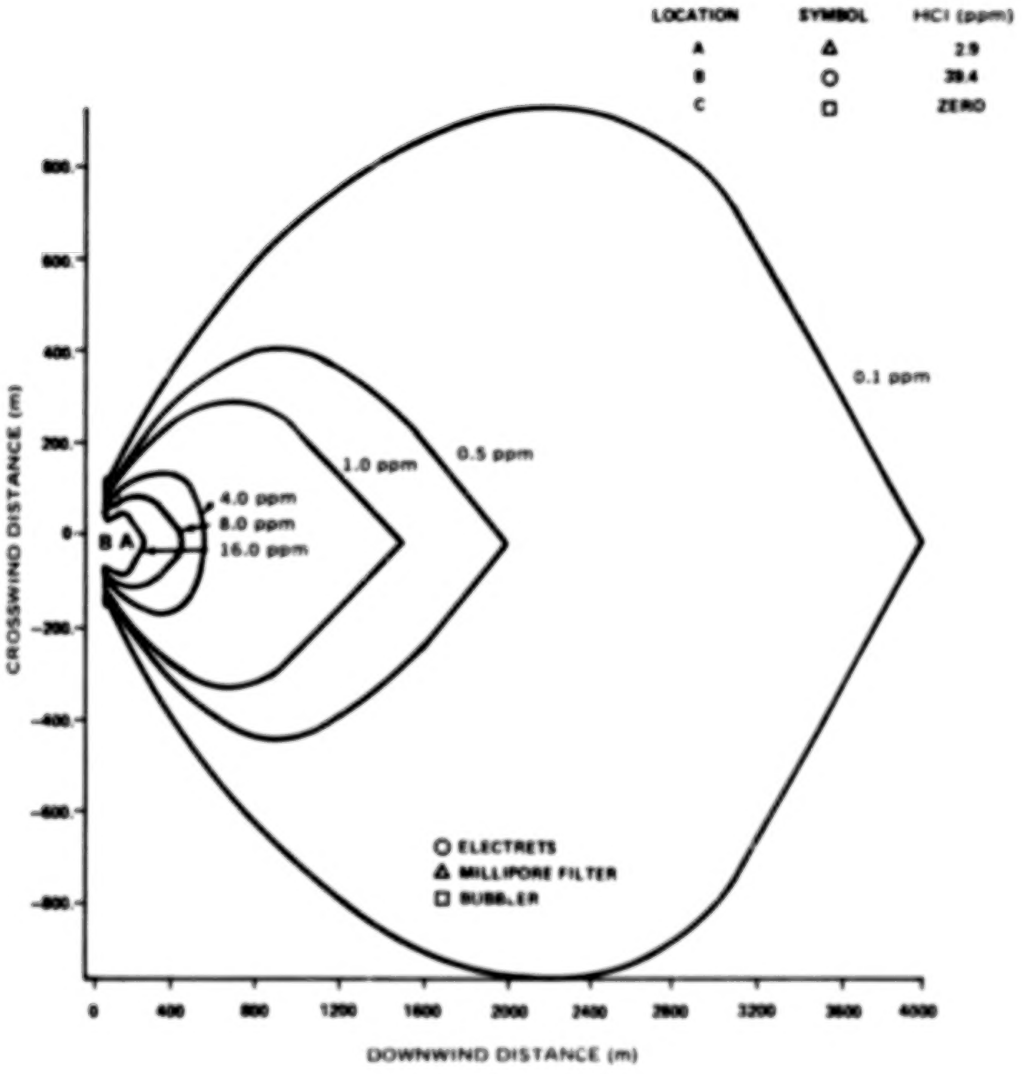

Figure 14. Comparison of HCl concentration isopleths computed by NASA/MSFC Multilayer Diffusion Model with measured values: Static Test No. 4 (height 2.0 m, azimuth bearing 307.6°).

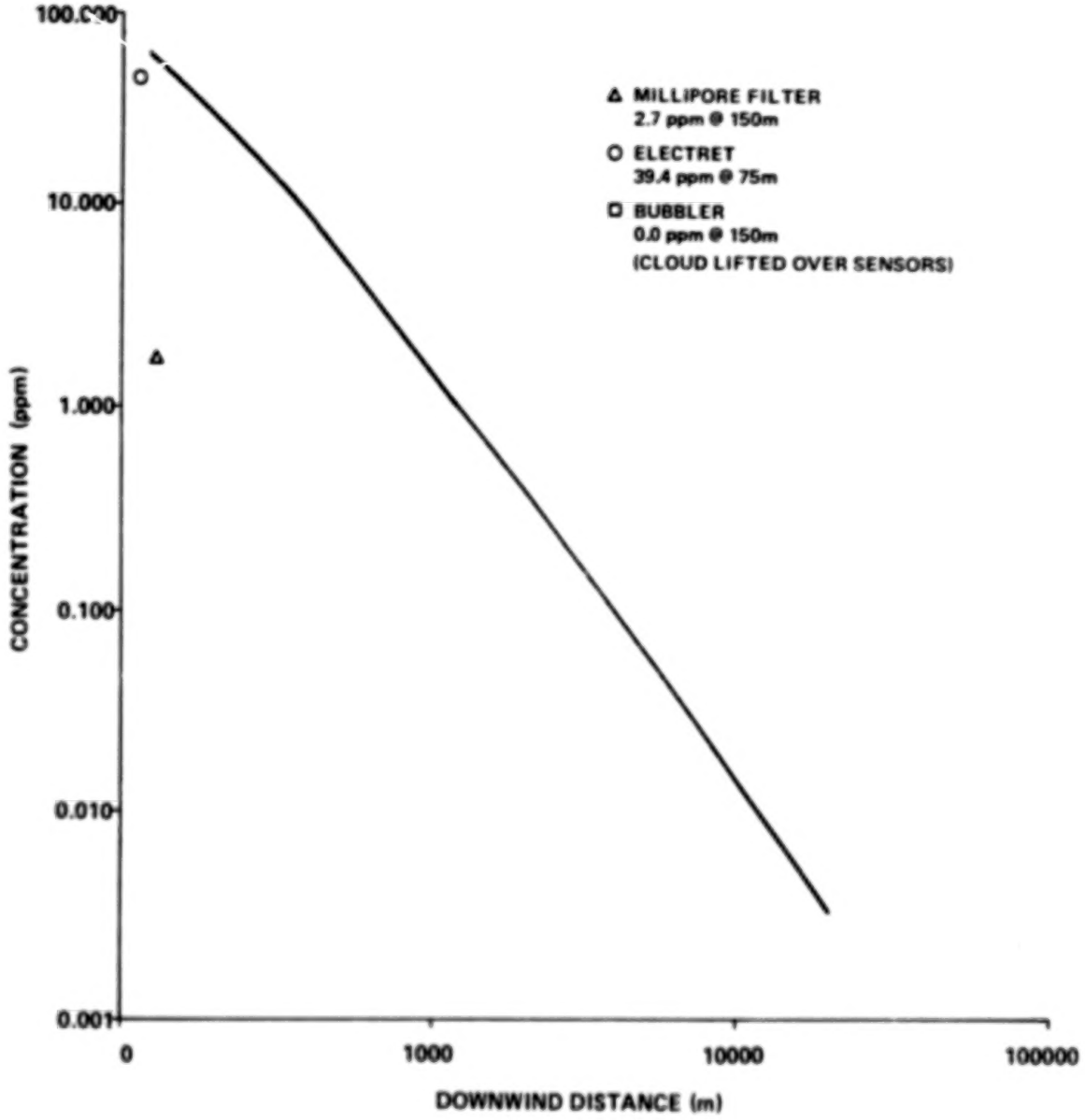

Figure 15. Computed maximum centerline HCl concentration from Model 4 and measured values: Static Test No. 4 (height 2.0 m, azimuth bearing 307.6°).

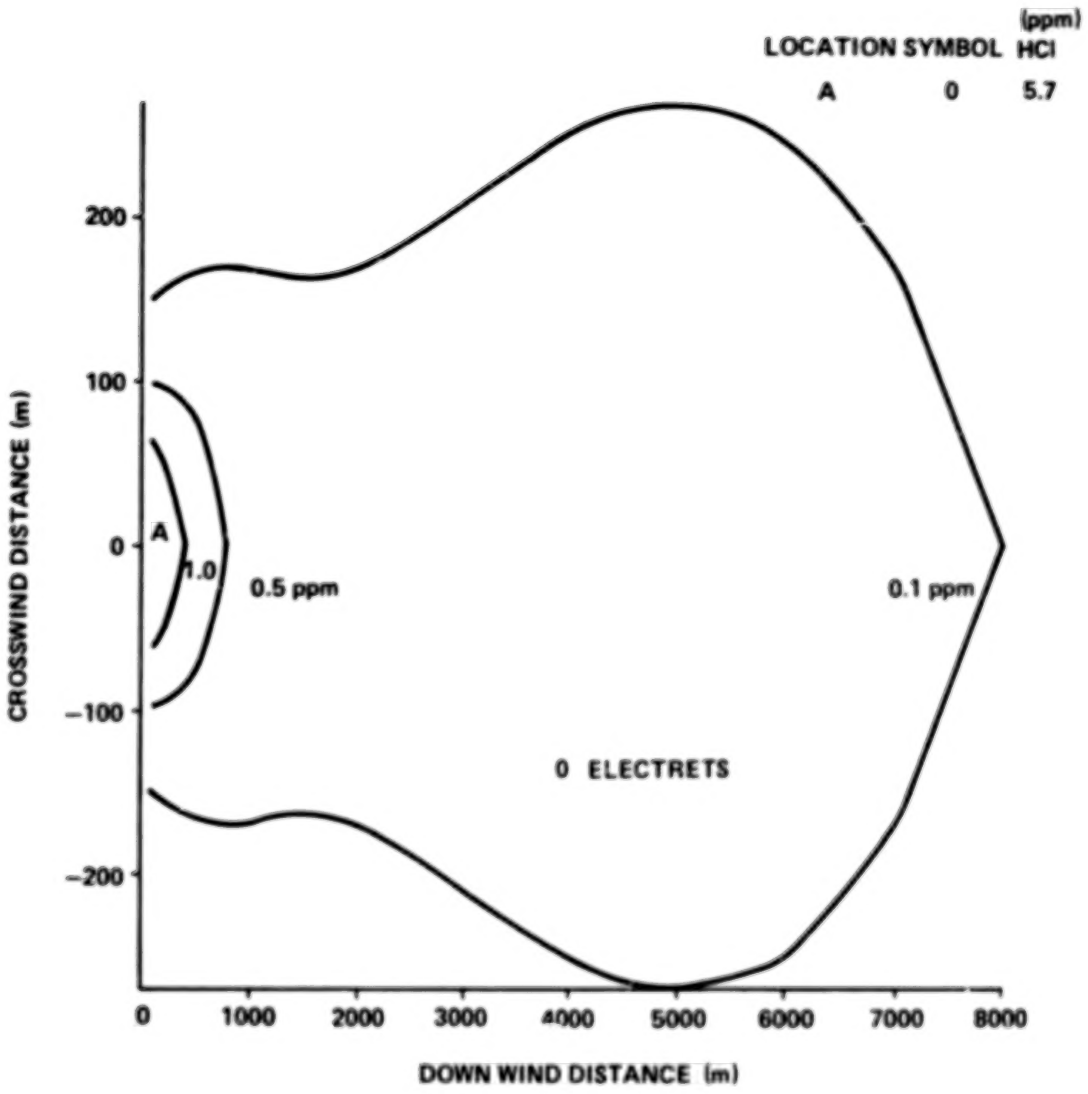

Figure 16. Comparison of HCl concentration isopleths computed by NASA/MSFC Multilayer Diffusion Model with measured values: Static Test No. 5 using Model 4 (height 2.0 m, azimuth bearing 10.4°).

distance and downwind distance obtained from the model. Figure 17 shows the HCl centerline concentration for downwind distance. At 100 m, the predicted value was approximately 1.7 ppm.

Static Test No. 6

Figure 18 shows the HCl isopleths versus crosswind and downwind distance and Figure 19 the HCl centerline concentration versus downwind distance obtained from the NASA/MSFC Multilayer Diffusion Model.

Static Test No. 7

This test was significant because the NASA/MSFC Multilayer Diffusion Model computed zero readings, and the instruments obtained zero readings. After deployment of the bubbler and millipore filter at 100 m, a delay occurred during the test. There was no chance to realign the instruments for the variable wind. Observations indicated that the positioning of the array of instrumentation missed the cloud completely, and zero values were indicated on the millipore filter and bubbler. Zero values were obtained on the HCl isopleths versus crosswind distance and downwind distance from the model as shown in Figure 20. Figure 21 shows the HCl maximum centerline concentration versus downwind distance obtained from the model.

Static Test No. 8

Figures 22 and 23 illustrate the predicted values obtained from the NASA/MSFC Multilayer Diffusion Model. The HCl isopleths versus downwind distance are shown in Figure 22, while Figure 23 illustrates the HCl maximum centerline concentration.

Static Test No. 9

Figures 24 and 25 illustrate the predicted measurements obtained from the NASA/MSFC Multilayer Diffusion Model. The HCl isopleths versus crosswind and downwind distance are presented in Figure 24, while the maximum HCl centerline concentration is illustrated in Figure 25.

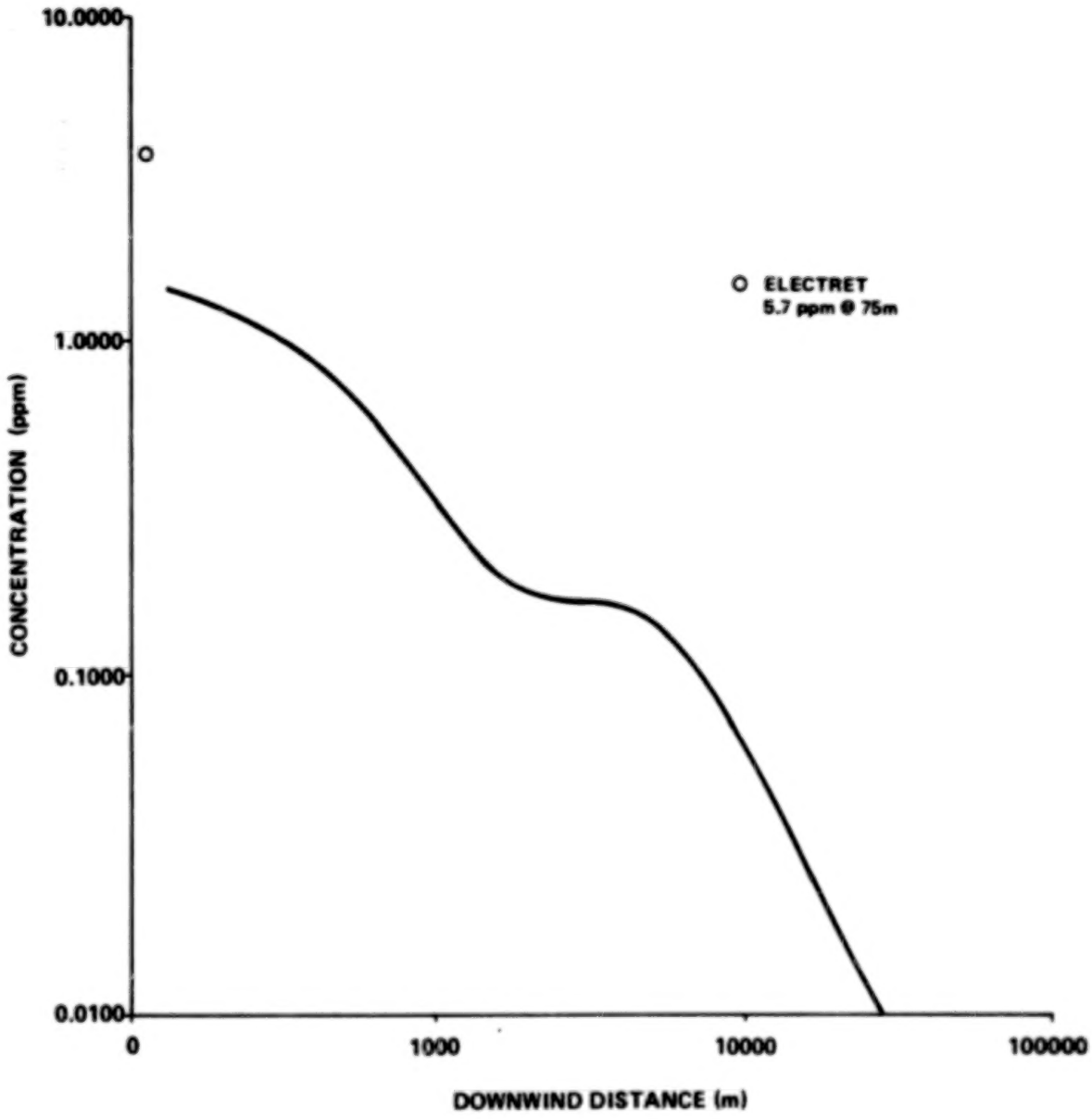

Figure 17. Computed maximum centerline HCl concentration from Model 4 and measured values: Static Test No. 5 (height 2.0 m, azimuth bearing 10.4°).

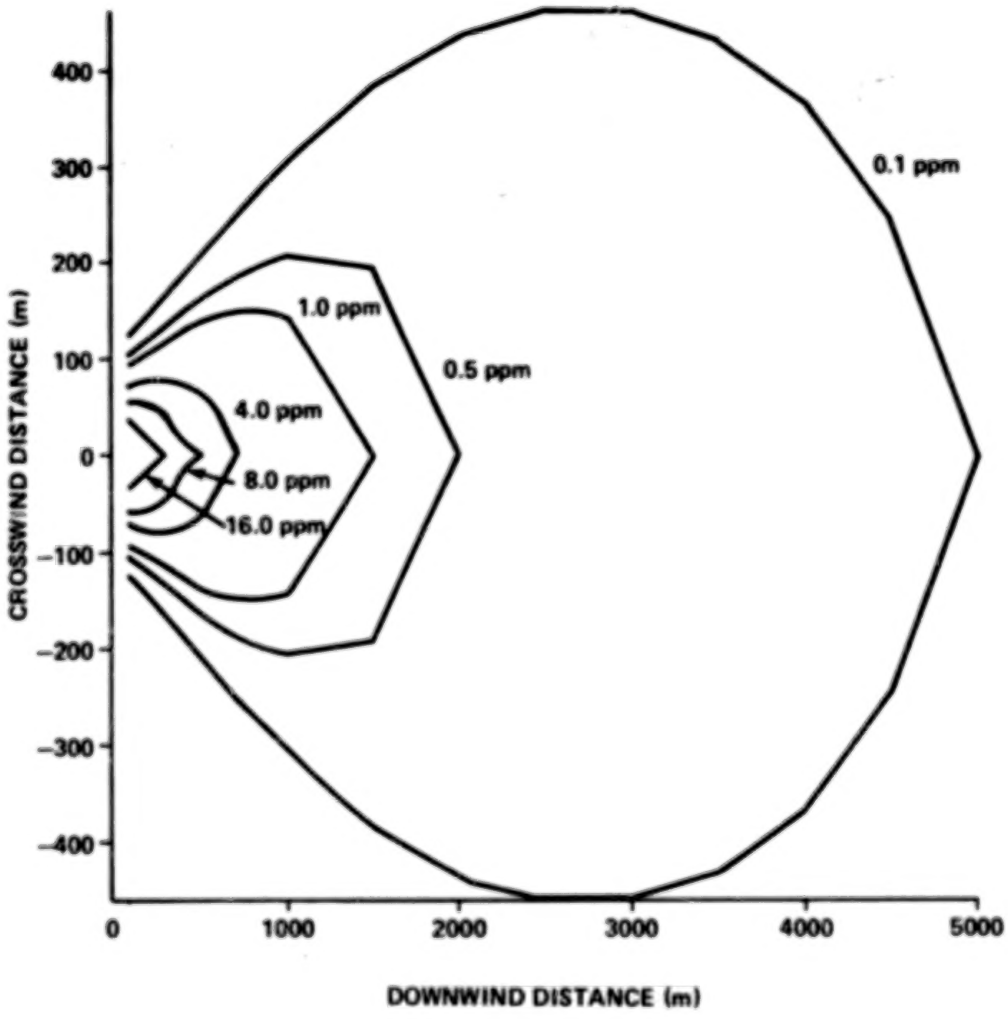

Figure 18. Computed HCl concentration isopleths by NASA/MSFC Multilayer Diffusion Model: Static Test No. 6 using Model 4 (height 2.0 m, azimuth bearing 324.4°).

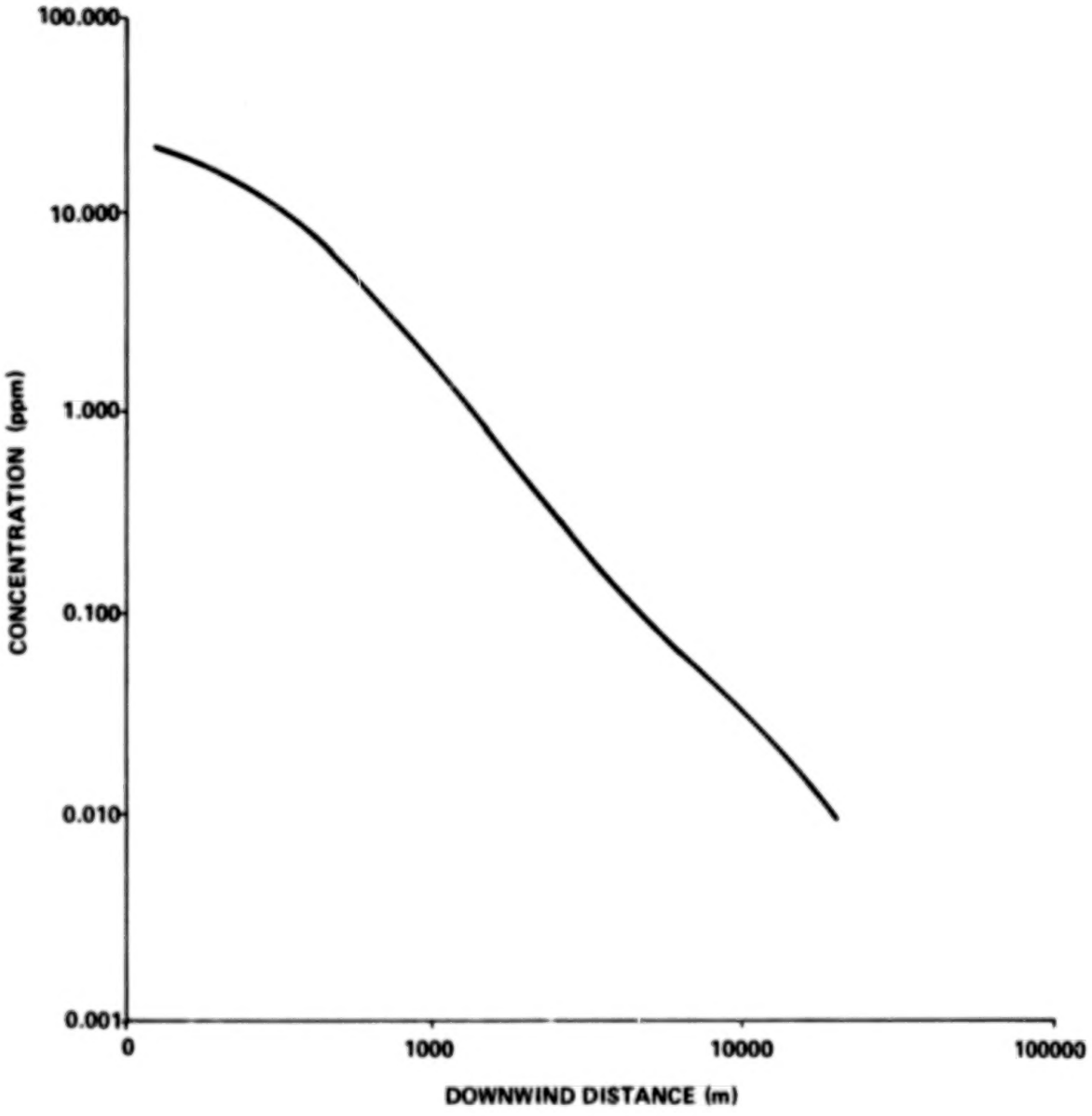

Figure 19. Computed maximum centerline HCl concentration from Model 4 for Static Test No. 6 (height 2.0 m, azimuth bearing 324.4°).

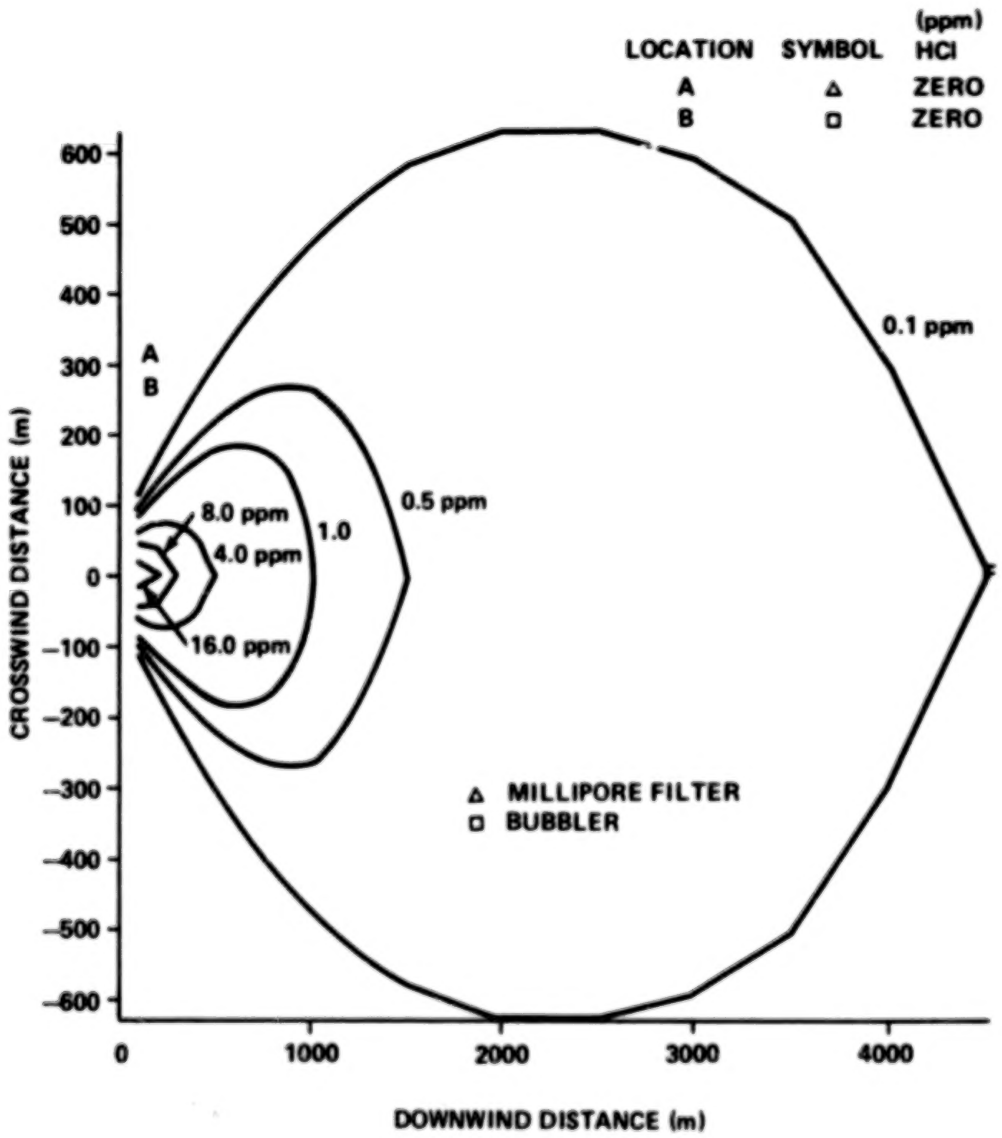

Figure 20. Comparison of HCl concentration isopleths computed by NASA/MSFC Multilayer Diffusion Model with measured values: Static Test No. 7 using Model 4 (height 2.0 m, azimuth bearing 43.0°).

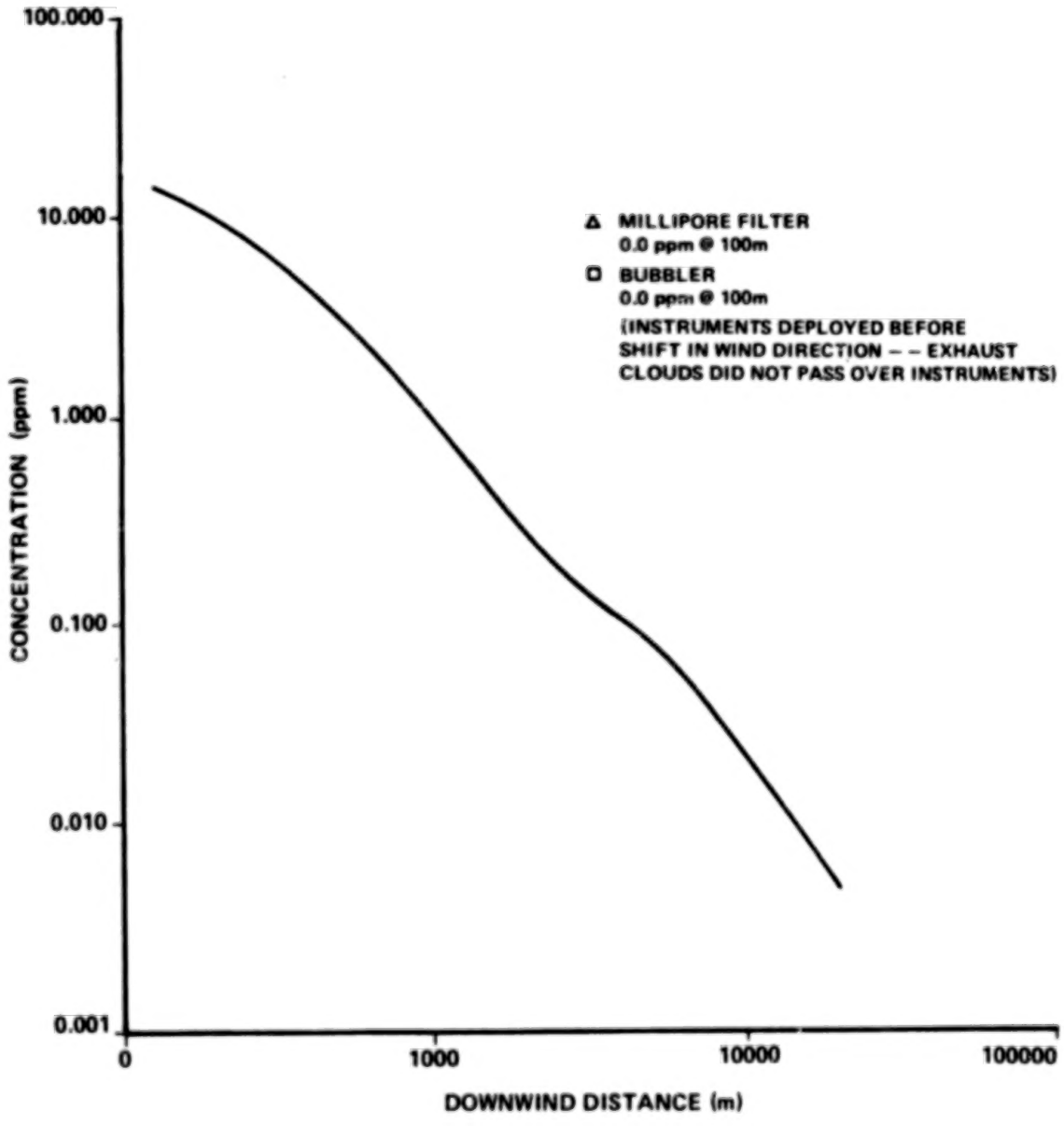

Figure 21. Computed maximum centerline HCl concentration from Model 4 for Static Test No. 7 (height 2.0 m, azimuth bearing 316.4°).

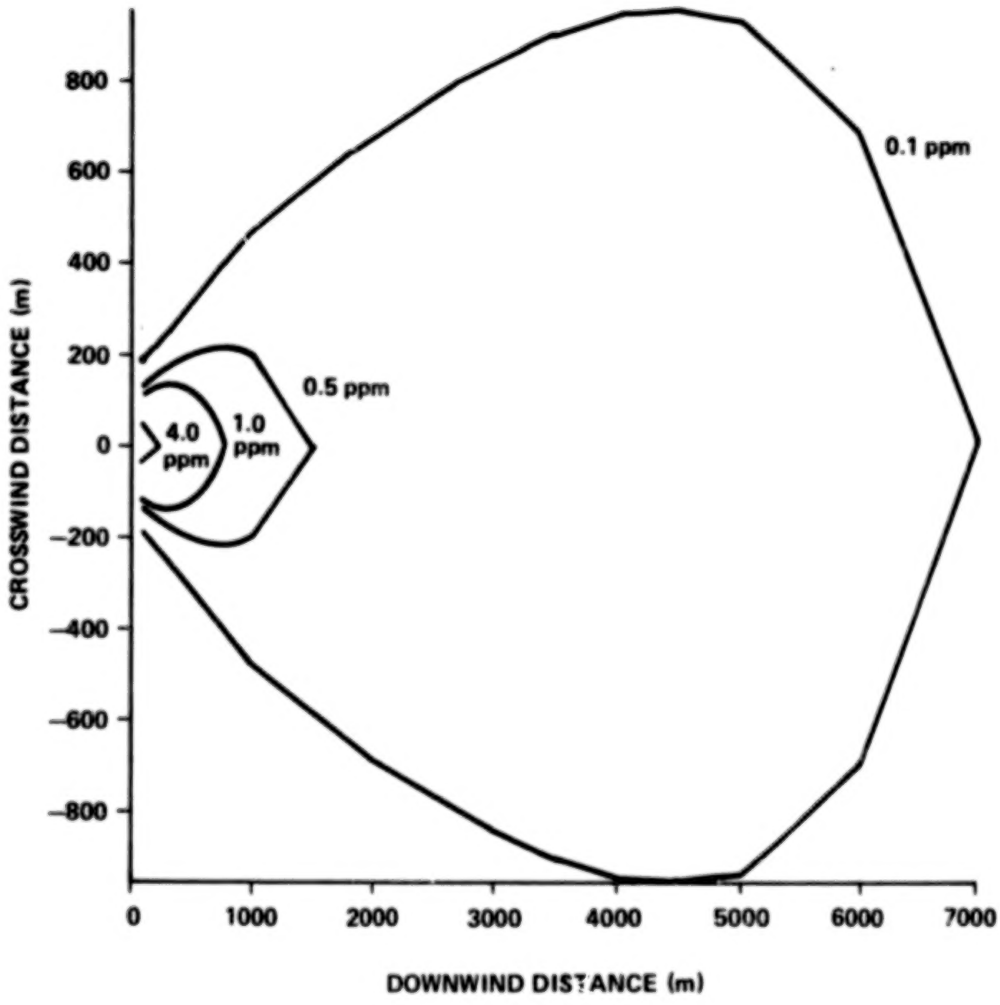

Figure 22. Computed HCl concentration isopleths by NASA/MSFC Multilayer Diffusion Model: Static Test No. 8 using Model 4 (height 2.0 m, azimuth bearing 75.0°).

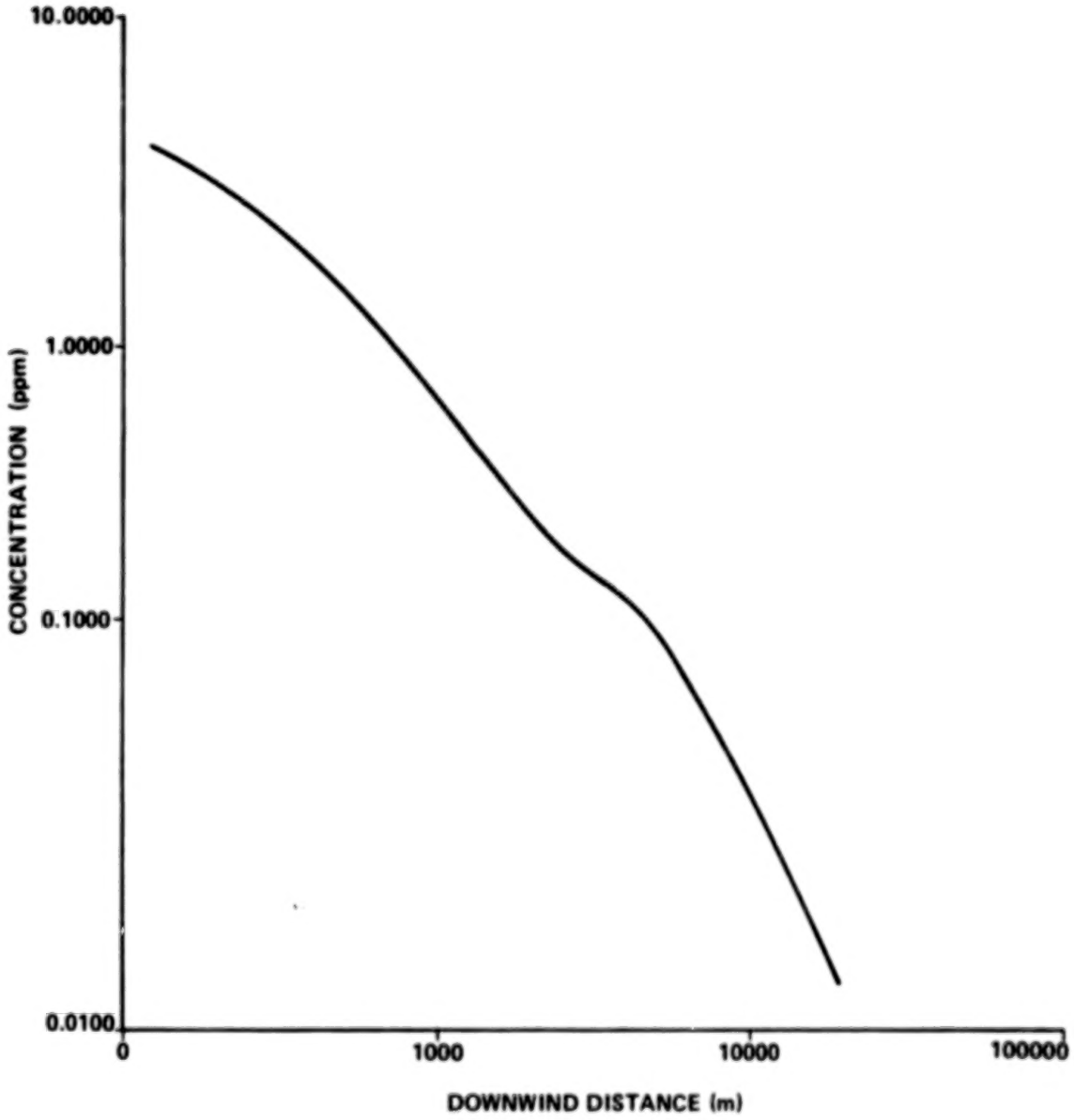

Figure 23. Computed maximum centerline HCl concentration from Model 4 for Static Test No. 8 (height 2.0 m, azimuth bearing 75.0°).

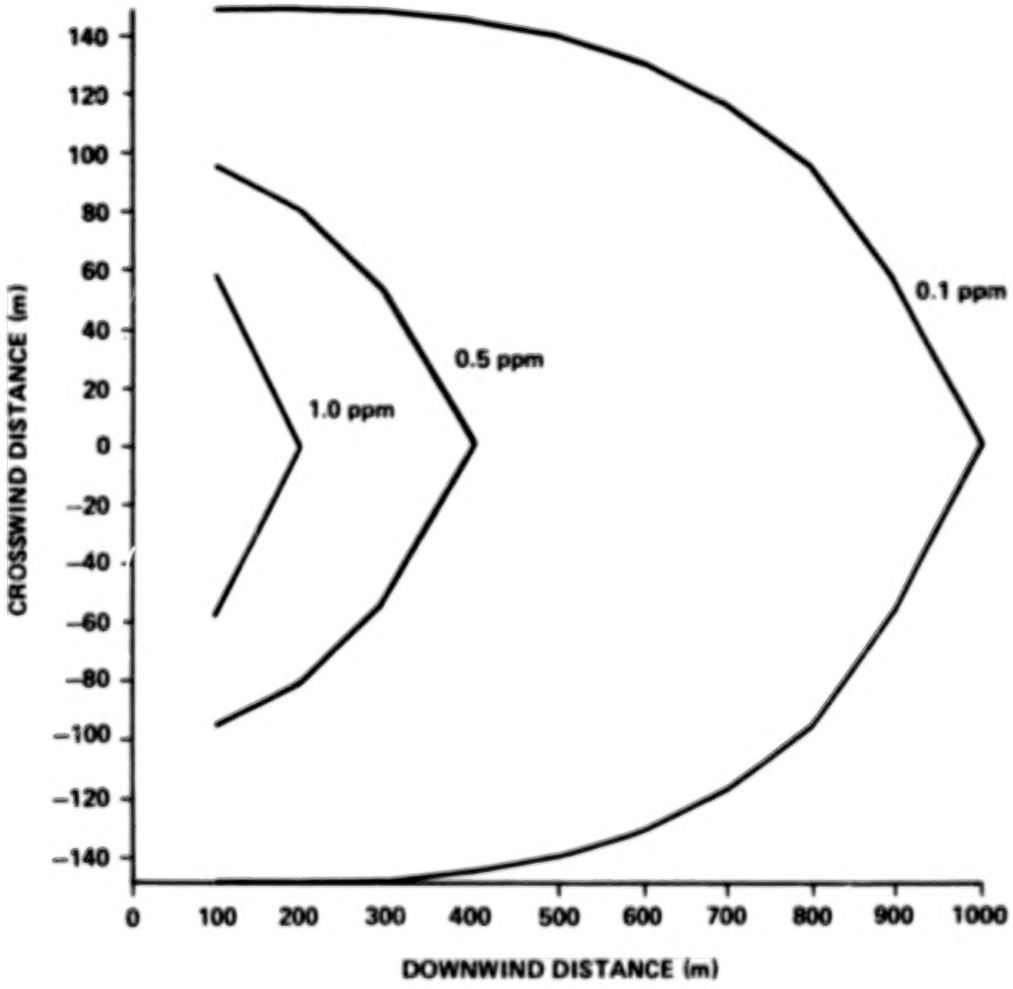

Figure 24. Computed HCl concentration isopleths by NASA/MSFC Multilayer Diffusion Model: Static Test No. 9 using Model 4 (height 2.0 m, azimuth bearing 75.8°).

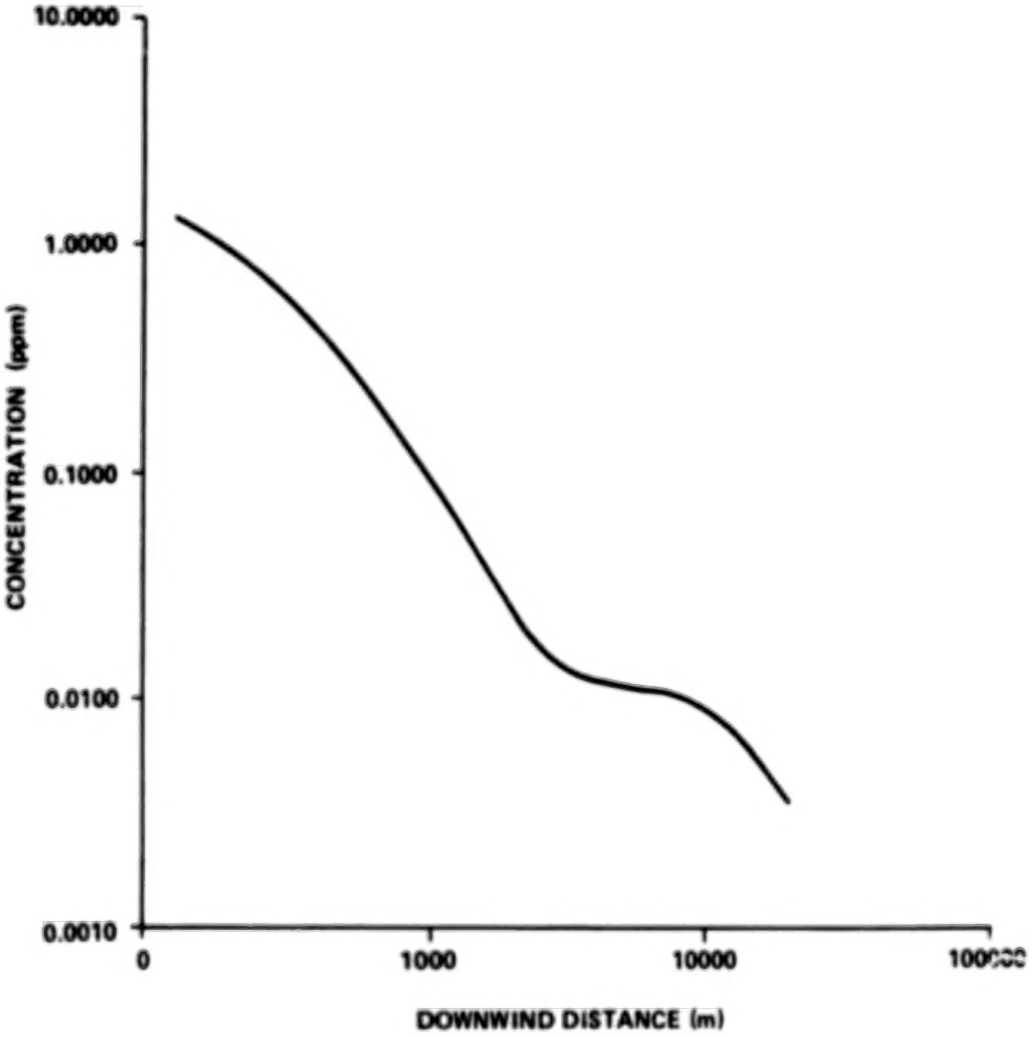

Figure 25. Computed maximum centerline HCl concentration from Model 4 for Static Test No. 9 (height 2.0 m, azimuth bearing 75.8°).

Static Test No. 10

From previous tests it was learned that to get good test results, it was necessary to have the instrumentation close to the launch pad. The cloud passes over the sensors in 10 to 12 s and once the cloud becomes airborne, measurements are difficult to obtain. Hence, the millipore filters and bubblers were placed 75 m from and in line with the flame trench which directs the rocket exhaust. Figure 26 illustrates the comparison of the predicted HCl isopleths versus crosswind and downwind distance and the measured values of the HCl detectors. The millipore filters and bubbler measured from 3.2 to 10.0 ppm, which corresponded very well with the NASA/MSFC Multilayer Diffusion Model of 8.0 ppm at 100 m downwind distance in Figure 27.

Static Test No. 11

Figures 28 and 29 illustrate the predicted values obtained from the NASA/MSFC Multilayer Diffusion Model. The HCl concentration isopleths versus crosswind and downwind distances are shown in Figure 28, while Figure 29 illustrates the maximum HCl centerline concentration values.

Static Test No. 12

Figures 30 and 31 illustrate the predicted values of HCl obtained from the NASA/MSFC Multilayer Diffusion Model. The HCl concentration isopleths versus crosswind and downwind distances are shown in Figure 30, while Figure 31 depicts the maximum centerline HCl concentration versus downwind distance.

Static Test No. 13

Figures 32 and 33 are the plots of the predicted values obtained from the NASA/MSFC Multilayer Diffusion Model. The HCl concentration isopleths versus crosswind and downwind distances are shown in Figure 32, while Figure 33 illustrates the maximum HCl centerline concentration versus downwind distance. The electrets measurement of 39.5 ppm at 100 m (position A) compared favorably with the models maximum centerline HCl concentration of 44.7 ppm. At position B, approximately 150 m from the flame

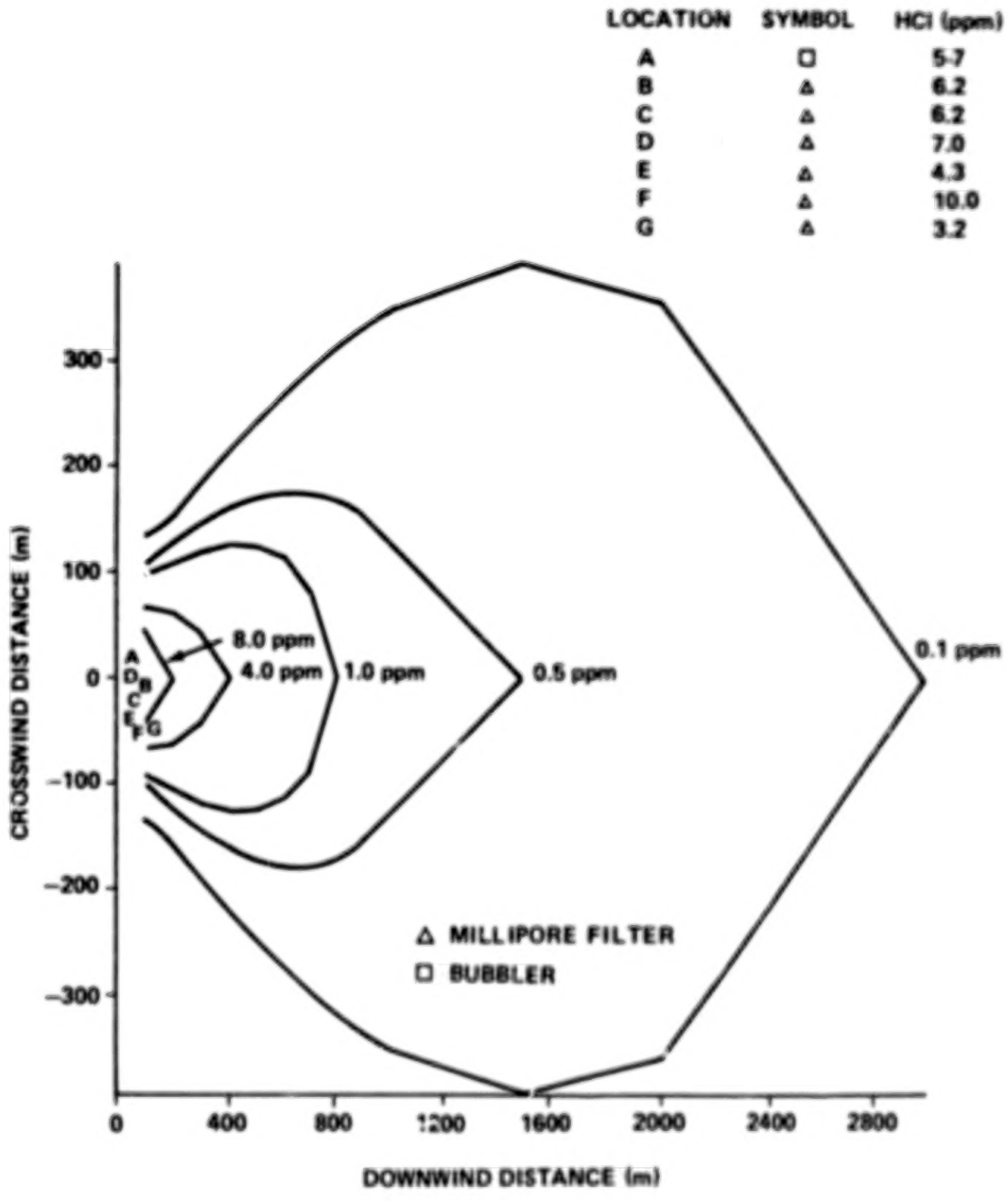

Figure 26. Comparison of HCl concentration isopleths computed by NASA/MSFC Multilayer Diffusion Model with measured values: Static Test No. 10 (height 2.0 m, azimuth bearing 171.4°).

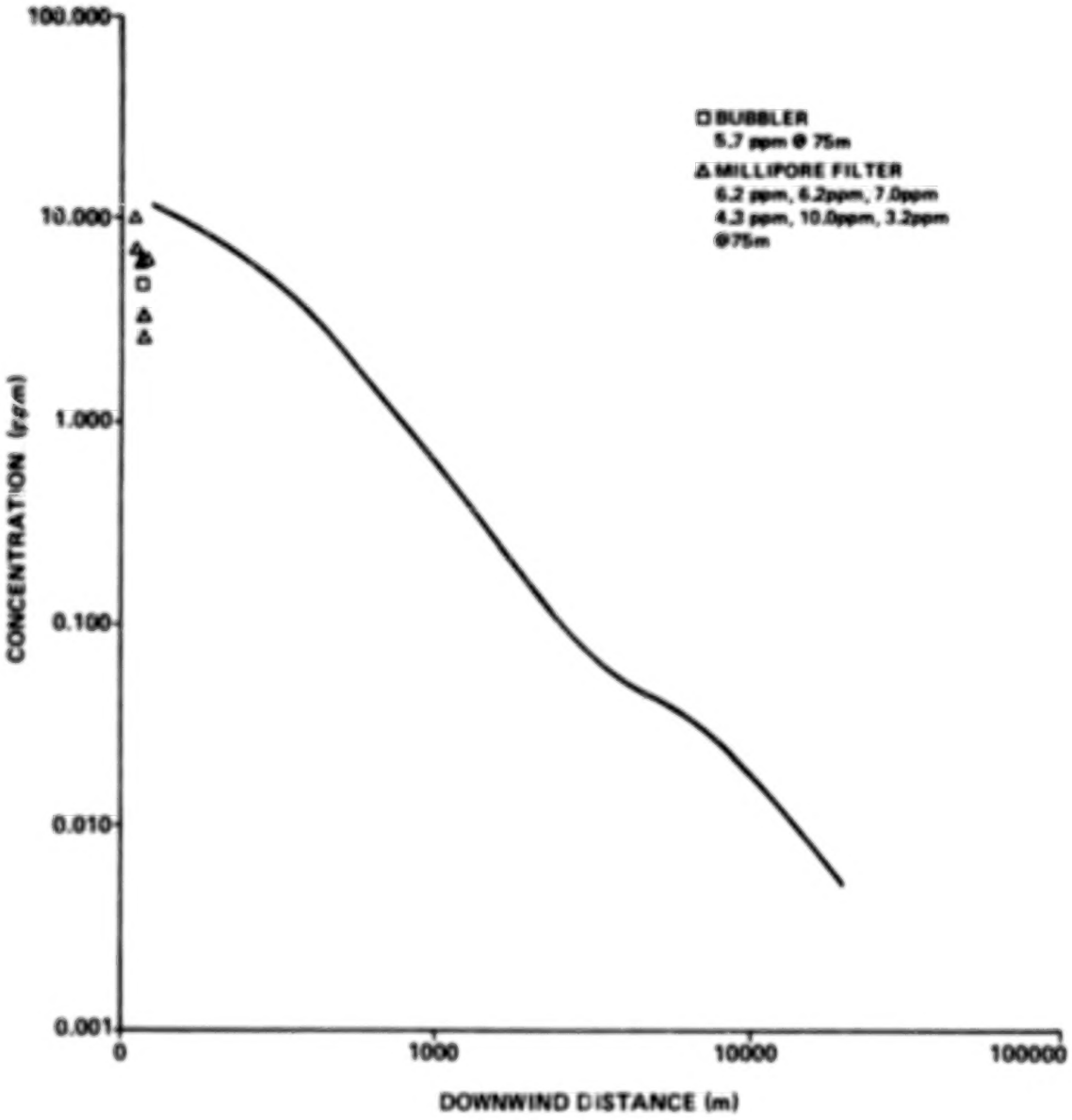

Figure 27. Computed maximum centerline HCl concentration from Model 4 and measured values: Static Test No. 10 (height 2.0 m, azimuth bearing 171.4°).

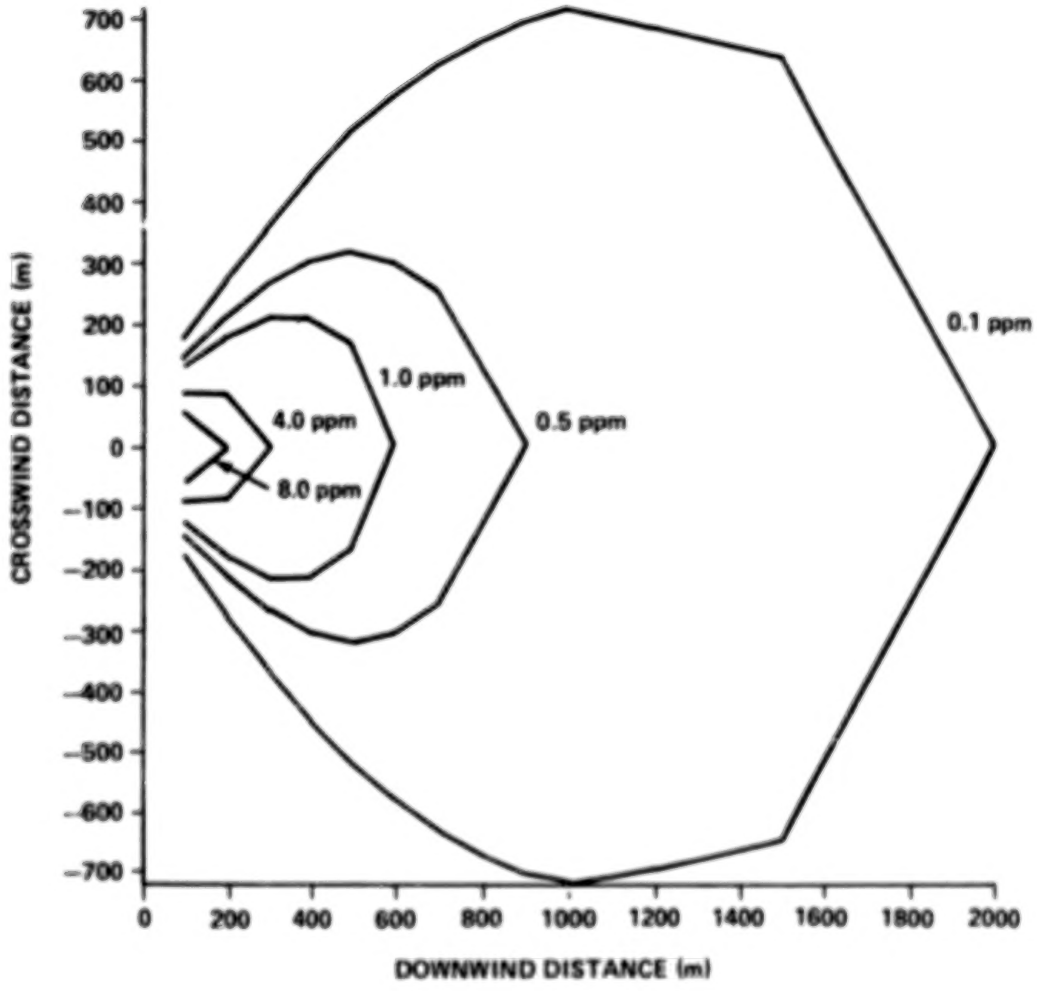

Figure 28. Computed HCl concentration isopleths by NASA/MSFC Multilayer Diffusion Model: Static Test No. 11 using Model 4 (height 2.0 m, azimuth bearing 114.2°).

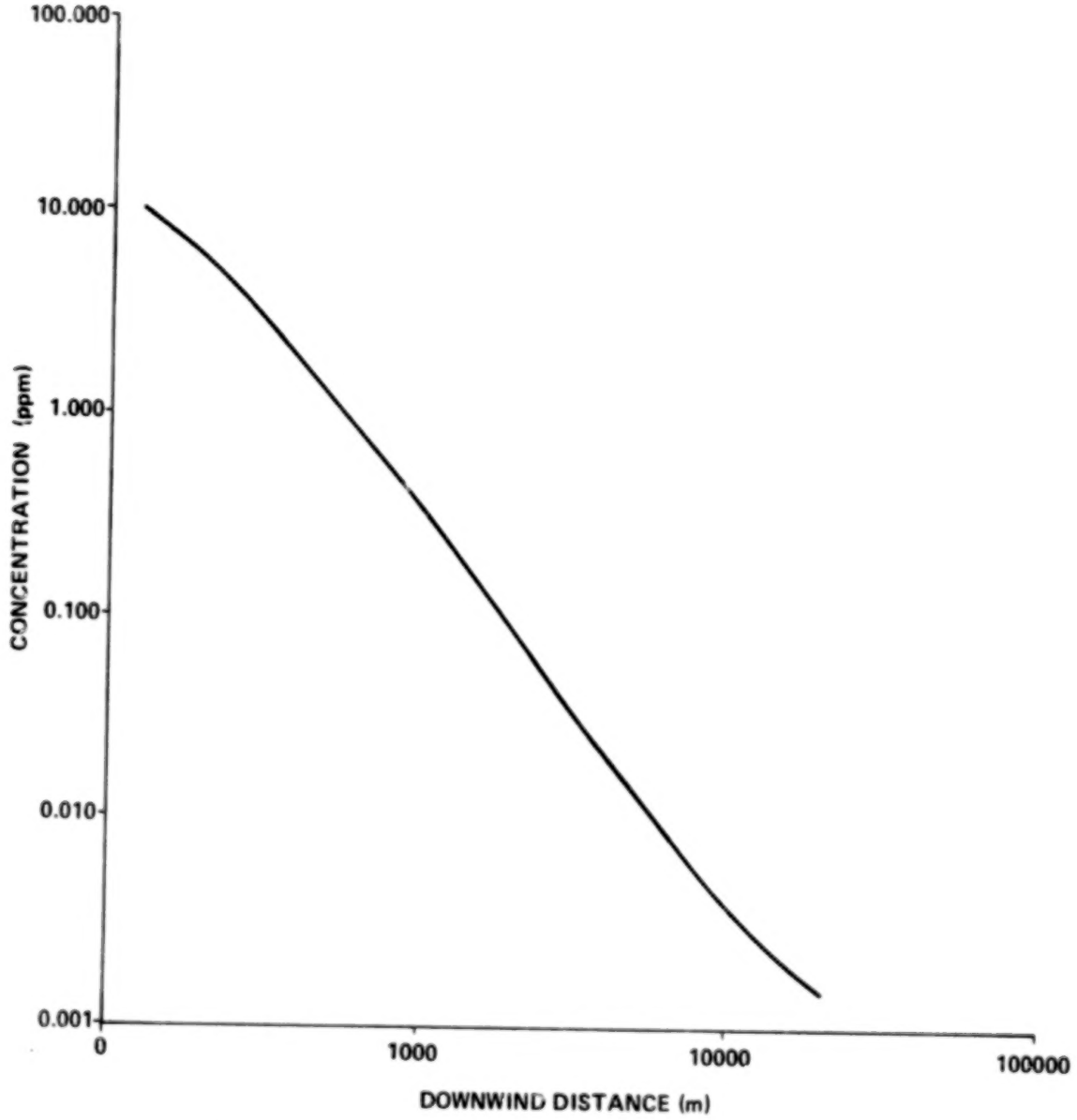

Figure 29. Computed maximum centerline HCl concentration from Model 4 for Static Test No. 11 (height 2.0 m, azimuth bearing 114.2°).

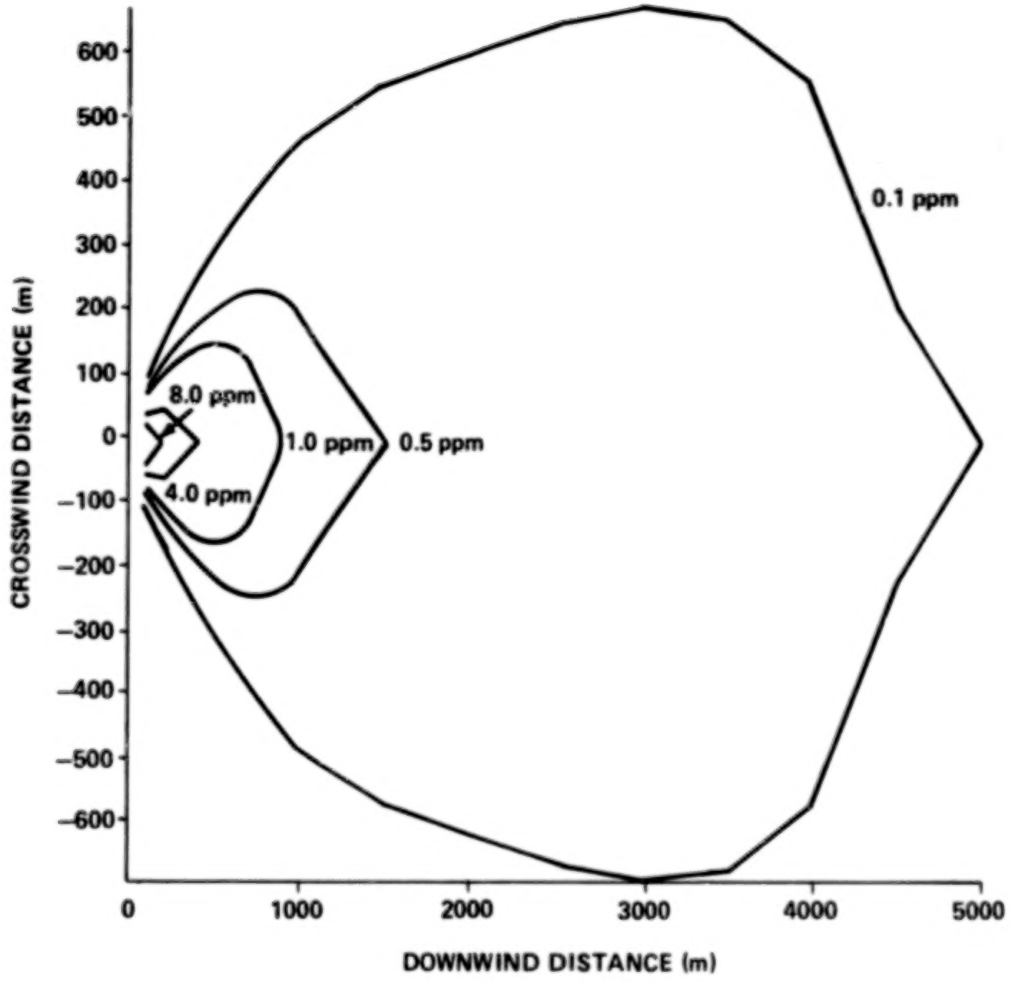

Figure 30. Computed HCl concentration isopleths by NASA/MSFC Multilayer Diffusion Model: Static Test No. 12 using Model 4 (height 2.0 m, azimuth bearing 328.6°).

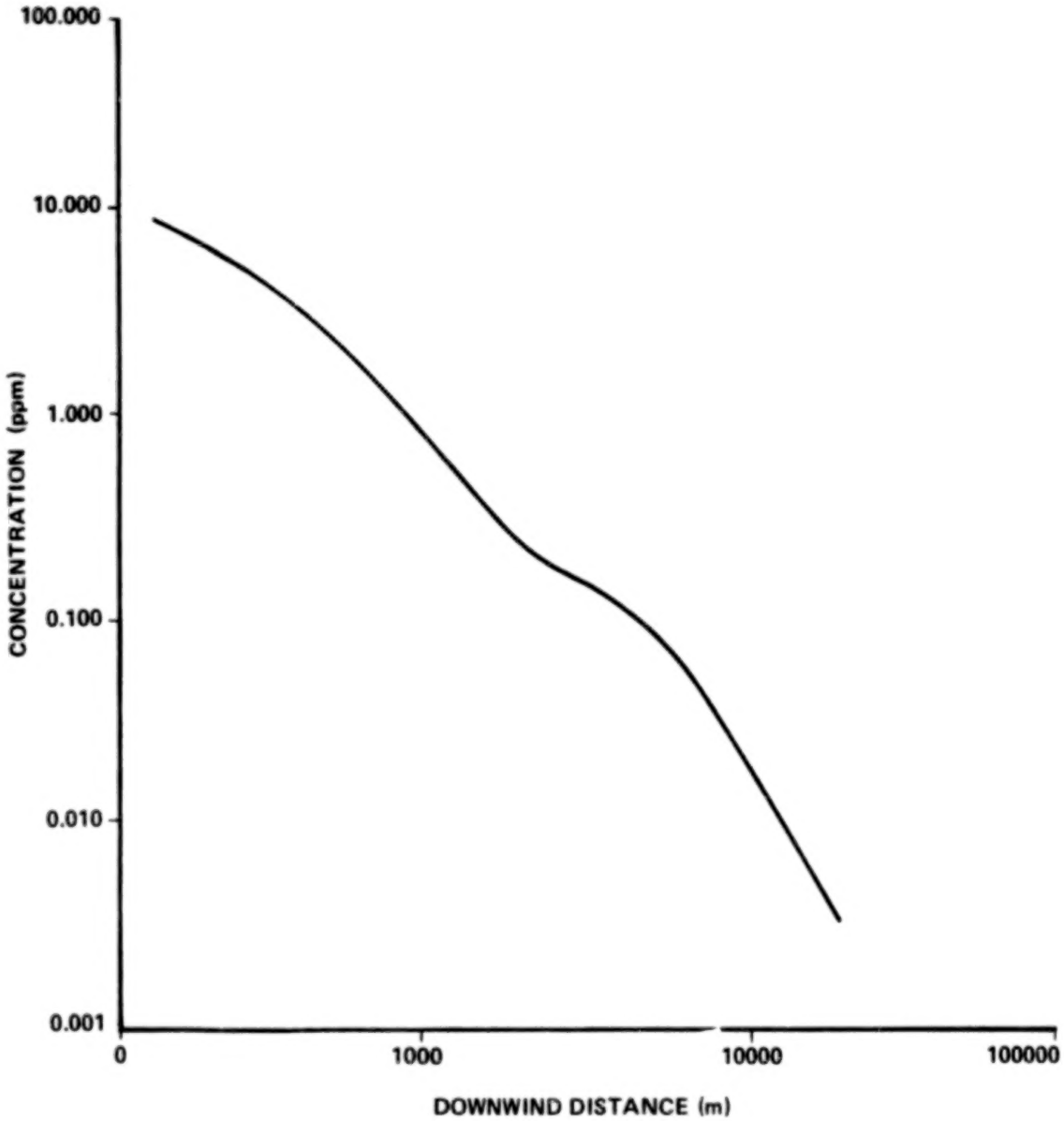

Figure 31. Computed maximum centerline HCl concentration from Model 4 for Static Test No. 12 (height 2.0 m, azimuth bearing 328.6°).

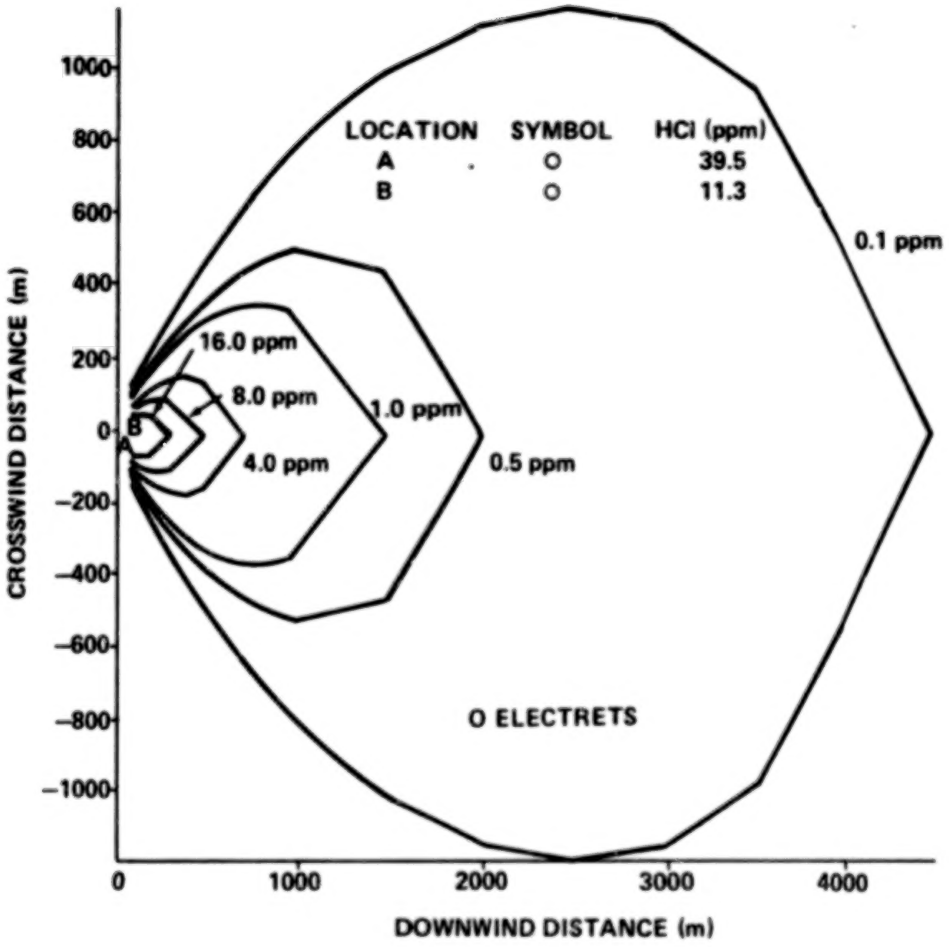

Figure 32. Comparison of HCl concentration isopleths computed by NASA/MSFC Multilayer Diffusion Model with measured values: Static Test No. 13 using Model 4 (height 2.0 m, azimuth bearing 260.7°).

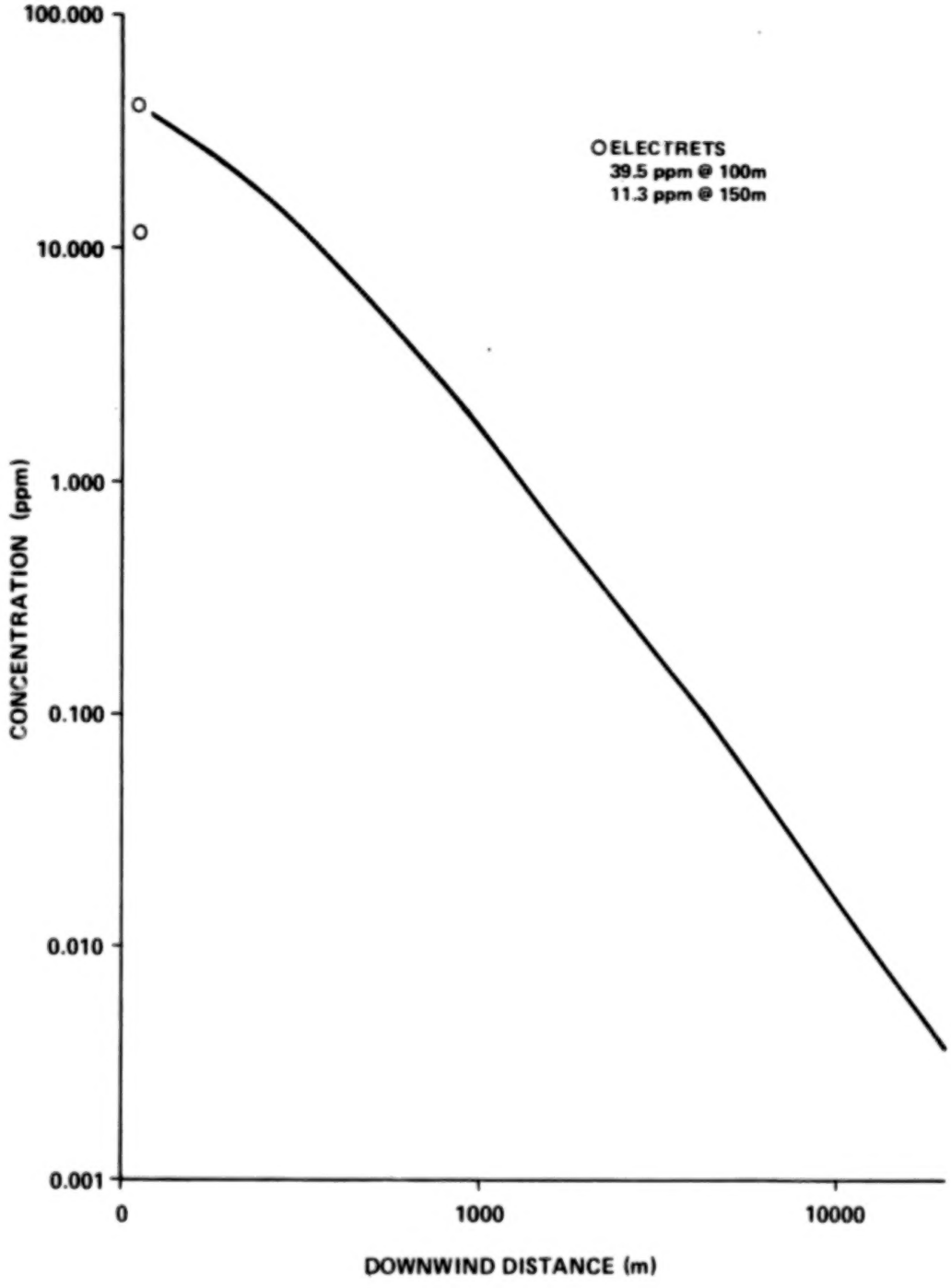

Figure 33. Computed maximum HCl concentration and measured values: Static Test No. 13 (height 2.0 m, azimuth bearing 260.7°).

trench and 20° off the direct line from the flame trench, a measurement of 11.3 ppm could be extrapolated between the isopleths of 8 and 16 ppm contour.

Static Test No. 14

Figures 34 and 35 illustrate the predicted values obtained from the NASA/MSFC Multilayer Diffusion Model. The HCl concentration isopleths versus crosswind and downwind distances are shown in Figure 34, while Figure 35 illustrates the maximum HCl centerline concentration values.

Static Test No. 15

Test No. 15 was an early Saturday morning test. The wind direction was from 220° and the wind speed was 2.1 m/s at the surface and at 158 m. At 325 m, the wind speed was 2.2 m/s from 210°. The potential temperature gradient was approximately 0.0005 K/m. Observation after firing indicated the exhaust cloud was a little more buoyant as compared to the previous tests and started to rise before the end of the launch pad at 100 m. With the low wind speed, the cloud lingered for approximately 25 s over the array of detectors and then slowly dissipated. Figures 36 and 37 illustrate the predicted values obtained from the NASA/MSFC Multilayer Diffusion Model. Figure 36 shows the HCl isopleths versus crosswind and downwind distances, and measured values from the HCl detectors which compared favorably. Figure 37 depicts the maximum HCl centerline concentration versus downwind distance of the model.

Static Test No. 16

Figures 38 and 39 illustrate the HCl predictions obtained from the NASA/MSFC Multilayer Diffusion Model. Figure 38 shows the HCl concentration isopleths versus crosswind and downwind distance, while Figure 39 illustrates the maximum HCl centerline concentration versus downwind distance.

Static Test No. 17

Figures 40 and 41 illustrate the HCl prediction values obtained from the NASA/MSFC Multilayer Diffusion Model. Figure 40 shows the HCl concentration isopleths versus crosswind and downwind distance, while Figure 41 illustrates the maximum HCl centerline concentration versus downwind distance.

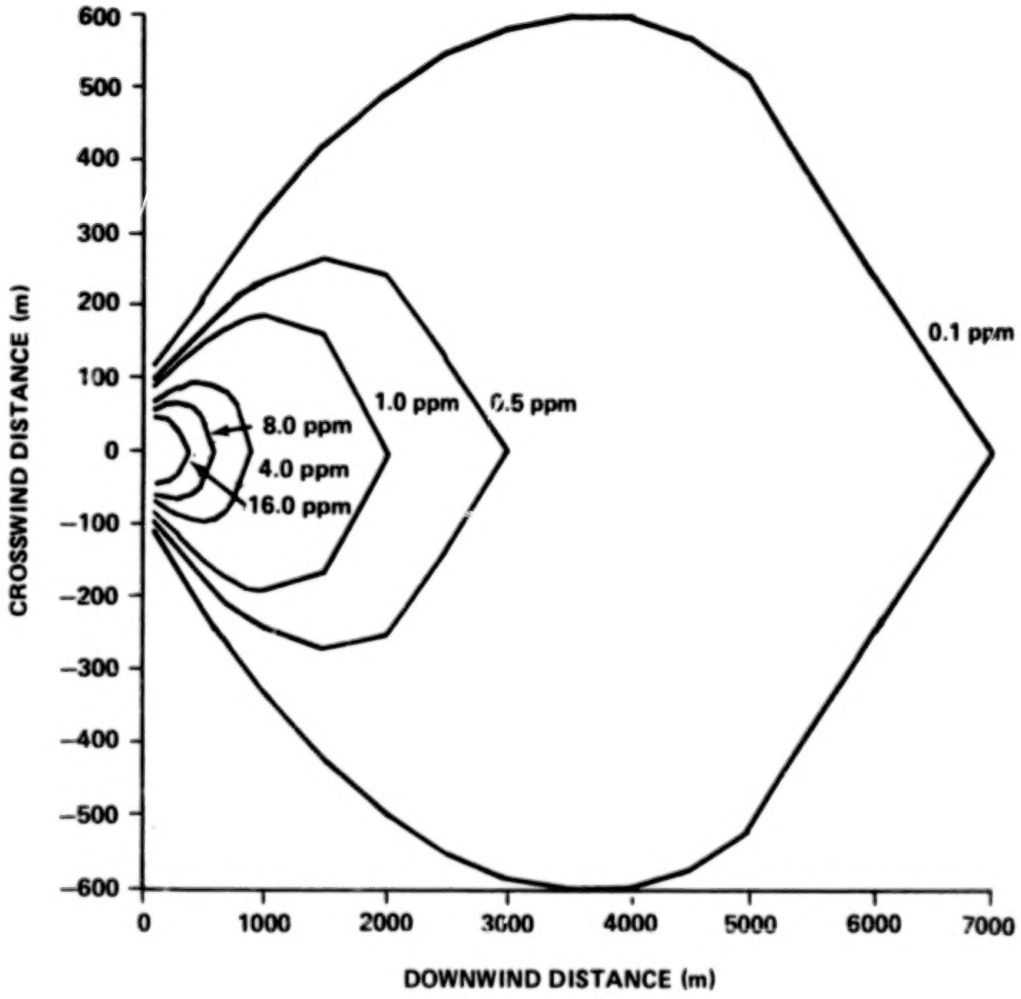

Figure 34. Computed HCl concentration isopleths by NASA/MSFC Multilayer Diffusion Model: Static Test No. 14 (height 2.0 m, azimuth bearing 354.3°).

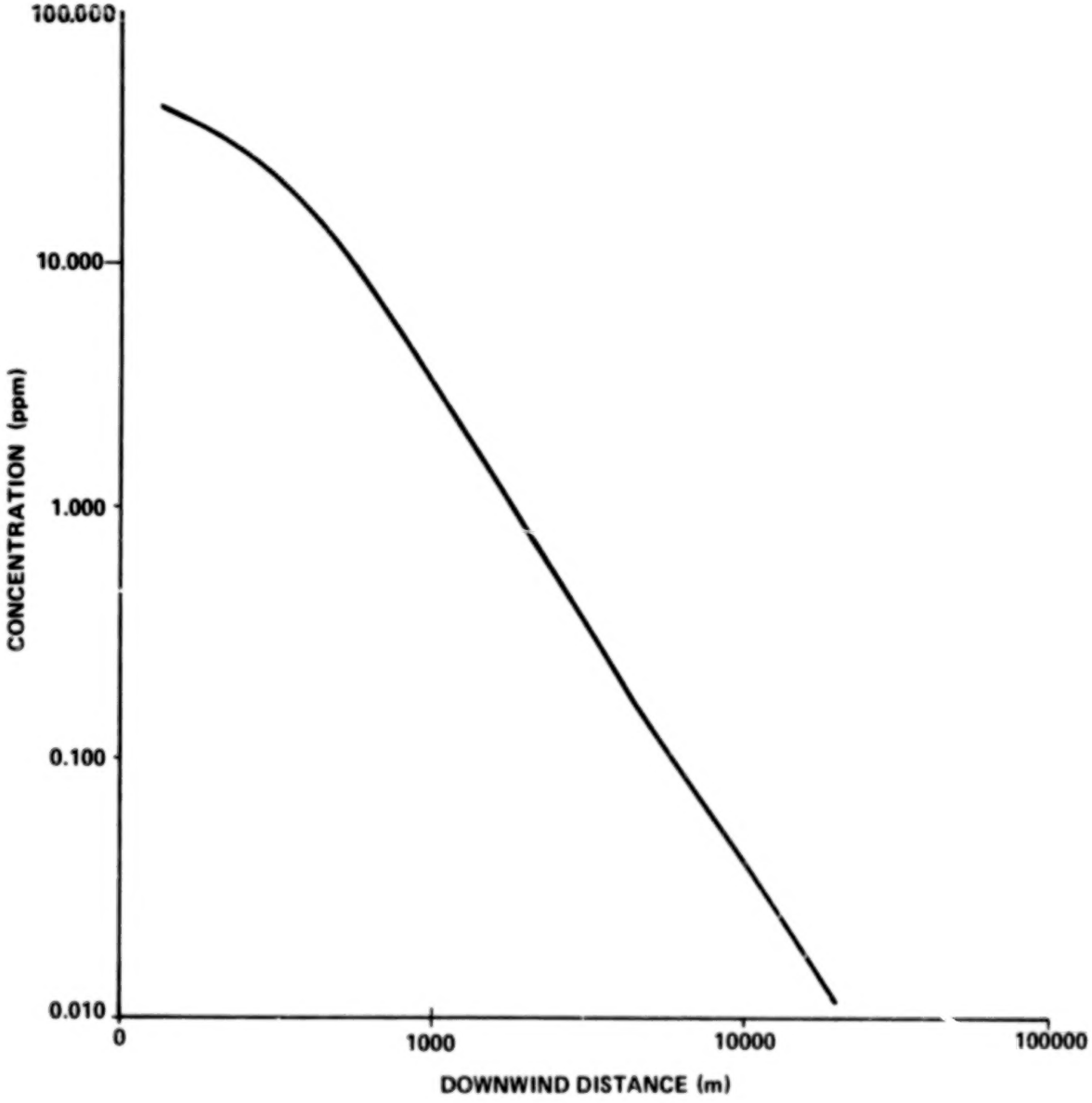

Figure 35. Computed maximum HCl concentration from Model 4 for Static Test No. 14 (height 2.0 m, azimuth bearing 354.3°).

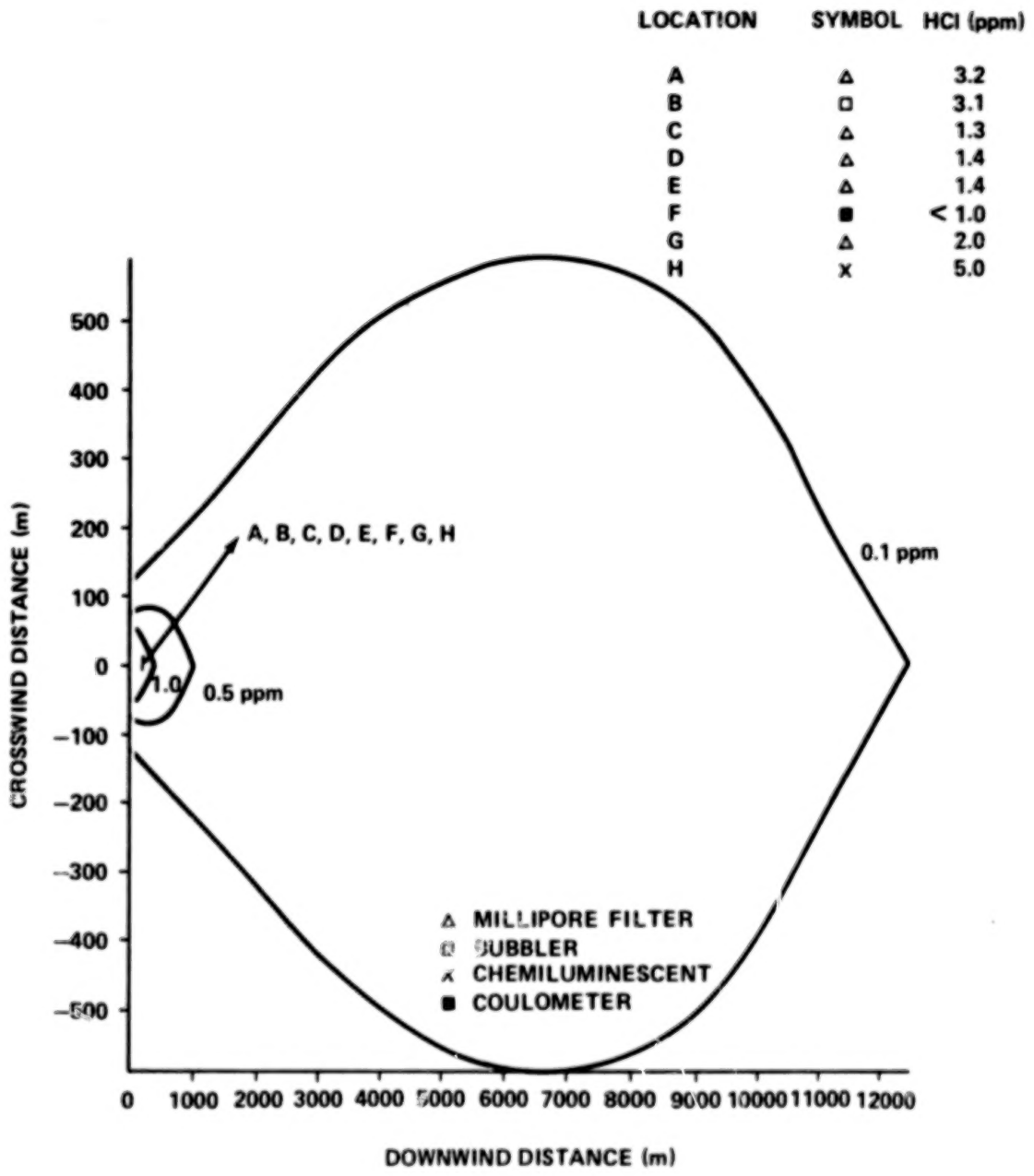

Figure 36. Comparison of HCl concentration isopleths computed by NASA/MSFC Multilayer Diffusion Model with measured values: Static Test No. 15 (height 2.0 m, azimuth bearing 35.1°).

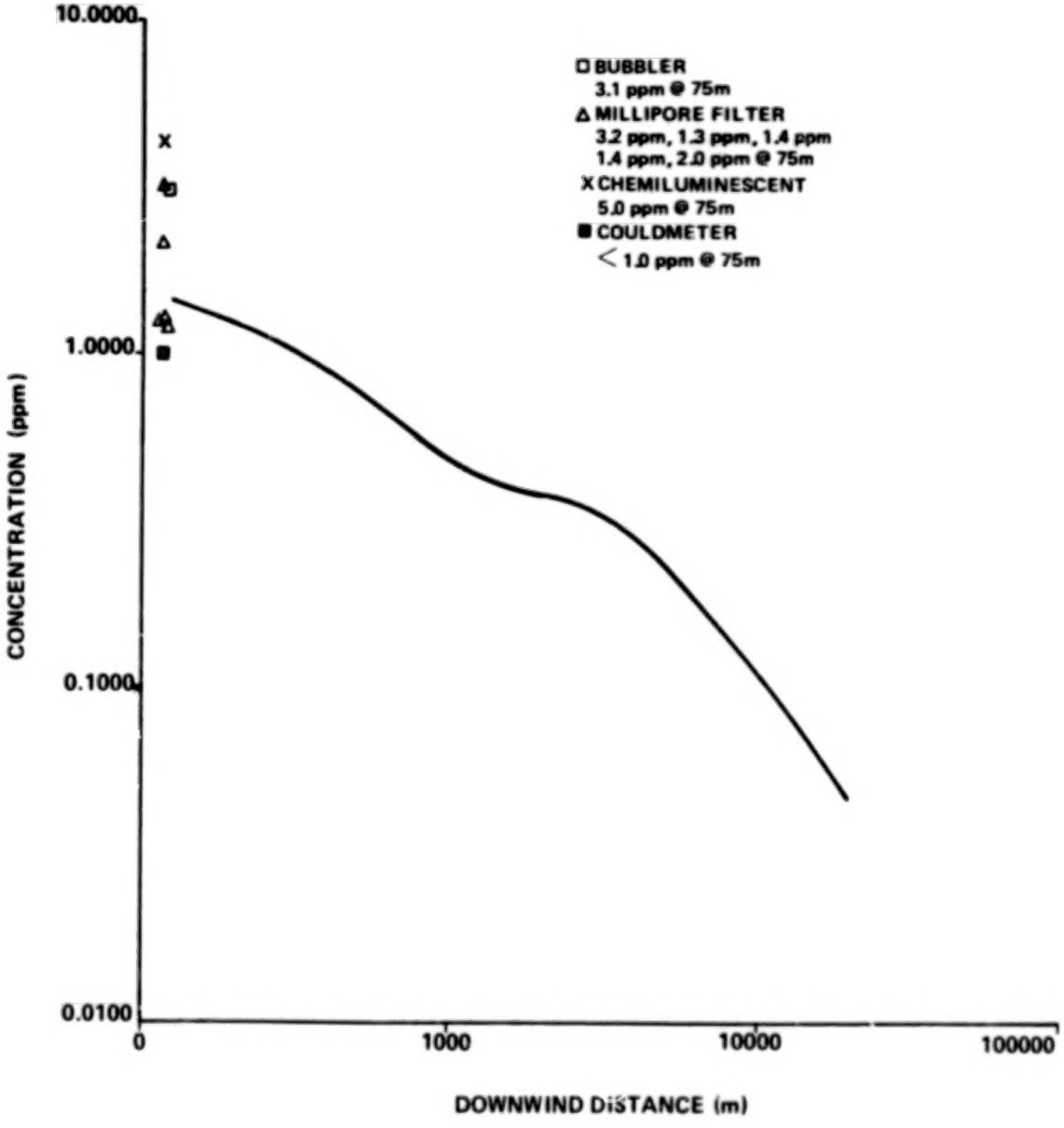

Figure 37. Computed maximum centerline HCl concentration from Model 4 and measured values: Static Test No. 15 (height 2.0 m, azimuth 35.1°).

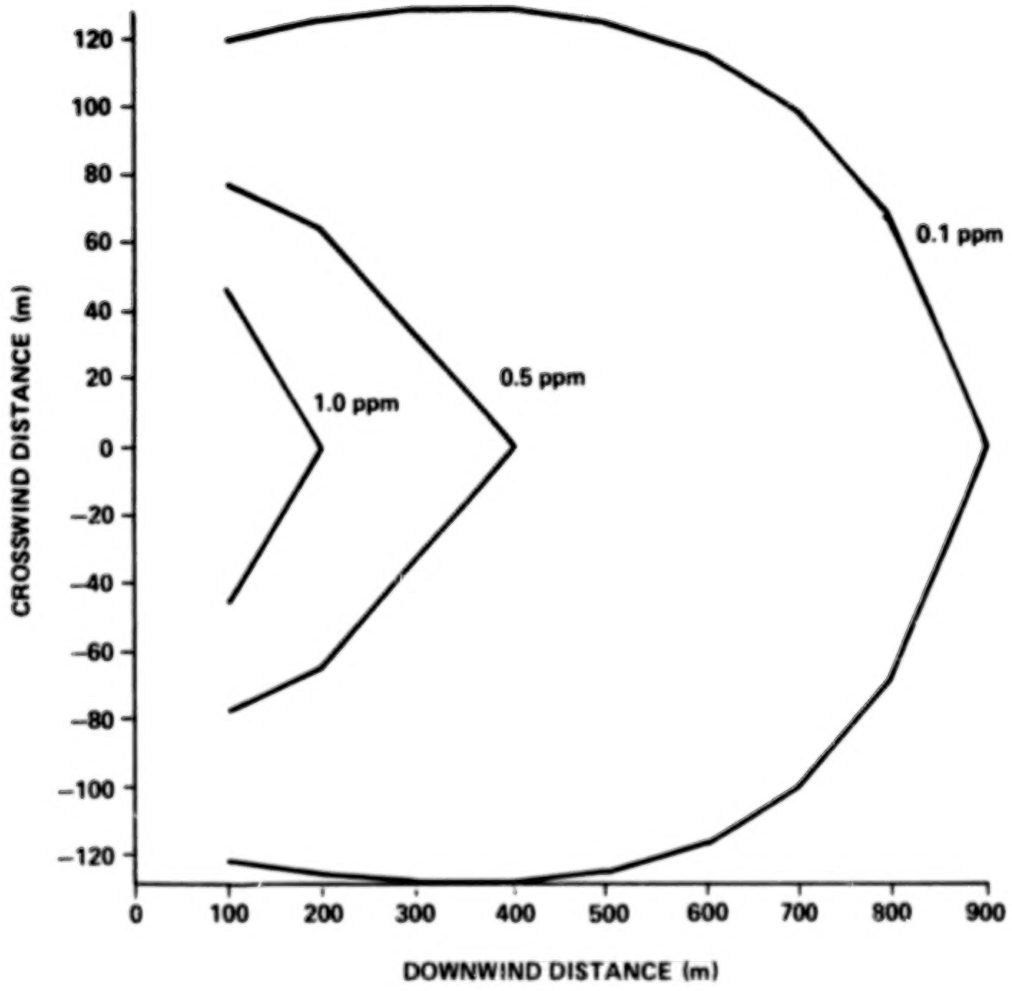

Figure 38. Computed HCl concentration isopleths by NASA/MSFC Multilayer Diffusion Model: Static Test No. 16 (height 2.0 m, azimuth bearing 182.2°).

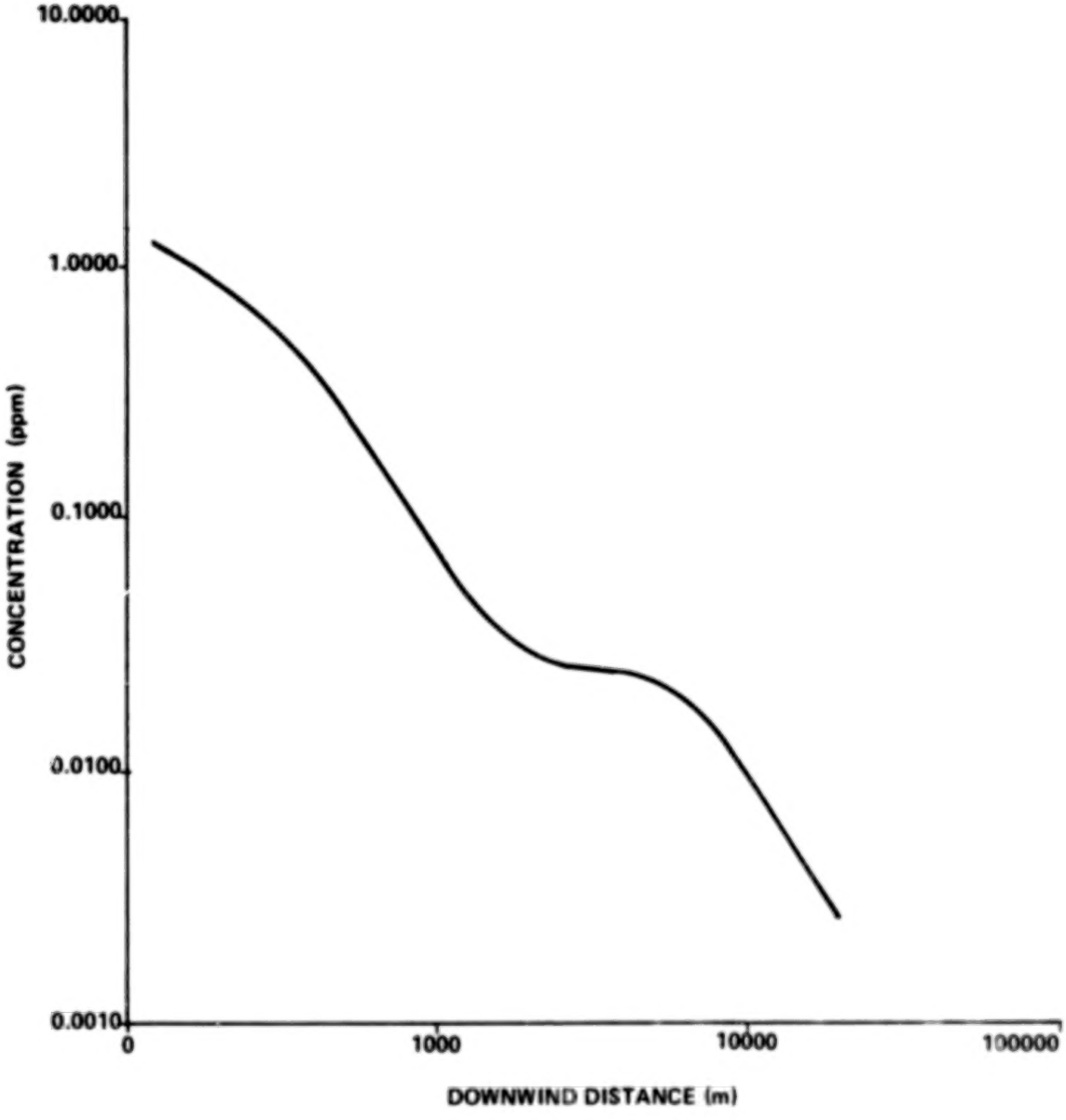

Figure 39. Computed maximum centerline HCl concentration from Model 4 for Static Test No. 16 (height 2.0 m, azimuth bearing 182.2°).

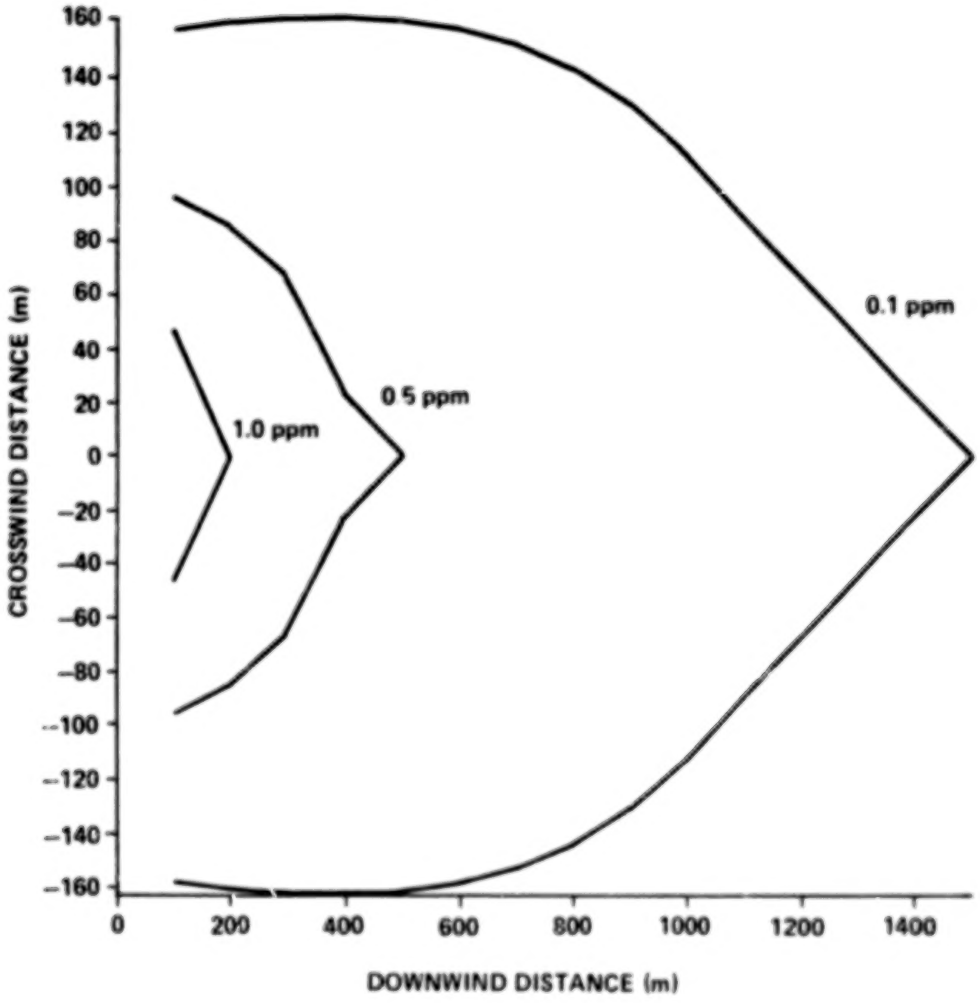

Figure 40. Computed HCl concentration isopleths by NASA/MSFC Multilayer Diffusion Model: Static Test No. 17 (height 2.0 m, azimuth bearing 322.0°).

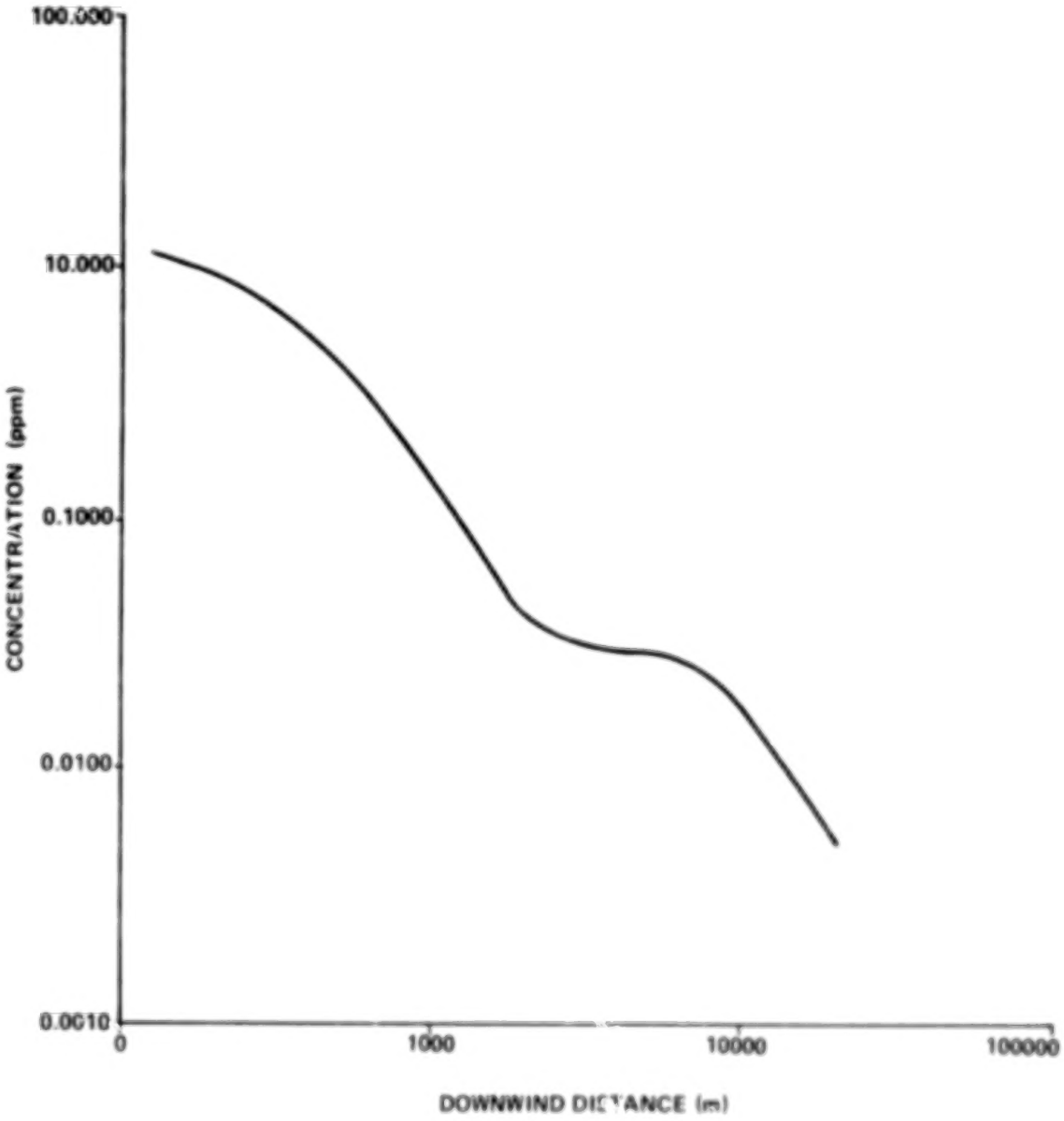

Figure 41. Computed maximum centerline HCl concentration from Model 4 for Static Test No. 17 (height 2.0 m, azimuth bearing 322.0°).

TABLE OF CONTENTS

LIST OF TABLES

LIST OF FIGURES

LIST OF SYMBOLS

Symbol	Definition
F_I	Instantaneous bouyancy term $\frac{3gQ_I}{4c_pT\pi\rho}$ (m^4/s^2)
FM	Percentage by weight of pollutant material in the fuel
H_L, H_S	Respective heat contents of liquid and solid fuels (cal/gm)
M	Molecular weight (gm/mole)
P	Ambient pressure (mb)
$P\ z_{TK}$	Integral of the Gaussian probability function between minus infinity and the top of the Kth layer z_{TK} $P\left\{\frac{z_{TK} - z_{mI}}{\sigma}\right\}$
Q	Total weight of exhaust products in the stabilized exhaust cloud (gm) $(Q_R)(t_R\{z_{mI}\})(FM)$
Q_F	Rate of heat released by burning fuel (cal/s) $H_L \cdot W_L + H_S \cdot W_S$
Q_I	Effective heat released (cal)
Q_K	Source strength in units of mass per unit depth of the Kth layer (gm/m)
T	Ambient air temperature (K)
W_L, W_S	Respective fuel expenditure rates, liquid and solid fuel (g/s)
z	Height above ground of any selected layer (m)
c_p	Specific heat of air at constant pressure 0.24 cal/K gm
g	Gravitational acceleration (9.8 m/s^2)

Symbol	Definition
r_R	Initial cloud radius at the surface (m)
$S=\frac{g}{T}\frac{\partial \Phi}{\partial z}$	Stability parameter ($1/s^2$)
t^*	Time of layer breakdown (s)
t_H	Time after ignition required for the cloud to reach the stabilization height (s)
t_R	Time after ignition (s)
t_{sI}	Time required for the cloud to achieve stabilization in an adiabatic atmosphere (s)
$t_R\{z_{mI}\}$	Time in seconds required for the vehicle to reach the height z_{mI} of maximum rise of the ground cloud (obtained from equation 1)
$\bar{u}$	Mean wind speed (m/s)
z	Height of stabilized cloud (m)
z'	Midpoint of the Kth layer (m)
	$(z_{BK} + z_{TK})/2$
z_{BK}	Height of the base of the Kth layer (m)
z_{TK}	Height of the top of the Kth layer (m)
z_{TL}	Height of the top of the Lth layer (m)
z_R	Altitude above the pad (m)
γ_C	Entrainment constant (continuous) (dimensionless)
γ_I	Entrainment constant (instantaneous) (dimensionless)
σ	Standard deviation of the concentration distribution of the stabilized ground cloud (m)
σ_{xK}	Standard deviation of the alongwind concentration distribution in the Kth layer at distance x (m)
σ_{xLK}	Standard deviation of the alongwind concentration distribution in the Lth layer for the source originating in the Kth layer (m)
$\sigma_{xo}\{K\}$	Standard deviation of the alongwind concentration distribution in the Kth layer at cloud stabilization (m)
$\sigma_{yo}\{K\}$	Standard deviation of the crosswind concentration distribution in the Kth layer at cloud stabilization (m)

Symbol	Definition
$\sigma_{zo}\{K\}$	Standard deviation of the vertical concentration distribution in the Kth layer at cloud stabilization (m)
$\sigma_{y}K$	Standard deviation of the crosswind concentration distribution in the Kth layer at distance x (m)
ρ	Density of ambient air (g/m^3)
$\frac{\partial \Phi}{\partial z}$	Vertical gradient of ambient potential temperature (K/m)
χ_p	Peak or centerline concentration (ppm)
keV	Kilo electron volt
s	Seconds

Test Firing No. 18

Shortly after ignition, the solid rocket motors broke loose from their mounts. One of the motors lodged in the test stand and the other landed in a wooded area. It was fortunate that all the instruments were close to the pad (approximately 75 m). Although it was not a normal static test firing because of the malfunction, it was a good test data event because the electrets were readily compared to other instruments. The average exposure time of the electrets and sensors to the ground cloud as observed from the block house and analysis of the photographs was 10 s. The dense exhaust cloud covered all the instruments simultaneously before it rose from the ground approximately 100 m from the test stand. The sensors were positioned prior to the test at 75 m. The sensors were placed in close because previous experience indicated once the exhaust cloud rises from the ground, measurements are hard to obtain.

Figures 42 and 43 illustrate the HCl predictions obtained from the NASA/MSFC Mulitlayer Diffusion Model.

An in-depth analysis is made of this test as the calibration of the electrets is determined from this test.

Table 22 lists results obtained from Test 18 for the various HCl measuring instruments. Concentrations obtained using the chemiluminescent HCl analyzer from the U.S. Air Force School of Medicine, Brooks Air Force Base, Texas, and bubblers, coulometers, and millipore filters from Arnold Engineering Development Center, Tullahoma, Tennessee, were compared to concentrations obtained simultaneously from the electrets studies.

Figure 44 illustrates the electrets and millipore filter positioned 75 m from the flame trench. Figure 45 shows the bubbler which was directly in line with the flame trench during the static test firing.

Direct comparisons were made at positions 1 and 8 of HCl measurements made with a millipore filter and a bubbler (Table 22). The electrets were kept beside the previously mentioned instruments to calibrate the pollution collected on the electrets surface. For example, at position 1, approximately 75 m from the flame trench and 85° from true north, the millipore filter measured 21.1 ppm. At the same angle and distance, the electrets measurement from the SEM and X-ray microprobe analysis gave 9682 counts. Also, at position 8, the bubbler measured 66.2 ppm, and 26 204 counts were obtained from the SEM and X-ray microscope analysis. From the above measurements, a

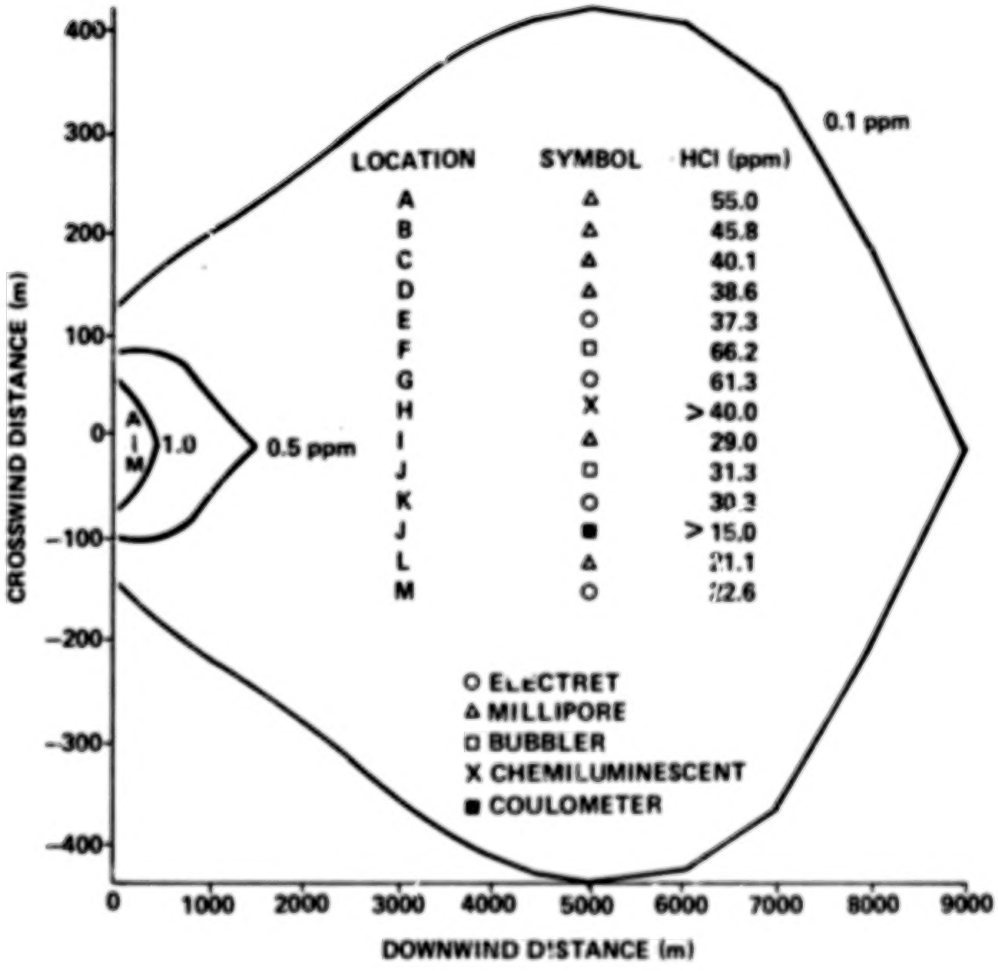

Figure 42. Comparison of HCl concentration isopleths computed by NASA/MSFC Multilayer Diffusion Model with measured values: Static Test No. 18 (height 2.0 m, azimuth bearing 122.7°).

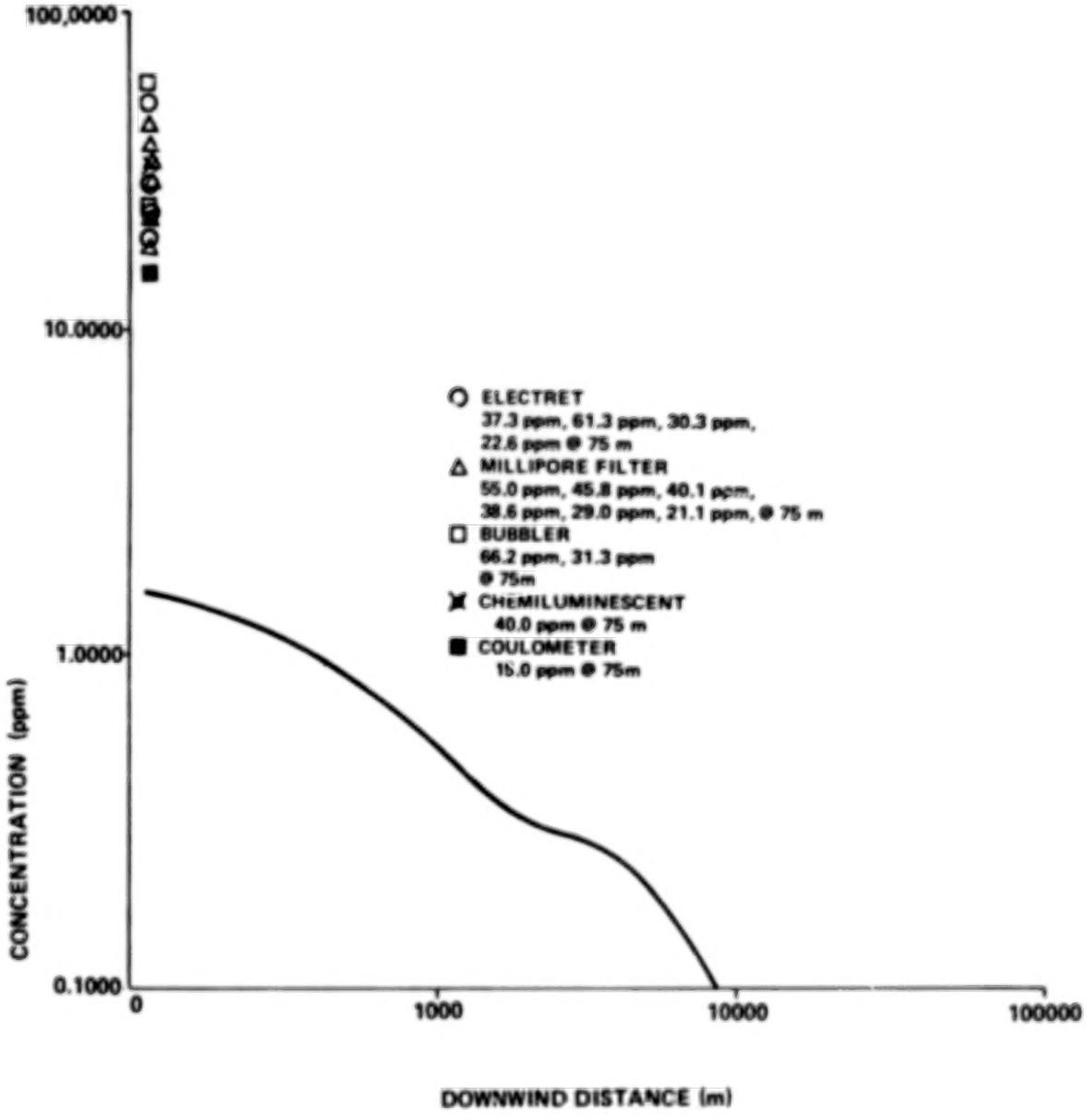

Figure 43. Computed maximum centerline HCl concentration from Model 4 and measured values: Static Test No. 18 (height 2.0 m, azimuth bearing 122.7°).

Table 22. Comparison of HCl Concentration Measurements Using Various Instruments to Electret Measurements During a 6.4 Percent Scale Model Test at MSFC Test Facility 116 (Test 18)

Position (P)	Angle (degree)/ Distance (m) (Measurement from True North)	Instrumentation	HCl Measurement (ppm)	Measurement Obtained Directly from Electrets Counts (Calibrated Values)[b]	Estimated Values (ppm)
1	85/75	Millipore Filter and Electret	21.1[a]	9 682[a]	22.65
2	30/75	Electret	30.32 (See Estimated Values)	12 961	30 32
3	75/75	Bubbler	31.3	13 375[b]	31.30
4	75/70	Electret	37.73 (See Estimated Values)	16 125	37.73
5	50/75	Millipore Filter	45.8	19 572[b]	45.79
6	45/75	Millipore Filter	55.0	23 503[b]	54.99
7	65/75	Chemiluminescent	65.4	27 948[b]	65.39
8	60/75	Bubbler and Electrets	66.2[a]	26 204[a]	61.31

a. Direct comparison made between millipore filter or bubbler and electrets.

b. Calibrated value (427.35 counts = 1 ppm).

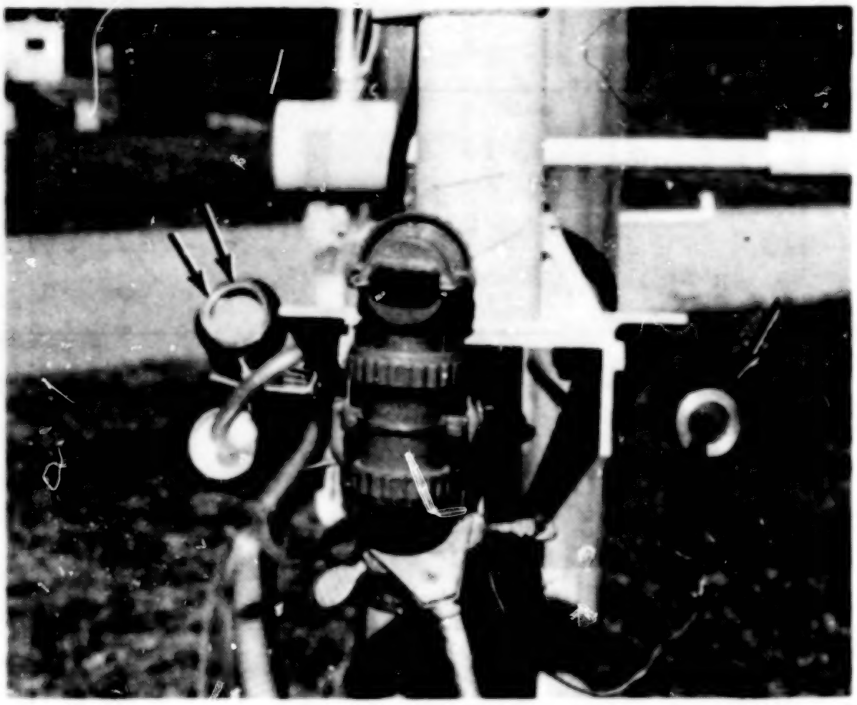

Figure 44. The electrets and millipore filter positioned 75 m from the flame trench (the single arrow points to the electrets position; the double arrow points to the millipore filter).

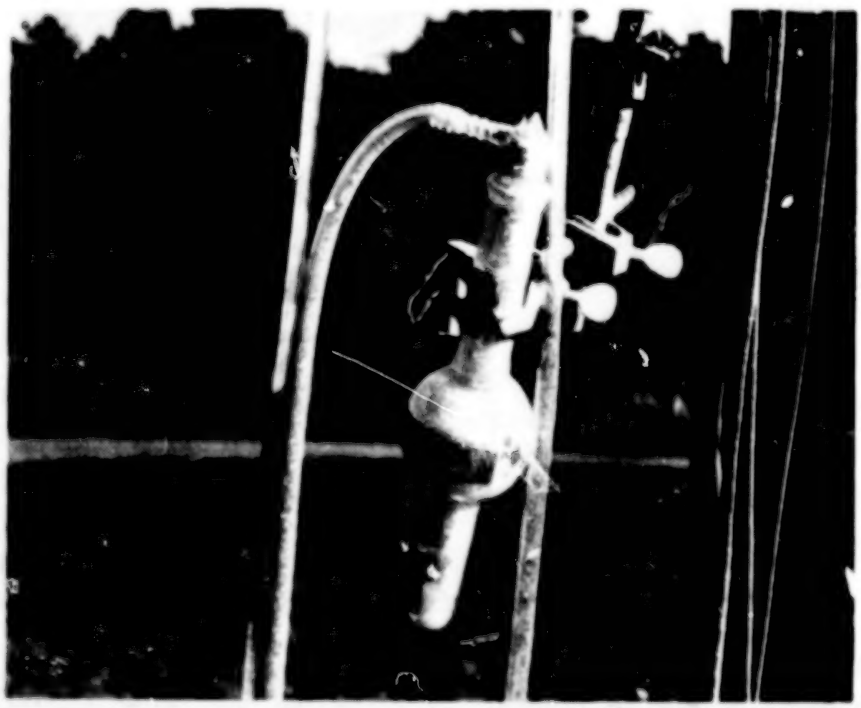

Figure 45. The bubbler directly in line with the flame trench (the bubbler was positioned directly in the ground cloud for measurement).

calibration of the counts from the electrets against the instruments (millipore filter and chemiluminescent analyzer) was obtained. This was found to be 427.35 counts equal 1 ppm. It may be noted that to obtain consistent results, the SEM analyses of the electrets were done under identical conditions. Also, the exhaust cloud passage time over the test instruments was approximately 10 s, which was determined from photographs taken during the test.

Figure 46 illustrates the comparison of the electrets measurements to HCl concentrations from various instruments such as the millipore filter, bubbler, and chemiluminescent HCl analyzer from Test 18.

In addition to the results in Figure 46, Figure 47 shows the distribution of concentrations of the pollution from the test site at various angles for a constant distance. It appears that when a dense flow of air from the rocket exhaust passes an electret that is adjacent to a millipore filter, bubbler, etc., the reading is high; and when a less dense flow of air from the rocket exhaust passes, a lower measurement of concentration is obtained. Figure 48 is a plot similar to that of Figure 46 but shows the dosage (ppm-s) versus electret electron counts from Test 18.

Figure 49 illustrates a summary of the measured data from the 18 static test firings at MSFC compared to the NASA/MSFC Multilayer Diffusion Model. It is important to note that the all the measured data from the electrets, millipore filter, bubbler, chemiluminescent detector, and coulometer were inside the upper and lower bounds of the diffusion model. These bounds were obtained by plotting the computed centerline HCl concentration from the 18 static tests and the upper and lower bounds of these tests encompassed the measured HCl values.

B. Chamber Tests

The chamber used for testing at Arnold Engineering Development Center is a 0.914 m^3 (3 ft^3) chamber made of plexiglass. The sample of the rocket fuel is ignited by triggering an electrically heated nichrome wire. The nichrome wire ignites the solid fuel which then burns for approximately 1 s. The holder of the millipore filter and electrets is placed into the chamber before the firing sequence. Exposure times of 30, 60, 90, and 120 s were determined using a digital timer. The mixing of the exhaust products results from the heat of the fuel and the resultant turbulent mixing. This lasts for several minutes, and observations indicated that it is a slow mixing process.

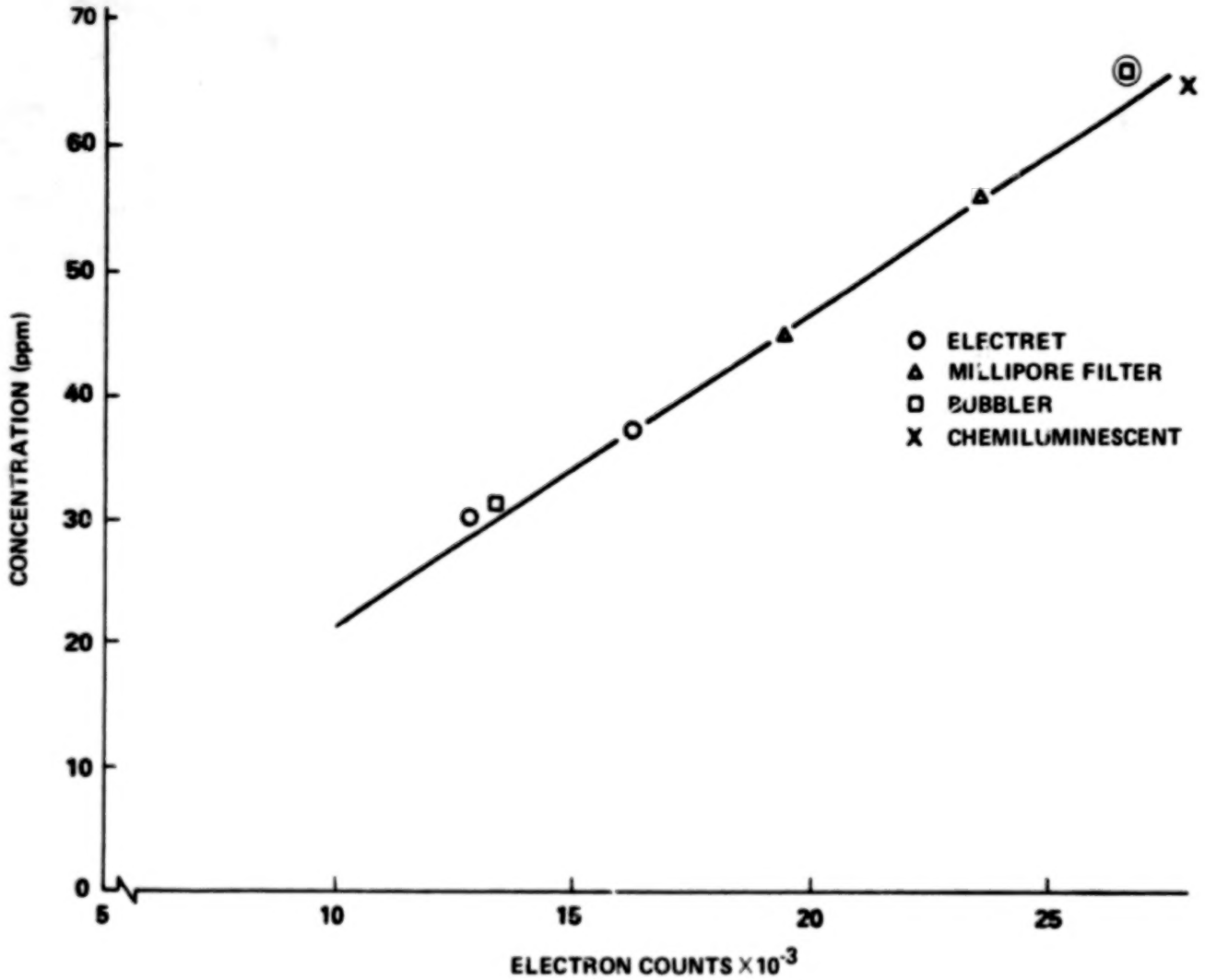

Figure 46. Comparison of HCl concentrations (ppm) from various instruments to electret electron counts during 6.4 percent SRB tests at MSFC (Test 18).

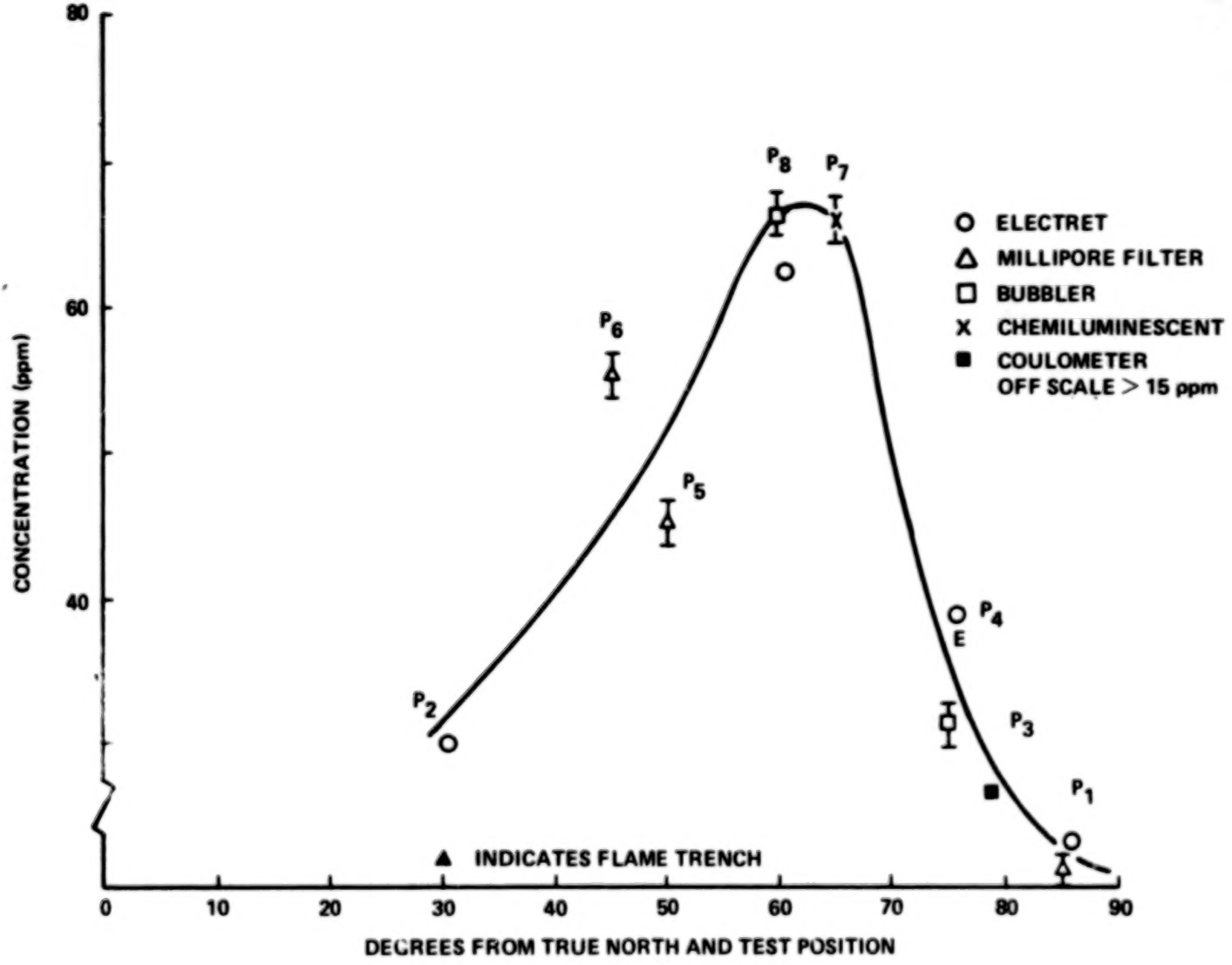

Figure 47. Measured distribution of rocket effluents (ppm) versus degrees from true north during 6.4 percent scale model testing at MSFC (Test 18).

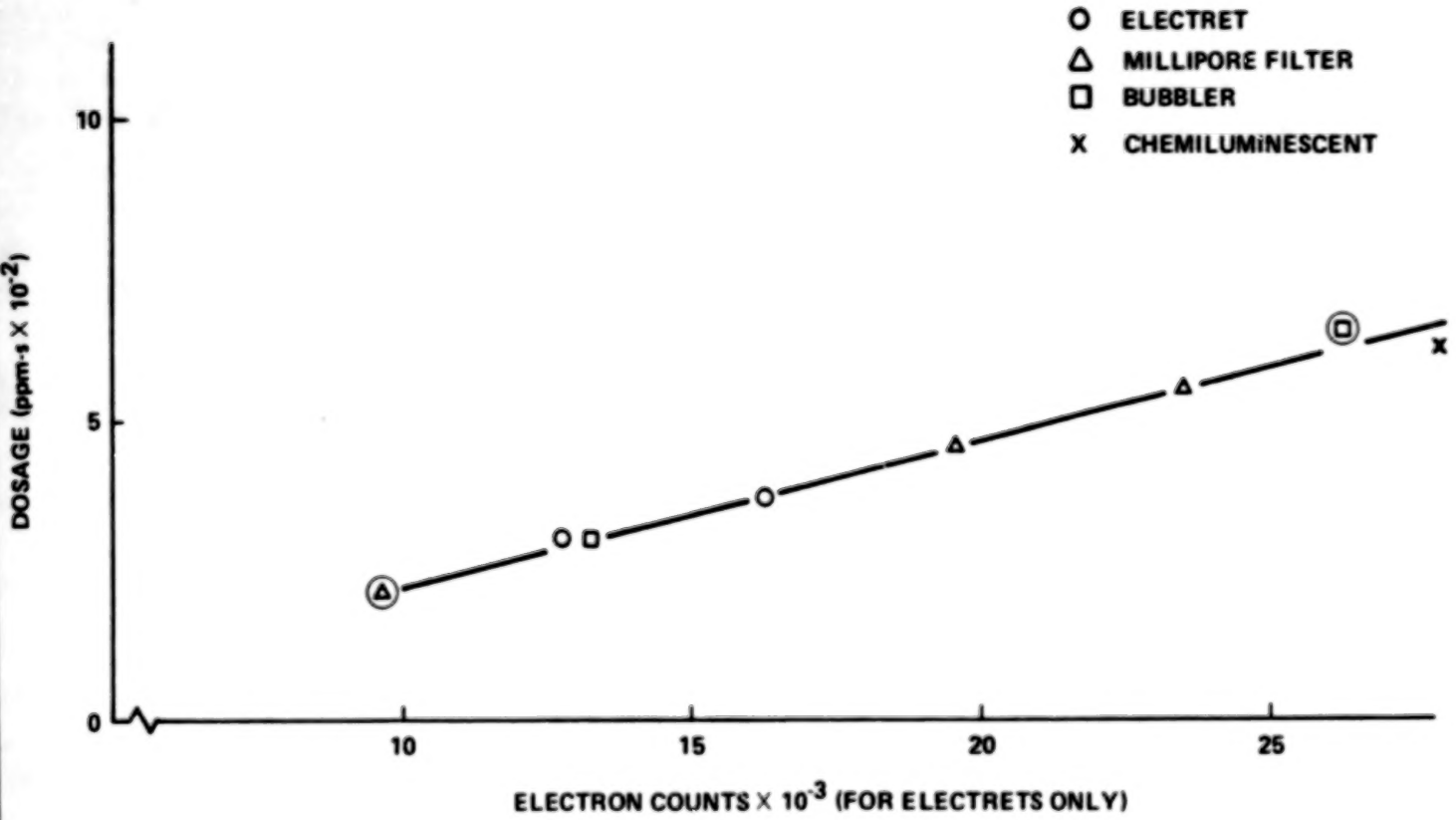

Figure 48. Comparison of HCl dosages (ppm-s) from various instruments to electret electron counts during 6.4 percent SRB tests at MSFC (Test 18).

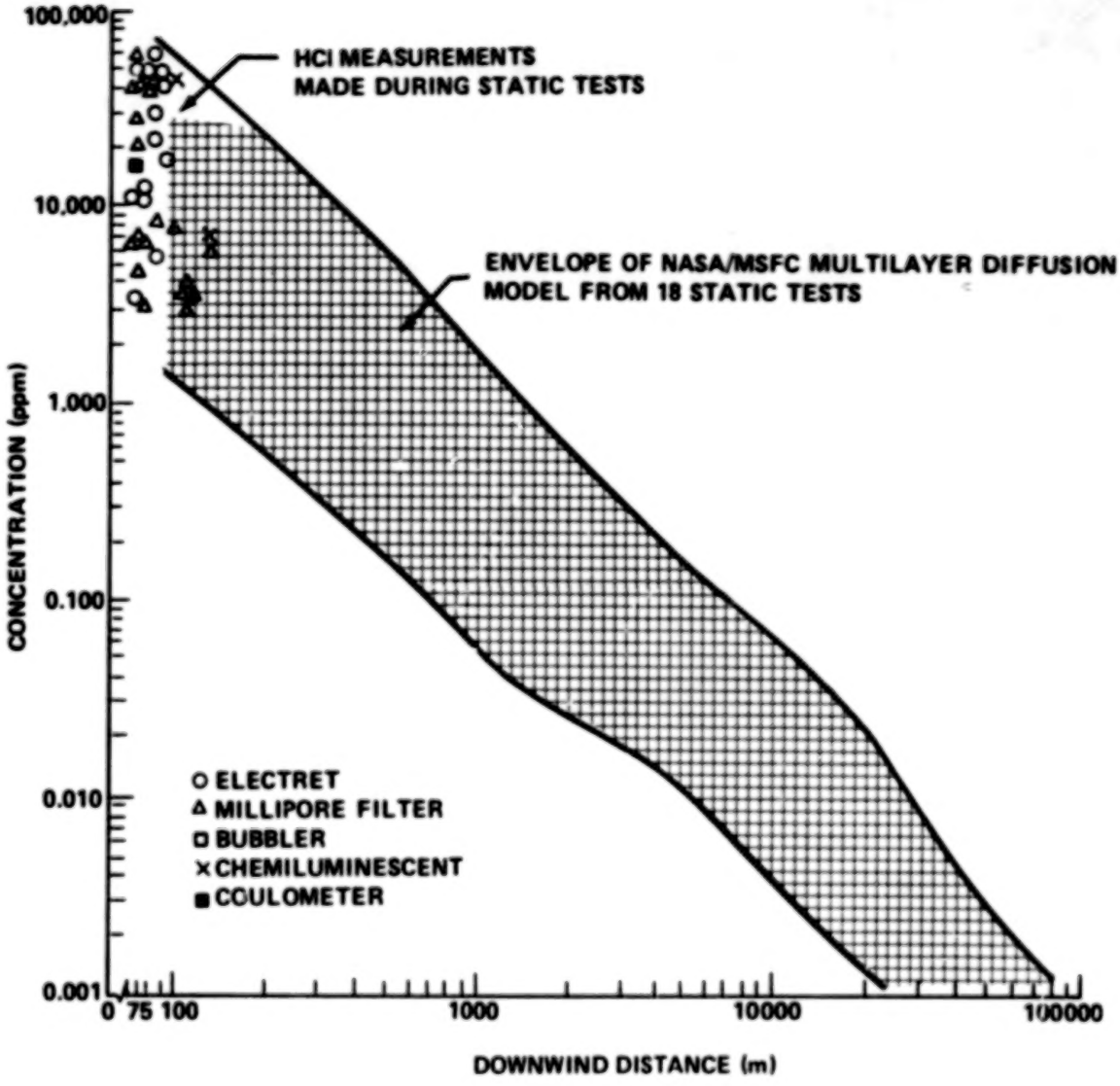

Figure 49. Comparison of measured values of HCl during 18 static tests at MSFC with the envelope of the upper and lower bounds obtained from the NASA/MSFC Multilayer Diffusion Model.

The density or distribution of the exhaust products for the 1 s firing in a chamber is not as uniform as a typical exhaust cloud observed [7,8,9] in the atmosphere where there is a mass flow of air over the instruments (wind speeds of 2 to 15 m/s depending on the test day). By observation the distribution sensed by the millipore filters and electrets in the chamber is a very slow mixing process in comparison to the mass flow of exhaust clouds observed in rocket testing in the atmosphere. It appears, however, that the initial reading for both instruments in the chamber is the best reading. The flow

at this point is more dense and uniform. After a period of time, the distribution becomes spotty in parts of the chamber and the exhaust gases decay. This can be seen in Figure 50 and Table 23. In Figure 50, the concentration for the millipore filter, after 60 s, two readings of 90 s, and 120 s drops off dramatically. In Figure 51, however, the electron counts generally increase with greater exposure time.

From Table 24, the localized instantaneous value for the electret count of 7366 and the millipore measurement of 20 ppm at 30s compares favorably when converted using 427.35 counts equal 1 ppm from the atmospheric tests. In this case, 17.25 ppm would be obtained from the electret measurement versus 20 ppm for the millipore filter.

Figure 52 illustrates the electret being positioned in the chamber alongside the millipore filter.

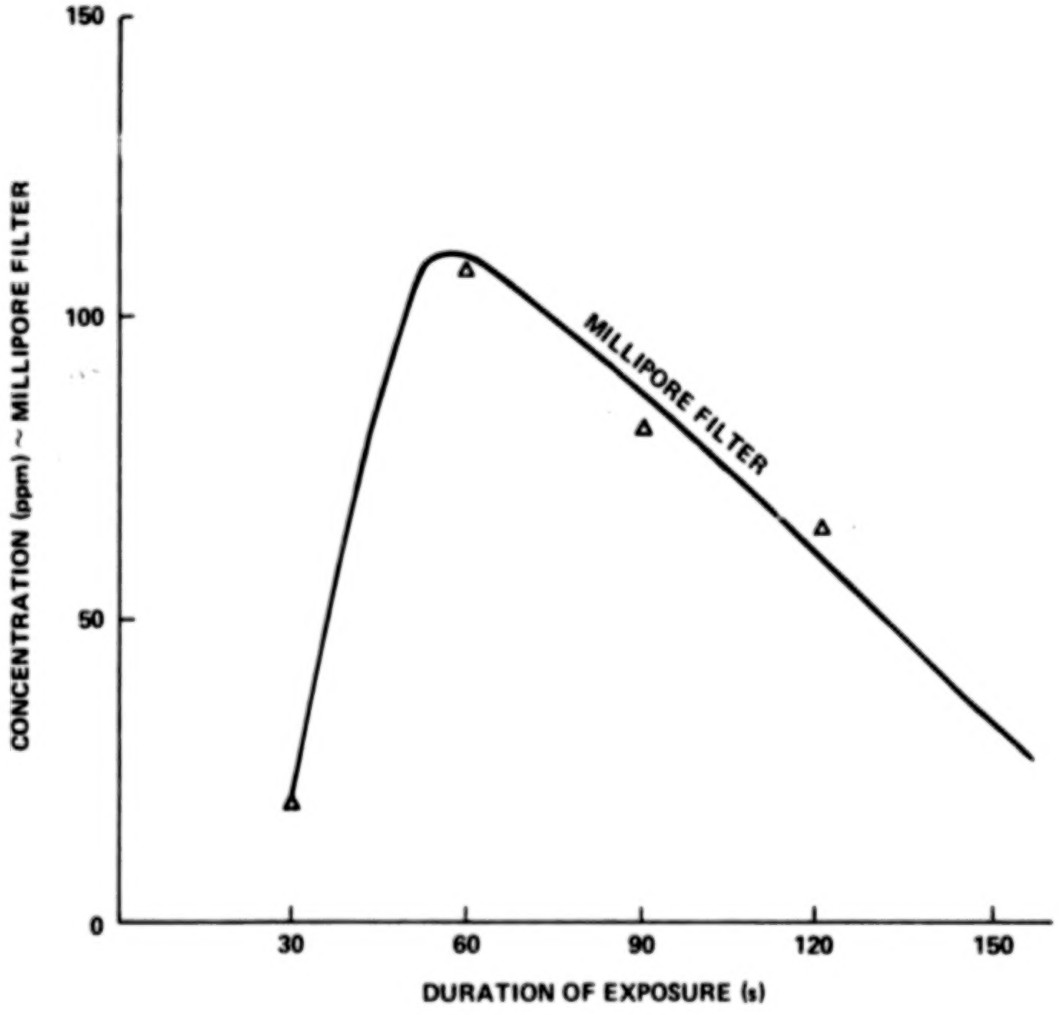

Figure 50. Duration of exposure (s) versus concentration measurements of HCl from millipore filter during chamber tests at Arnold Engineering Development Center.

Table 23. Chamber Test Data HCl Concentration Measurements from Millipore Filter Versus Electret Electron Counts for Times of 30, 60, 90, and 120 s at Arnold Engineering Development Center

Instrumentation	Time of Exposure (s)			
	30	60	90	120
Electret Electron Counts	7366	10 845	10 263	15 648
Millipore Filter (ppm)	20	107	263	67

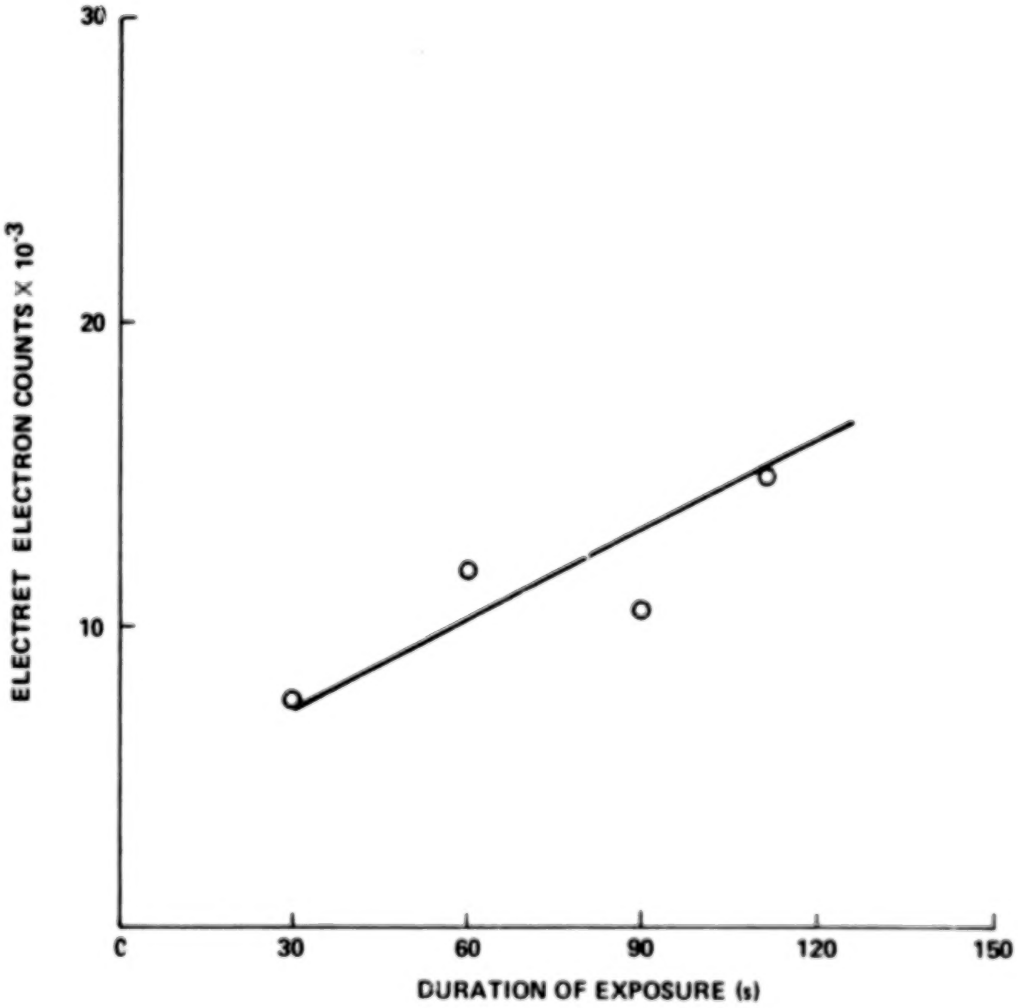

Figure 51. Duration of exposure (s) versus electret electron counts during chamber tests at Arnold Engineering Development Center.

Table 24. Viking I Test Matrix

Electret	Site	Time Out (CST)	Time in (CST)	Distance (km)	Azimuth (degree)	Counts	Counts Less Calibration	Counts Normalized for Time of Clouds Passage (counts/62.9)	$\frac{\text{Normalized Count}}{427.35 \text{ Counts/ppm}}$ = ppm	NASA/MSFC Model 4 (ppm)
V_1	Tower (Prelaunch Calibration)	1250	1334	0.25	85.0	4 076	–	–	–	–
V_2	Tower (Launch)	1250	1930	0.25	85.0	9 453	5 377	85.4	0.20	0.15
V_3	Tower (Launch)	1250	1930	0.25	85.0	16 277	12 201	193.97	0.45	0.15
V_4	Tower (Launch)	1255	Lost (Blast)	0.25	85.0	Lost	–	–	–	–
V_5	FB1	1323	2045	2.53	147.3	37 688	33 612	534.3	1.25	1.09
V_6	FB2	1348	2008	2.03	170.0	9 534	5 438	86.4	0.20	0.79
V_7	FB3	1310	2037	2.59	344.7	35 608	31 532	501.3	1.17	1.11
V_8	Tower (Postlaunch Calibration)	1930	1941	0.25	85.0	7 786	–	–	–	–
V_9	Boat (Prelaunch Calibration)	1500	1600	6.80	18.0	3 110	–	–	–	–
V_{10}	Boat (Vertical)	1500	1900	6.80	18.0	5 286	2 176	34.6	0.08	1.10
V_{11}	Boat (Horizontal)	1500	1910	6.80	18.0	24 992	21 882	347.8	0.81	1.10
V_{12}	Boat (Post Calibration)	1900	2000	6.80	18.0	5 940	–	–	–	–

Figure 52. Comparison of electrets (single arrow) and millipore filter (double arrow) in a chamber at Arnold Engineering Development Center.

C. Viking I Launch

The Titan IIIC missile at Launch Complex 41 ready for liftoff on August 20, 1975, for the Viking I mission to Mars is shown in Figure 53.

It is apparent during the deployment of the instruments to measure the effluents from the exhaust cloud that the potential cloud trajectory is of major importance. Synoptic weather data from the National Weather Service Network at T minus eight hours indicated a nearly equal potential for both land and sea trajectory for the cloud. The repositioning and reevaluation of the cloud path took place at T minus four hours. The land cloud trajectory became more probable than the sea cloud trajectory. Haze as well as cloud expansion resulted in loss of visible cloud tracking after 26 min. Observation of the cloud trajectory appeared to be 320° to 340° from the pad.

Since the Viking Project Team cut the power off from T minus 10 minutes to T plus ten minutes during the Viking I launch, a direct comparison of the instruments at the sites could not be made with the electrets.

The counts from the SEM as presented in Table 24 were adjusted by subtracting the background counts from the measurements. From the calibration of the 6.4 percent rocket motor firing, the exhaust cloud took an average of 10 s to travel over the sensors, and the calibration of 427.35 counts/ppm was based on this 10 s value. During the Viking I mission, the cloud took 629 s to pass over the sensor or 62.9 times more as compared to the 6.4 percent model on the Tomahawk missile at MSFC. A comparison of the results of the electrets and the NASA/MSFC Multilayer Diffusion Model is given in Table 24.

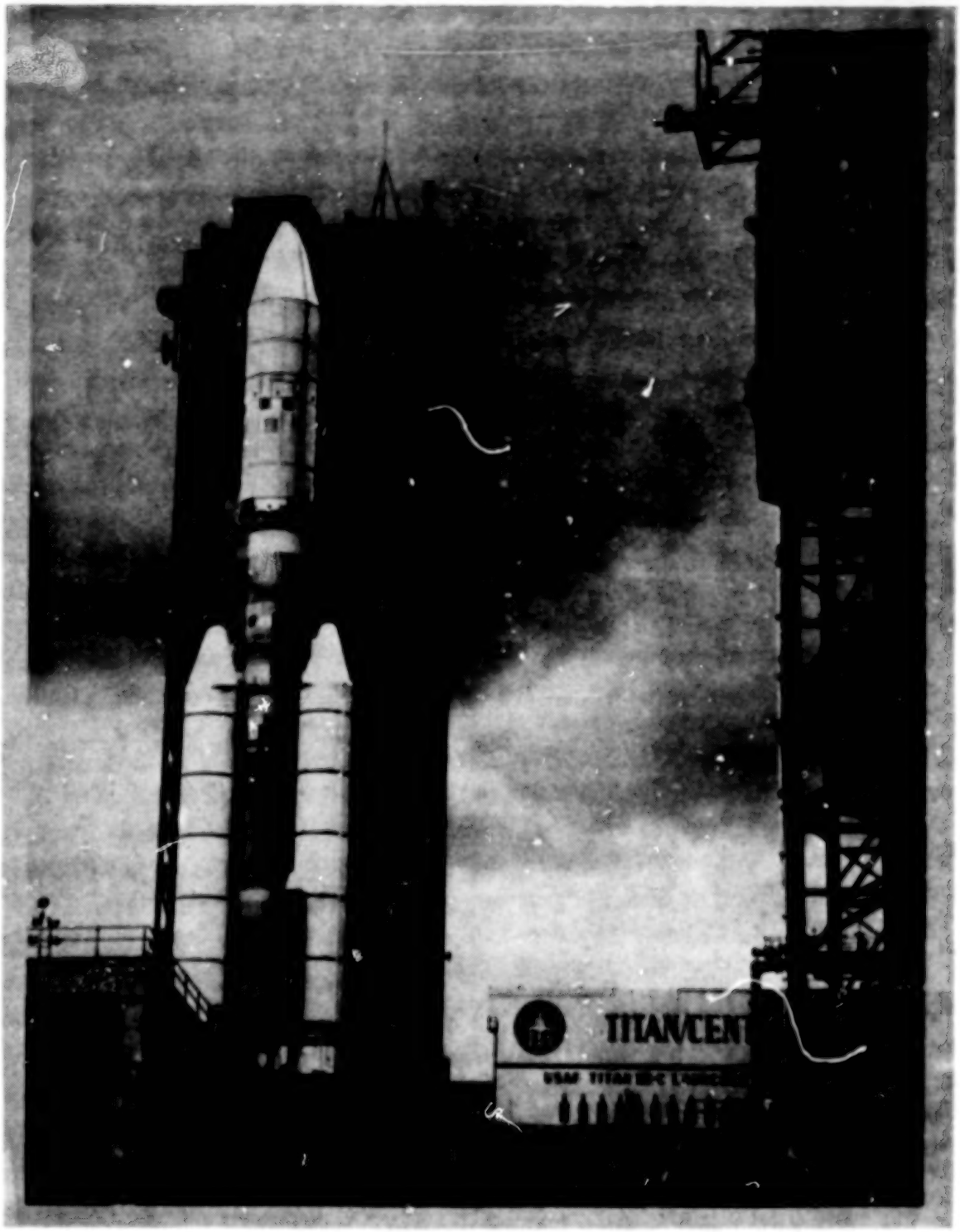

Figure 53. Titan IIIC poised at Launch Complex 41 KSC for launching of Viking I mission to Mars on August 20, 1975.

CHAPTER VII

CONCLUSIONS

The purpose of this research investigation was to evaluate the electrets, a new detecting contamination device used to assess the chemical compositions of rocket effluents. In assessing the effectiveness of the electrets, the following was concluded:

The electrets have been used successfully in collecting rocket exhaust effluents. It was possible by the use of the SEM and X-ray microprobe analysis to obtain spectra, giving the electret a multipollutant capability. In addition, simplicity of deployment and speed of assessment and analysis make the electrets a valuable tool in measuring pollutants from a space vehicle rocket exhaust.

The electret compared favorably with other HCl measuring devices. It is a valuable complementary device to other measuring systems. Summary of the measured data from the electrets and other HCl detectors is within the upper and lower bounds of the computed HCl concentrations using the NASA/MSFC Multilayer Diffusion Model.

Future research should be designed for extensive investigations to obtain quantitative results. Ideally, the measurements should be repeated so that reliability of the results could be assured. Continued chamber and field tests should achieve these results.

REFERENCES

1. Pillai, P. K. C. and Shriver, Edward L.: Electrets and Their Applications in Contamination Studies. NASA Technical Report R-457, 1975.

2. Wells, Oliver C.: Scanning Electron Microscope. McGraw-Hill, New York, 1974.

3. Gregory, Gerald L.; Hudgins, Charles H.; and Emerson, Burt R., Jr.: Proceedings of JANNAF Propulsion Meeting. San Diego, California, 1974.

4. Dawborn, R. and Kinslow, M: Studies of the Exhaust Products from Solid Propellant Rocket Motors. Arnold Engineering Development Center. Tullahoma, Tennessee, 1976.

5. Dumbauld, R. K.; Bjorklund, J. R.; and Bowers, J. F.: NASA/MSFC Multilayer Diffusion Models and Computer Programs for Operational Prediction of Toxic Fuel Hazards. H. E. Cramer Co., TR 73-301-02, NASA Contract NAS8-29033, 1973.

6. Landau, L. D. and Lifshitz, E. M.: Fluid Mechanics. Course of Theoretical Physics, Vol. 6, Pergamon Press, 1959.

7. Susko, M.; Kaufman, J. W.; and Hill K.: Rise Rate and Growth of Static Test Vehicle Engine Exhaust Clouds. NASA TM X-53782, Aero-Astrodynamics Research Review, No. 7, 1968, pp. 146-166.

8. Susko, Michael and Kaufman, J. W.: Exhaust Cloud Rise and Growth for Apollo Saturn Engines. Journal of Spacecraft and Rockets, Vol. 10, 1973, pp. 341-345.

9. Stephens, J. Briscoe; Susko, Michael; Kaufman, J. W.; and Hill, C. Kelly: An Analytical Analysis of the Dispersion Predictions for Effluents from the Saturn V and Scout-Algol III Rocket Exhausts. NASA TM X-2935, 1973.

10. Fichtl, George H.; Kaufman, J. W.; and Vaughan, W. W.: Characteristics of Atmospheric Turbulence as Related to Wind Loads on Tall Structures. Journal of Spacecraft and Rockets, Vol. 4, 1969, pp. 1396-1403.

11. Tyldesley, J. B. and Wallington, C. E.: The Effect of Wind Shear and Vertical Diffusion on Horizontal Dispersion. Quart. J. Royal Meteorological Society, Vol. 91, 1967, pp. 158-174.

12. Daniel, O. H.: Digital Computer of an AN/GMD-2 Rawinsonde Data. Pan American World Airways, Guided Missile Range Division, Patrick Air Force Base, Florida, 1962.

13. Anonymous: National Primary and Secondary Ambient Air Quality Standards. Environmental Protection Agency, Part II of Federal Register, Vol. 36, No. 84, 1971.

14. Anonymous: National Environmental Policy Act, Public Law 91-190, 42 U. S. Congress, 1969, p. 4321.

15. Anonymous: Basis for Establishing Guides for Short-Term Exposures of the Public to Air Pollutants. National Academy of Sciences, National Research Council Report PB 203 464, 1971.

16. Anonymous: Guides for Short-Term Exposures of the Public to Air Pollutants, Vol. 11. Guide for Hydrogen Chloride. Committee on Toxicology of the National Academy of Sciences National Research Council, Washington, D.C., National Research Council Report PB 199 904, 1971.

APPENDIX

APPENDIX A

CALCULATION OF THERMODYNAMIC VARIABLES FROM RAWINSONDE DATA

The equations used for calculation of thermodynamic variables from measurements of altitude, temperature, and relative humidity obtained from the GMD-4, AMQ-9 rawinsonde system are summarized herein; these equations, originally developed for the GMD-2 system [11], must be used in conjunction with the list of symbols and units provided at the end of this appendix.

Atmospheric Density, ρ

$$\rho = 348.38 \frac{P}{T_v} \tag{A-1}$$

Pressure, P

$$P = P' 10^{-(h-h')/(221.266\, T_{vm})} \tag{A-2}$$

Geopotential Height, h

$$h = \frac{g_o}{9.8} \frac{r_e H}{r_e + H} \tag{A-3}$$

Virtual Temperature, T_v

$$T_v = T(1 + 0.376932\, e/P') \tag{A-4}$$

Mean Virtual Temperature, T_{vm}

$$T_{vm} = \frac{T_v' + T_v}{2} \tag{A-5}$$

Vapor Pressure, e

$$e = 6.11\, f_D\, 10^{7.5t/(t+237.3)} \tag{A-6}$$

Dew Point Temperature, t_d

$$t_d = \frac{237.3 \log e - 186.527}{8.236 - \log e} \tag{A-7}$$

Potential Temperature, θ

$$\theta = T \frac{1000^{0.288}}{P} \tag{A-8}$$

Virtual Potential Temperature, θ_v

$$\theta_v = T_v \frac{1000^{0.288}}{P} \tag{A-9}$$

Absolute Humidity, ρ_w

$$\rho_w = 216.7\ e/P \tag{A-10}$$

Microwave Refractive Index, n

$$n = 1 + \left[\frac{1}{T}\left(77.6P - 11e + \frac{374808e}{T}\right)\right] 10^{-6} \tag{A-11}$$

For data tabulation, use:

$$N = (n - 1)10^6 \tag{A-12}$$

Speed of Sound, V_s

$$V_s = 643.855\left(\frac{T}{273.16}\right)^{0.5} \tag{A-13}$$

LIST OF SYMBOLS

Symbol	Definition
e	Vapor pressure (mb)
f_D	Relative humidity expressed as a decimal
g_o	Acceleration of gravity at geographical location of the rawinsonde station (m/s^2)
h	Geopotential height at the top of the layer bounded by h and h′ (ft)
h'	Geopotential height at the bottom of the layer bounded by h and h′ (ft)
H	Geometric altitude at the top of the layer bounded by H and H′ (ft)
H'	Geometric altitude at the bottom of the layer bounded by H and H′ (ft)
n	Microwave refractive index
N	Unit of refractive index used for simplification of data tabulation
P	Pressure at geopotential height h (mb)
P'	Pressure at geopotential height h′ (mb)
r_e	Radius of the Earth (ft)
t	Temperature (°C)
T	Temperature (K)
t_d	Dew point temperature (°C)
T_v	Virtual temperature at geopotential height h (K)
T'_v	Virtual temperature at geopotential height h′ (K)
T_{vm}	The mean virtual temperature of layer bounded by h and h′ (K)
V_s	Speed of sound (kn)
ρ	Atmospheric density (gm/m^3)
ρ_w	Absolute humidity (gm/m^3)
θ	Potential temperature (K)
θ_v	Virtual potential temperature (K)

1. REPORT NO.	2. GOVERNMENT ACCESSION NO.	3. RECIPIENT'S CATALOG NO.
NASA TP-1073		

4. TITLE AND SUBTITLE	5. REPORT DATE
Research in the Use of Electrets in Measuring Effluents from Rocket Exhaust of the Space Shuttle (6.4 Percent Scaled Model) and Viking I Launch	November 1977
	6. PERFORMING ORGANIZATION CODE
7. AUTHOR(S)	8. PERFORMING ORGANIZATION REPORT #
Michael Susko	M-231
9. PERFORMING ORGANIZATION NAME AND ADDRESS	10. WORK UNIT NO.
George C. Marshall Space Flight Center Marshall Space Flight Center, Alabama 35812	11. CONTRACT OR GRANT NO.
	13. TYPE OF REPORT & PERIOD COVERED
12. SPONSORING AGENCY NAME AND ADDRESS	Technical Paper
National Aeronautics and Space Administration Washington, D. C. 20546	14. SPONSORING AGENCY CODE

15. SUPPLEMENTARY NOTES

Prepared by Space Sciences Laboratory, Science and Engineering

16. ABSTRACT

The purpose of this experimental research was to investigate electrets, a new device used to detect the chemical composition of rocket exhaust effluents. In assessing the effectiveness of electrets, comparisons were made with hydrogen chloride measuring devices from chamber and field tests and computed results from the NASA/MSFC Multilayer Diffusion Model.

The experimental data used in this investigation were obtained from the 18 static test firings at Marshall Space Flight Center, Huntsville, Alabama, chamber tests at Arnold Engineering Development Center, Tullahoma, Tennessee, and the Viking I launch to Mars on August 20, 1975, from Kennedy Space Center, Florida.

The results show that electrets have multipollutant measuring capabilities, simplicity of deployment, and speed of assessment. The electrets compared favorably with other hydrogen chloride measuring devices. The summary of the measured data from the electrets and the hydrogen chloride detectors is within the upper and lower bounds of the computed hydrogen chloride concentrations from the NASA/MSFC Multilayer Diffusion Model.

17. KEY WORDS	18. DISTRIBUTION STATEMENT
Aerospace effluents Atmospheric modeling Diffusion modeling Electrets Fluid mechanics	STAR Cagetory 45

19. SECURITY CLASSIF. (of this report)	20. SECURITY CLASSIF. (of this page)	21. NO. OF PAGES	22. PRICE
Unclassified	Unclassified	120	$5.50

* For sale by the National Technical Information Service, Springfield, Virginia 22161

NASA-Langley, 1977